A QUANTUM CHEMICAL STUDY OF WATER AND AMMONIA ADSORPTION MECHANISMS ON TITANIUM DIOXIDE SURFACES

A THESIS SUBMITTED TO
THE GRADUATE SCHOOL OF NATURAL AND APPLIED SCIENCES
OF
MIDDLE EAST TECHNICAL UNIVERSITY

BY

REZAN ERDOĞAN

IN PARTIAL FULFILLMENT OF THE REQUIREMENTS
FOR
THE DEGREE OF MASTER OF SCIENCE
IN
CHEMICAL ENGINEERING

JANUARY 2010

Approval of the thesis:

A QUANTUM CHEMICAL STUDY OF WATER AND AMMONIA ADSORPTION MECHANISMS ON TITANIUM DIOXIDE SURFACES

submitted by **REZAN ERDOĞAN** in partial fulfillment of the requirements for the degree of **Master of Science in Chemical Engineering Department, Middle East Technical University** by,

Prof. Dr. Canan Özgen
Dean, Graduate School of **Natural and Applied Sciences** _____

Prof. Dr. Gürkan Karakaş
Head of Department, **Chemical Engineering** _____

Prof. Dr. Işık Önal
Supervisor, **Chemical Engineering Dept., METU** _____

Examining Committee Members:

Prof. Dr. Hayrettin Yücel
Chemical Engineering Dept., METU _____

Prof. Dr. Işık Önal
Chemical Engineering Dept., METU _____

Prof. Dr. Güngör Gündüz
Chemical Engineering Dept., METU _____

Prof. Dr. Şinasi Ellialtıoğlu
Physics Dept., METU _____

Assoc. Prof. Dr. Göknur Bayram
Chemical Engineering Dept., METU _____

Date: January 15, 2010

I hereby declare that all information in this document has been obtained and presented in accordance with academic rules and ethical conduct. I also declare that, as required by these rules and conduct, I have fully cited and referenced all material and results that are not original to this work.

Name, Last name : Rezan Erdoğan

Signature :

ABSTRACT

A QUANTUM CHEMICAL STUDY OF
WATER AND AMMONIA ADSORPTION MECHANISMS ON
TITANIUM DIOXIDE SURFACES

Erdoğan, Rezan
M.Sc., Department of Chemical Engineering
Supervisor : Prof. Dr. Işık Önal

January 2010, 106 pages

Theoretical methods can be used to describe surface chemical reactions in detail and with sufficient accuracy. Advances, especially in density functional theory (DFT) method, enable to compare computational results with experiments.

Quantum chemical calculations employing ONIOM DFT/B3LYP/6-31G**-MM/UFF cluster method provided in Gaussian 03 are conducted to investigate water adsorption on rutile (110), and water and ammonia adsorption on anatase (001) surfaces of titanium dioxide. Water and ammonia adsorption on anatase (001) surface is studied by also performing PW:DFT-GGA-PW91 periodic DFT method by using VASP code and the results are compared with the results of ONIOM method.

The results obtained by means of ONIOM method indicate that dissociative water adsorption on rutile (110) surface is not favorable due to high activation barrier, whereas on anatase (001) surface, it is favorable since molecular and dissociative water adsorption energies are calculated to be -23.9 kcal/mol and -58.12 kcal/mol. Moreover, on anatase (001) surface, dissociative ammonia adsorption is found energetically more favorable than molecular one (-37.17 kcal/mol vs. -23.28 kcal/mol). Thermodynamic functions at specific experimental temperatures for water and ammonia adsorption reactions on anatase (001) surface are also evaluated.

The results obtained using periodic DFT method concerning water adsorption on anatase (001) surface indicate that dissociative adsorption is more favorable than molecular one (-32.28 kcal/mol vs. -14.62 kcal/mol) as in ONIOM method. On the same surface molecular ammonia adsorption energy is computed as -25.44 kcal/mol.

The vibration frequencies are also computed for optimized geometries of adsorbed molecules. Finally, computed adsorption energy and vibration frequency values are found comparable with the values reported in literature.

KEYWORDS: DFT; ONIOM; periodic DFT; rutile; water adsorption; anatase; water and ammonia adsorption.

ÖZ

SU VE AMONYAĞIN TİTANYUM DİOKSİT YÜZEYLERİ ÜZERİNDE ADSORPSİYON MEKANİZMALARININ KUANTUM KİMYASAL ÇALIŞMASI

Erdoğan, Rezan
Yüksek Lisans, Kimya Mühendisliği Bölümü
Tez Yöneticisi: Prof. Dr. Işık Önal

Ocak 2010, 106 sayfa

Kimyasal yüzey reaksiyonlarını ayrıntılı olarak ve yeterli doğrulukta tanımlamak için teorik metotlar kullanılabilir. Özellikle 'density functional theory' (DFT) metodundaki gelişmeler, hesaba dayalı sonuçları deneylerle karşılaştırmaya olanak sağlar.

Titanyum dioksitin rutil (110) yüzeyi üzerinde su adsorpsiyonunu, anataz (001) yüzeyi üzerinde su ve amonyak adsorpsiyonlarını incelemek için Gaussian 03 programında ONIOM DFT/B3LYP/6-31G**-MM/UFF küme metodu kullanılarak kuantum kimyasal hesaplamalar yapılmıştır. Ayrıca, anataz (001) yüzeyi üzerinde su ve amonyak adsorpsiyonları VASP kodu kullanılarak PW:DFT-GGA-PW91 periyodik DFT metoduyla da çalışılmış ve sonuçlar ONIOM metodunun sonuçlarıyla karşılaştırılmıştır.

ONIOM metodu kullanılarak elde edilen sonuçlar, rutil (110) yüzeyi üzerinde suyun ayrışma adsorpsiyonunun yüksek aktivasyon bariyerinden dolayı avantajlı olmadığını, bununla birlikte anataz (001) yüzeyi üzerinde, suyun molekül olarak ve ayrışarak gerçekleşen adsorpsiyon enerjileri -23.9 kcal/mol ve -58.12 kcal/mol olarak hesaplandığından, suyun ayrışma adsorpsiyonunun molekül olarak gerçekleşen su adsorpsiyonuna göre daha avantajlı olduğunu göstermektedir. Ayrıca, anataz (001) yüzeyi üzerinde amonyağın ayrışma adsorpsiyonunun molekül olarak gerçekleşen amonyak adsorpsiyonundan enerjiler açısından daha avantajlı olduğu bulunmuştur. (-37.17 kcal/mol'e karşın -23.28 kcal/mol). Anataz (001) yüzeyi üzerinde su ve amonyak adsorpsiyon reaksiyonları için belirli deneysel sıcaklıklarda termodinamik fonksiyonlar da hesaplanmıştır.

Periyodik DFT metodu kullanılarak, anataz (001) yüzeyi üzerinde su adsorpsiyonuna dair elde edilen sonuçlar, ONIOM metodunda olduğu gibi, suyun ayrışma adsorpsiyonunun molekül olarak gerçekleşen su adsorpsiyonundan enerjiler açısından daha avantajlı olduğunu işaret etmektedir (-32.28 kcal/mol'e karşın -14.62 kcal/mol). Aynı yüzey üzerinde, moleküler olarak gerçekleşen amonyak adsorpsiyonunun enerjisi -25.44 kcal/mol olarak bulunmuştur.

Adsorplanmış moleküllerin optimize edilmiş geometrilerinin vibrasyon frekans değerleri de hesaplanmıştır. Son olarak, adsorpsiyon enerji ve vibrasyon frekans değerlerinin literatürde belirtilen değerlerle kıyaslanabilir olduğu bulunmuştur.

ANAHTAR SÖZCÜKLER: DFT; ONIOM; periyodik DFT; rutil; su adsorpsiyonu; anataz; su ve amonyak adsorpsiyonları.

To my mother Filiz Erdoğan

ACKNOWLEDGEMENTS

I wish to express my sincere thanks to my supervisor Prof. Dr. Işık Önal for his guidance and interest throughout this study.

I would like to thank my colleague Dr. M. Ferdi Fellah for his helps, suggestions, solutions to my problems, and conveying his invaluable experiences to me. I wish also thank my colleague Oluş Özbek for his helps and criticism in periodic DFT calculations using VASP. Thanks also to all my lab mates for their helpful and enjoyable friendships throughout this study.

I would like to thank also my dear friend Volkan Çankaya for not only editing the whole thesis with me but also his endless support and understanding.

This research was supported in part by TÜBİTAK through TR-Grid e-Infrastructure Project. TR-Grid systems are hosted by TÜBİTAK ULAKBİM and Middle East Technical University. Visit http://www.grid.org.tr for more information.

TABLE OF CONTENTS

LIST OF TABLES

TABLES

LIST OF FIGURES

FIGURES

LIST OF SYMBOLS AND ABBREVATIONS

CI 77891	: Color index number for TiO_2
E171	: E number (food additive) for TiO_2
MOSFET	: Metal oxide semiconductor field effect transistor
TPD	: Temperature programmed desorption
XPS	: X-ray photoelectron spectroscopy
HREELS	: High resolution electron energy loss spectroscopy
UHV	: Ultra high vacuum
STM	: Scanning tunneling microscope
DFT	: Density functional theory
HF	: Hartree Fock
MP2	: Møller Plesset perturbation theory 2
PW91	: Perdew Wang 1991 functional
PBE	: Perdew Burke Ernzerhof functional
FTIR	: Fourier transform infrared
MO	: Molecular orbital
SINDO1	: Semi-empirical MO
MSINDO	: Semi-empirical molecular orbital
MSINDO-CCM	: Semi-empirical molecular orbital method-cyclic cluster model
CPU	: Central processing unit
MM	: Molecular mechanics
ONIOM	: Our own n-layered integrated molecular orbital and molecular mechanics
SM	: Small model
IM	: Intermediate model
R	: Real

B3LYP	: Becke's three-parameter hybrid method involving the Lee et al. correlation functional formalism
QST3	: Synchronous quasi-Newtonian method of optimization
XRD	: X-ray diffraction
BET	: Brunauer et al. 1938
VASP	: Vienna ab initio simulation package
PAW	: Projector augmented-wave
GGA	: Generalized gradient approximation
LDA	: Local density approximation
LCAO	: Linear combination of atomic orbital
RPBE	: Revised Perdew Burke Ernzerhof functional

CHAPTER 1

INTRODUCTION

TITANIUM DIOXIDE (TiO_2, also known as titanium (IV) oxide or titania), is the naturally occurring oxide of titanium. When TiO_2 is used as a pigment, it is called titanium white, Pigment White 6, or CI 77891, and it was given E number E171 for its applications, from paint to sunscreen to food coloring (Figure 1.1)

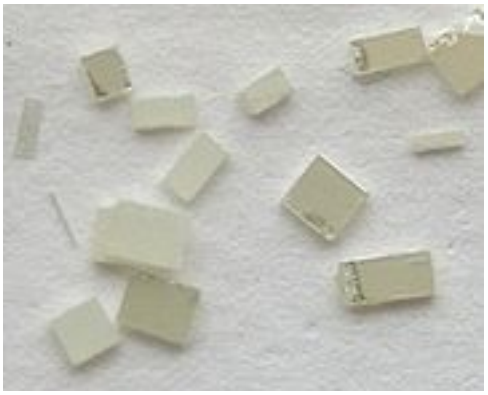

Figure 1.1 TiO_2 crystals (titanium white).

Titanium dioxide is presently produced at a rate over 4 million tones per year; half of the annual global production of titanium dioxide is used in paint or coating, a quarter in plastic such as carrier bags and refrigerator doors, and most of the rest in paper, synthetic fibers, and ceramics [1]. It is also used in a wide range of smaller applications such as catalyst support and photocatalyst.

In order to manufacture TiO_2 a source of titanium (Ti) is required. Titanium is never found in the pure state; rather, it occurs as an oxide, in the minerals ilmenite ($FeTiO_3$), rutile (TiO_2) or sphene ($CaO–TiO_2–SiO_2$). The first titanium ore, ilmenite (black sand), was discovered by Reverend William Gregor in 1789 [2].

Gregor's analysis of the ilmenite is illustrated in Table 1.1. Although most industrially produced TiO_2 is in rutile form, the rutile ore extracted from the ground is too impure to be used directly as a pigment, and must be processed just like the other ores.

Table 1.1 Gregor's analysis of the ilmenite.

Component	Percent %
Iron oxide	51.00
Titanium oxide	45.25
Silica	3.50
Manganese oxide	0.25

Data from [2].

The first step in the manufacture of TiO_2 pigment is to purify the ore, which is a refinement step, by either sulfate process or chloride process [3]. In the sulfate process, the titania value from the ore is extracted by using sulfuric acid, and a solution of titanium, iron, and other metal sulfates is obtained. Through a series of steps including chemical reduction, purification, precipitation, washing, and calcination, pigment-sized TiO_2 is produced. On the other hand, most of the titanium dioxide in the world is produced by the chloride process. It is a more technical process, which centers on the gas-phase oxidation of titanium tetrachloride ($TiCl_4$).

Once refined and developed to the appropriate particle size, the second step is finishing which is the surface treatment with inorganic oxides and an organic compound to achieve better technical performance. The production procedure of TiO_2 pigments is completed with drying, milling, and packing steps [3].

Titanium dioxide (industrially produced rutile and anatase pigments) is the brightest, whitest pigment available. These unique properties are derived from the refractive index of titanium dioxide. The refractive index expresses the ability to bend and scatter light. Titanium dioxide has the highest refractive index of any material known (2.95 for rutile, 2.55 for anatase). It is also chemically inert,

insoluble in polymers, and heat stable under harshest processing conditions. It has also high band gap energy (3.0 eV for rutile, 3.2 eV for anatase) [4].

Due to mixed ionic and covalent bonding in metal oxide systems, the surface structure has a strong influence on local surface chemistry [5]. The bulk properties of TiO_2 (rutile) can be seen in Table 1.2.

Table 1.2 Bulk properties of TiO_2 (rutile).

	Atomic radius (nm)
O (covalent)	0.066
Ti (metallic)	0.146
	Ionic radius (nm)
O (-2)	0.140
Ti (+4)	0.064

Data from [5].

The surface of TiO_2 is saturated by coordinatively bonded water, which then forms hydroxyl ions. Depending on the type of bonding of the hydroxyl groups, TiO_2 shows acidic or basic character. The surface of TiO_2 is thus always polar. The presence of hydroxyl groups makes photochemically induced reactions possible, e.g., the decomposition of water into hydrogen and oxygen and nitrogen into ammonia and hydrazine (N_2H_4) [6].

Five polymorphs (crystalline forms) of TiO_2 exist: anatase and brookite, which are low-temperature, low-pressure forms; TiO_2-II and TiO_2-III, which are formed from anatase or brookite under pressure; and rutile, the stable phase at all temperature and ambient pressure [6].

The polymorphic transformations anatase to rutile and brookite to rutile do not occur reversibly. This fact and heat of transformation data show that anatase and brookite are not stable at any temperature. Similarly, the transformations of anatase and brookite to the high-pressure forms, TiO_2-II and TiO_2-III, occur irreversibly. The transformations of anatase → rutile, anatase → TiO_2-II, and TiO_2-II → rutile in a nonequilibrium temperature-pressure diagram is shown in

Figure 1.2. The transformations of brookite → rutile, brookite → TiO_2-II, and TiO_2-II → rutile in a nonequilibrium temperature-pressure diagram can be seen in Figure 1.3 [7].

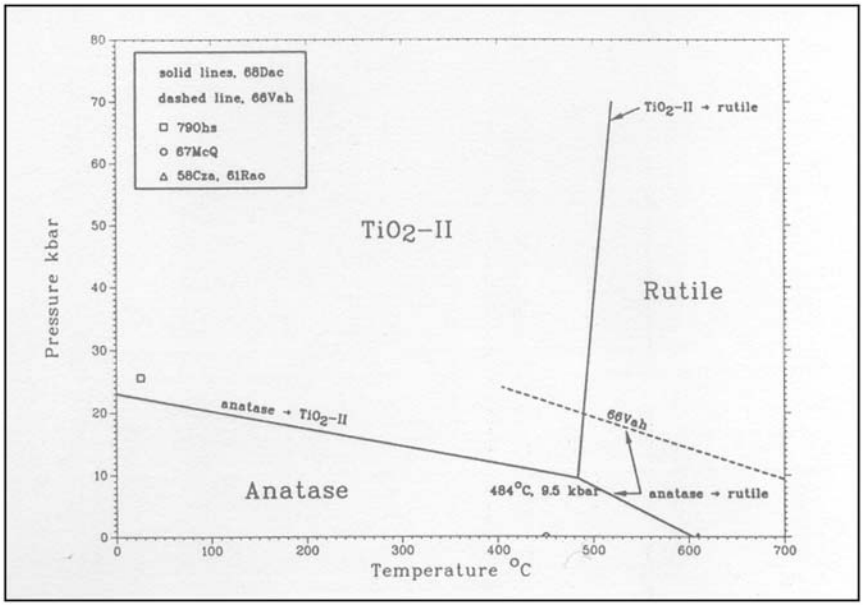

Figure 1.2 Observed conditions for persistence or induced transformation of unstable anatase [7].

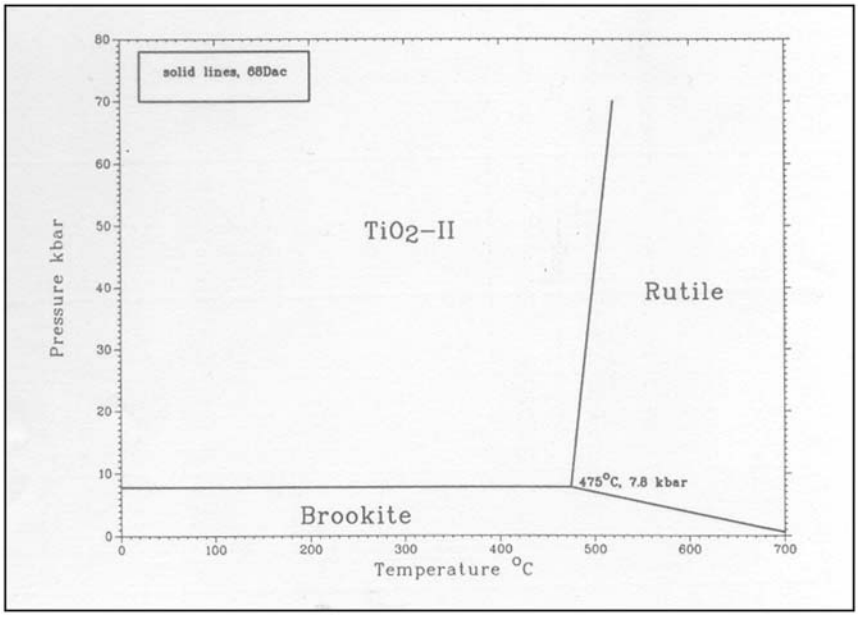

Figure 1.3 Observed conditions for persistence or induced transformation of unstable brookite [7].

The diagrams in Figures 1.2 and 1.3 indicate conditions for which the rate of transformation in the appropriate direction is appreciable. Of the high-pressure phases, TiO_2-II is formed more easily and the only one that can be retained during quenching. The transformation of anatase → rutile occurs infinitely slowly at 610 ˚C. Transformation of rutile to TiO_2-II occurs at pressures above 7 GPa and temperatures above 700 ˚C. The transformation of TiO_2-II to TiO_2-III occurs at about 20 to 30 GPa [7].

Among the crystalline forms of titania, rutile and anatase have given importance since they play any role in the applications of TiO_2. Their unit cells are shown in Figure 1.4.

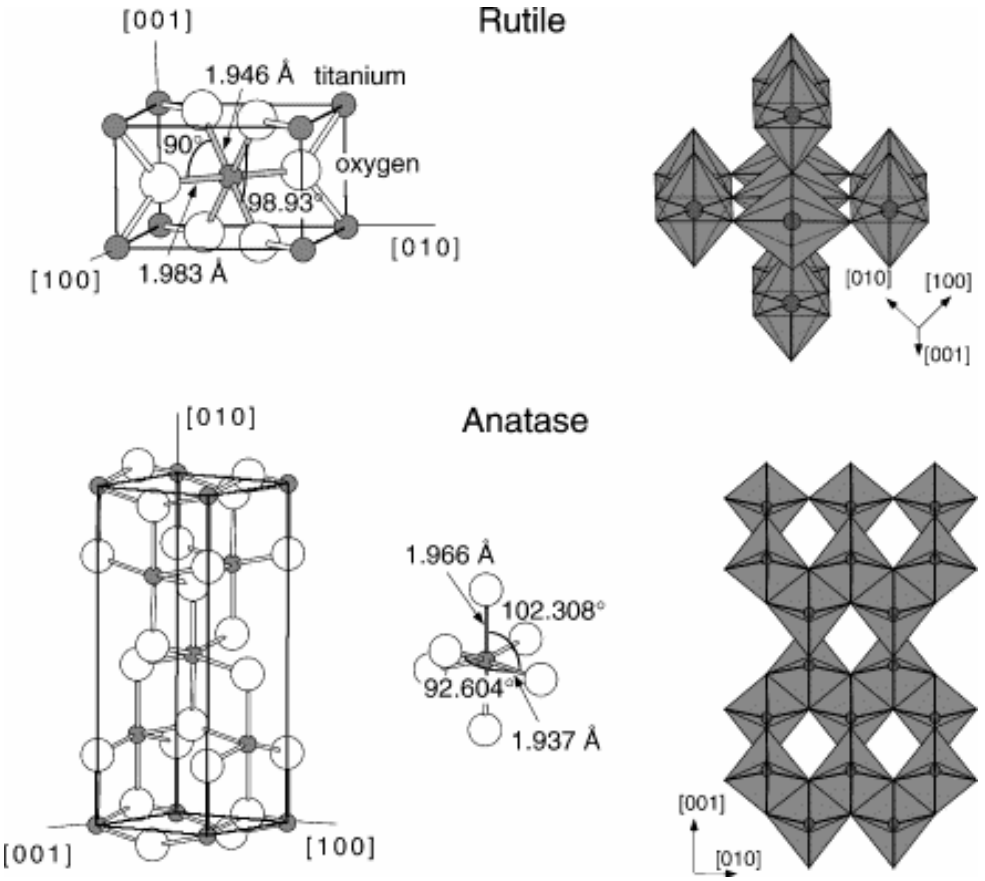

Figure 1.4 Bulk structures of rutile and anatase. The tetragonal bulk unit cell of rutile has the dimensions, a=b=4.587 Å, c=2.953 Å, and the one of anatase a=b=3.782 Å, c=9.502 Å [4].

In both rutile and anatase phases, the basic building block consists of a titanium atom in the lattice surrounded octahedrally by six oxygen atoms and each oxygen atom surrounded by three titanium atoms in trigonal arrangement.

Rutile, which is the most thermodynamically stable one, has the highest density and the most compact atomic structure [6]. Many surface science studies focused on single crystal rutile TiO_2 (110) surface, because of its thermodynamic stability and relatively easy preparation as a model surface [4]. Ramamoorthy and Vanderbilt [8] calculated the total energy of periodic TiO_2 slabs using a self-consistent ab-initio method and they found that the (110) surface has the lowest surface energy, and the (001) surface has the highest. From the calculated energies, they constructed a three-dimensional Wulff plot, which gives the equilibrium crystal shape of a macroscopic crystal, is shown in Figure 1.5.

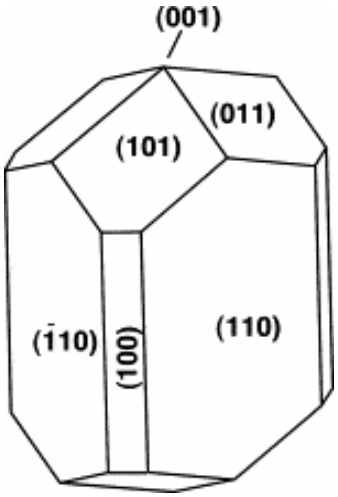

Figure 1.5 The equilibrium shape of a macroscopic TiO_2-rutile crystal using the Wulff construction [8].

Most commercial titania powder catalysts are a mixture of rutile and anatase (e.g., the most often used Degussa P25 contains approx. 80–90% anatase and the rest rutile [9]). Such mixtures work best for certain photocatalytic reactions and non-photo induced catalysis [10].

There is growing evidence that anatase is more active than rutile, especially in catalysis, anatase phase of titanium dioxide is used much more often as a support or a catalyst by itself [4,11,12].

TiO_2-anatase nanoparticles have predominantly (101) and (100)/(010) majority surfaces, together with minority (001) surface [13]. However, many studies concerning the structure and reactivity of different anatase surfaces suggest that the minority (001) surface is more reactive and plays a key role in the reactivity of anatase nanoparticles [13-16]. The calculated Wulff shape of an anatase crystal and the shape of naturally grown mineral samples can be seen in Figure 1.6.

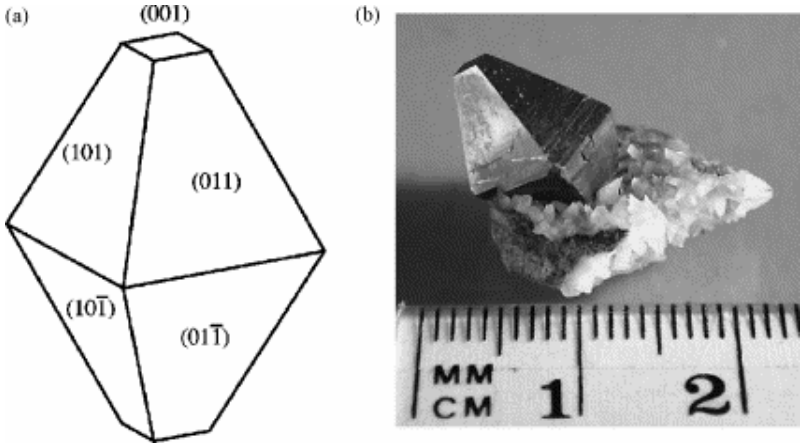

Figure 1.6 (a) The equilibrium shape of a TiO_2-anatase crystal according to the Wulff construction [17]. **(b)** Picture of an anatase mineral crystal.

TiO_2 has wide range of technological applications. It is used in heterogeneous catalysis (metal/TiO_2 systems) [9,18], as a photocatalyst, in solar cells for the production of hydrogen and electric energy [19], as a gas sensor [20], as a white pigment (e.g. in paint, food, and cosmetic products) [21,22,23], as a corrosion-protective coating [24], as an optical coating [25], in ceramics, and in electric devices such as varistors [26]. It is used also in toxic material conversion [27,28] and bone implants [29], air purifying, and self-cleaning window [30] applications. It is utilized as a gate insulator for the new generation of MOSFETS (metal oxide semiconductor field effect transistor) [31], as a spacer material in magnetic spin-valve systems [32,33], and finds applications in nanostructured form in Li-based batteries and electrochromic devices [34].

One good reason for pursuing research on single-crystalline TiO_2 surfaces is that it is a model system in surface science studies of metal oxides. The thermodynamically stable rutile (110) surface certainly falls into this category. Furthermore, TiO_2 is a preferred system for experimentalists because it is well suited for many experimental techniques. A second reason for studying TiO_2 surfaces is the wide range of its applications in many fields including catalysis.

Water commands a fundamental interest as an adsorbate on TiO_2 surfaces. To illustrate, many of the applications, almost all photocatalytic processes, are performed in an aqueous environment. In addition, TiO_2 exposed to air will always be covered by a water film and the presence of water can affect adsorption and reaction processes. The adsorption of water on TiO_2 have been extensively reported both in experimental and theoretical literature. Therefore, in this study, H_2O adsorption on rutile and anatase TiO_2 surfaces is studied to check the reliability of the methodology used. In other words, this is a validation test for future calculations on ammonia adsorption. NH_3 adsorption on anatase TiO_2 can be important for industrial catalytic reactions such as selective catalytic reduction (SCR) of NO and photo-oxidation of NH_3 over TiO_2. There are very few experimental studies and theoretical calculations concerning adsorption of ammonia on anatase TiO_2. Moreover, for H_2O and NH_3 adsorptions on anatase TiO_2 surface, theoretical ONIOM and periodic DFT methods are intended to be compared. It is known that periodic DFT methods involve heavy computations but they are also more accurate methods.

The aim of this thesis is to theoretically investigate adsorption mechanisms of H_2O and NH_3 molecules on different titania surfaces by using quantum chemical calculations. More precisely, water adsorption on rutile TiO_2 (110) surface is studied by ONIOM method, water adsorption on anatase TiO_2 (001) surface is studied and compared by both ONIOM and periodic DFT methods, and finally ammonia adsorption on anatase TiO_2 (001) surface is studied and compared by both ONIOM and periodic DFT methods.

CHAPTER 2

LITERATURE SURVEY

2.1 Water Adsorption on Rutile TiO_2 (110) Surface

2.1.1 Experimental Studies

There are some experimental studies with regard to the surface properties and adsorption mechanisms of water on rutile TiO_2 (110) surface. Using synchrotron radiation and photoemission spectroscopy Kurtz et al. [35] reported that water molecules adsorbed on the perfect (stoichiometric) rutile (110) surface molecularly or dissociatively depending on temperature.

Hugenshmith et al. [36] studied interaction of H_2O with rutile TiO_2 (110) surface by TPD (temperature programmed desorption), XPS (x-ray photoelectron spectroscopy) and work function measurements. They reported that water is mainly molecularly adsorbed and not dissociated on this surface.

Henderson et al. [37] reached the same results as Hugenshmith et al. by performing HREELS (high resolution electron energy loss spectroscopy) and TPD studies. Henderson et al. [37] reported that water adsorbed on rutile TiO_2 (110) surface predominately in a molecular state with exothermic adsorption energy of 17-19 kcal/mol, little or no water dissociates on ideal TiO_2 (110) surface under UHV (ultra high vacuum) conditions; but that dissociation may be linked to structural and/or point defects.

Brinkley et al. [38] investigated the adsorption properties of water on rutile TiO_2 (110) surface using modulated molecular beam scattering and TPD studies. They

detected that very few of the molecules dissociate, even in the limit of zero coverage and they found molecularly adsorbed H_2O with -(17–24) kcal/mol which is also in agreement with TPD studies reported in [36,37].

Recent STM (scanning tunneling microscope) studies, most notably the ones published by Brookes et al. [39] and Schaub et al. [40] support the earlier experimental results that dissociative adsorption occurs at defects or at oxygen vacancies as active sites for water dissociation. Molecular adsorption is more favorable than dissociation on the defect-free surface.

2.1.2 Theoretical Studies

There are many theoretical studies about adsorption reactions and surface properties on rutile TiO_2 (110). Unlike the experimental results, Goniakowski et al. [41] found that dissociative adsorption of water molecule is thermodynamically more stable than molecular adsorption with 6 kcal/mol lower in adsorption energy.

Lindan et al. [42] also indicated that dissociation of the water molecule is thermodynamically favored on low coverages but both molecular and dissociative adsorption were confirmed at high coverages on rutile TiO_2 (110) surface by use of both DFT (density functional theory) and HF (Hartree-Fock) methods.

Casarin et al. [43] and Stefanovich et al. [44] predicted that molecular water adsorption is more favorable than dissociative chemisorption as shown in recent experimental studies. Casarin et al. [43] studied molecular adsorption of water on rutile TiO_2 (110) surface by use of DFT calculations and obtained -19.3 kcal/mol molecular adsorption energy that in good agreement with experimental data.

Stefanovich et al. [44] have studied adsorption of a single water molecule in both molecular and dissociative geometries by using HF, MP2 (Møller–Plesset perturbation theory 2), and DFT/B3LYP methods. They concluded that isolated

water molecule adsorbs on the rutile TiO_2 (110) surface in the molecular form and adsorption energy was estimated to be about -30 kcal/mol.

Menetrey et al. [45] performed periodic DFT calculations to study the effect of oxygen vacancies. They found that the reactivity at reduced surface differs from that on the stoichiometric perfect surfaces. For the water molecule, the dissociative adsorption energy (-31.6 kcal/mol) is lower than on the perfect surface (-29.3 kcal/mol).

Most recent plane wave (PW:DFT-GGA-PW91) calculations performed by Bandura et al. [46] pointed out that adsorption energy values for molecular and dissociative adsorption of water molecule on rutile TiO_2 (110) surface are -21.9 kcal/mol and -18.4 kcal/mol, respectively. They also employed ab-initio (LCAO:HF LANL1-CEP) calculations on the same surface and reported that molecular and dissociative adsorption energies of water are -22.5 kcal/mol and -11.5 kcal/mol, respectively.

Wendt et al. [47] studied water adsorption on stoichiometric and reduced rutile TiO_2 (110) surfaces. Their results obtained using DFT calculations indicate that on stoichiometric surface, the molecular and dissociative adsorption of water are exothermic by 15.22 kcal/mol and 18.22 kcal/mol, respectively. In their other study [48], they reported a high activation barrier (27 kcal/mol) for the diffusion dissociation reaction of water by applications of periodic slab calculations.

Lindan and Zhang [49] studied water dissociation on rutile TiO_2 (110) surface by using periodic slab calculations. They reported that molecular and dissociative adsorption energy and activation barrier values for water are -11.8 kcal/mol, -6.5 kcal/mol and 5.8 kcal/mol at 1 ML (monolayer) water coverage, respectively. In their study, they also pointed out that, the barrier increases with decreasing coverage.

Perron et al. [50] performed periodic DFT calculations to investigate water adsorption process to determine whether molecular and/or dissociative adsorptions take place. It was determined that molecular adsorption of water is

energetically favorable but dissociative one can also be envisaged because it could be stabilized with hydrogen bonding.

Kamisaka et al. [51] studied the surface stresses and adsorption energies of clean and water-adsorbed (110) and (100) surfaces of rutile. Two forms of water, molecularly and dissociatively adsorbed water, and water adsorbed at surface oxygen vacancies, were studied. In all cases, the effect of functionals was discussed by using the PW91 (Perdew Wang 1991) and PBE (Perdew Burke Ernzerhof) functionals provided in VASP software. In their calculations, the H_2O (molecular) adsorbate had a larger adsorption energy than that of the H_2O (dissociative) adsorbate by 5.8 kcal/mol with either functional. However, they reported that these values should not be regarded as evidence of a preferred molecular form since convergence properties and effect of functionals should be considered.

2.2 Water and Ammonia Adsorption on Anatase TiO_2 (001) Surface

2.2.1 Experimental Studies

There are some experimental studies with regard to the surface properties and adsorption reactions of water and ammonia on TiO_2-anatase surfaces. Srnak et al. [52] reported that they observed two states of water desorption from anatase titania and estimated desorption activation energies of adsorbed states as -11 kcal/mol and -18 kcal/mol from vacuum TPD studies.

In the study of Munuera et al. [53] a heat of desorption value for water adsorption on TiO_2-anatase was reported as -12 kcal/mol.

For the case of ammonia, using combined temperature-programmed in situ FTIR (Fourier transform infrared) and on-line mass spectrometric studies, Topsøe et al. [54,55] indicated that ammonia adsorption on pure titania surface occurs predominantly on Lewis acid sites.

Ramis and Busca et al. [56-58] reported that ammonia is activated by coordination over Lewis acid sites on TiO_2-anatase and this activated ammonia is easily transformed to amide NH_2 species by the abstraction of hydrogen.

Srnak et al. [52] reported that they observed two states of ammonia desorption from titania, as in the case of water and their estimated desorption activation energy of strongly adsorbed state is -27 kcal/mol.

Sprinceana et al. [59] carried out a calorimetric study of the acidity and interface effects of tin dioxide layers deposited on another metal oxide and reported a differential heat of -31 to -36 kcal/mol for ammonia adsorption on anatase titania.

2.2.2 Theoretical Studies

There are many theoretical studies about water adsorption reactions and surface properties on anatase TiO_2 (001). Fahmi and Minot [60] investigated water adsorption on TiO_2-anatase surfaces by using periodic Hartree-Fock method and they reported that water adsorbs on acidic site (fivefold coordinated titanium atom) and afterwards it dissociates to give hydroxyl groups.

Bredow and Jug [61] studied molecular and dissociative adsorption of water on rutile (110) and anatase (001) surfaces simulated with model clusters by means of a semi-empirical molecular orbital method called SINDO1. They reported that dissociative adsorption is energetically favored on both surfaces.

In their other study, Jug et al. [62] investigated water adsorption on various TiO_2-anatase surfaces by means of a semi-empirical molecular orbital method called MSINDO. They reported molecular and dissociative water adsorption energies on anatase TiO_2 (001) as -23.9 and -49.7 kcal/mol, respectively and according to their results, dissociative adsorption of water is thermodynamically more favorable than molecular one.

Vittadini et al. [13] investigated structure and energetics of water adsorption on TiO_2-anatase (101) and (001) surfaces at various coverages by use of DFT calculations and they reported that on the (001) surface, for θ=0.5, H_2O is adsorbed dissociatively, with an adsorption energy of -33.2 kcal/mol. At θ=1, H_2O can be adsorbed molecularly (-18.9 kcal/mol), but a state with half of the H_2O adsorbed dissociatively and the other half H bonded in a "second layer" is energetically more favorable.

Kachurovskaya et al. [63] reported a molecular adsorption energy value of -13.6 kcal/mol for water adsorption on TiO_2-anatase (001) surface and did not study any dissociation case.

Nair [64] investigated water adsorption on anatase by means of MSINDO-CCM (semi-empirical molecular orbital method-cyclic cluster model) calculations and they reported that dissociative adsorption of water is thermodynamically more favorable than molecular one on anatase (001) surface with the adsorption energy values of -32.98 and -18.64 kcal/mol, respectively.

Arrouvel et al. [65] investigated surface hydroxylation states for anatase-TiO_2 by density functional simulations and thermodynamic analysis. Their results concerning the (001) surface showed that water is mainly dissociated and adsorption energy varies strongly with increasing coverage from -39.44 to -24.14 kcal/mol.

In agreement with previous theoretical studies, Gong and Selloni [66] found that dissociative adsorption is favored, with average adsorption energies of -28.8, -25.6, and -27 eV per H_2O at 1/6, 1/3, and 1/2 ML coverages, respectively, by use of PW:DFT-GGA and Car-Parrinello methods.

Barnard et al. [67] studied TiO_2 nanoparticles in water by means of DFT calculations, and they reported energy values of molecular and dissociative water adsorption on anatase TiO_2 (001) surface as -5.3 and -10.4 kcal/mol, respectively.

Ignatchenko et al. [68] studied interaction of water with anatase form of titania by means of isotopic exchange of water and periodic DFT calculations. Their experimental data support computational results showing that interaction of water with anatase (001) surface proceeds through insertion into a Ti-O bond.

Wahab et al. [69] studied adsorption of water molecule onto (100), (010), and (001) surfaces of nano-sized anatase TiO_2 with semi-empirical MSINDO method, and they reported molecular and dissociative water adsorption energy values on anatase TiO_2 (001) as -17.7 and -24.6 kcal/mol, respectively. Their results were in agreement with other computational studies and they stated that dissociated form of water molecule adsorption on anatase TiO_2 surfaces is always more stabilized than the molecular one.

In our research group, Onal et al. [70] have performed a cluster study with regard to water and ammonia adsorption on anatase TiO_2 (101) and (001) surfaces. In the study of Onal et al. [70] on relaxed (001) cluster, it was reported that non-activated dissociation of water takes place with an exothermic relative energy difference of 54.12 kcal/mol that is calculated via DFT-B3LYP/6-31G** method in SPARTAN 04 program package.

There are few theoretical studies [70,71], one of which is our own research group's study [70], concerning ammonia adsorption on (001) anatase TiO_2. In the study of Onal et al. [70] it was reported that on fixed cluster anatase TiO_2 (001) surface, ammonia dissociation turns out to be an energetically unfavorable process, while on relaxed cluster surface dissociation occurs with a slight activation barrier of 3.63 kcal/mol and an adsorption energy value of -36.32 kcal/mol.

Calatayud et al. [71] studied ammonia adsorption on anatase TiO_2 (001) surface and determined molecular adsorption energy value as -19.4 kcal/mol by using periodic calculations, however; they did not study or could not find a dissociation case.

CHAPTER 3

METHODOLOGY

3.1 Overview of Computational Quantum Chemistry

The term theoretical chemistry may be defined as a mathematical description of chemistry, whereas computational chemistry is a branch of chemistry that uses computers to assist in solving chemical problems. Computational quantum chemistry uses the results of theoretical chemistry, incorporated into efficient computer programs, to calculate the structures and properties of molecules and solids. Examples of such properties are structure (i.e. the expected positions of the constituent atoms), absolute and relative (interaction) energies, electronic charge distributions, dipoles and higher multipole moments, vibrational frequencies, reactivity or other spectroscopic quantities, and cross sections for collision with other particles [72].

A wide variety of different procedures or models have been developed to calculate the molecular structure and energetics. These have generally been broken down into two categories, quantum chemical models and molecular mechanics models.

Quantum chemical models, explained in Appendix section in detail, all ultimately stem from the Schrödinger equation. It treats molecules as collections of nuclei and electrons without any reference whatsoever to chemical bonds. One drawback of Schrödinger equation is that it cannot be solved for exactly for multi-electron systems, and approximations need to be made. Quantum chemical models differ in the nature of these approximations, and span a wide range, both in terms of their capability, reliability, and their computational cost [73]. For an overall view,

quantum chemical models can be mainly classified as ab-initio models, density functional models, and semi-empirical models. Ab-initio models are derived directly from theoretical principles with no inclusion of experimental data and the simplest type of Ab-initio models is Hartree-Fock (HF) model. Density functional theory (DFT) models are often considered to be ab-initio models for determining the molecular electronic structure, even though many of the most common functionals use parameters derived from empirical data, or from more complex calculations. In DFT, total energy is expressed in terms of the total one-electron density rather than the wave function. Semi-empirical quantum chemistry models are based on the Hartree-Fock formalism, but use many approximations and obtain some parameters from empirical data [72].

Molecular mechanics (MM) models, alternative to quantum chemical models, do not start from an exact-theory (the Schrödinger equation), but rather from a simple but chemically reasonable picture of molecular structure. In this picture, molecules are made up of atoms and bonds (as opposed to nuclei and electrons) and atom positions are adjusted to best match known structural data (bond lengths and angles) as well as to accommodate non-bonded interactions [73].

Taking both quality of results (accuracy) and computational cost into account some comparison can be made among theoretical models, but it is not possible to say exactly which model is the best for a particular application.

However, in general, molecular mechanics allows the modeling of enormous molecules, such as proteins and segments of DNA. It also models intermolecular forces well. The disadvantage of molecular mechanics is that there are many chemical properties that are not even defined within the method, such as electronic excited states. Molecular mechanics models are easy, but not necessarily good, way to describe a system [72].

Ab-initio calculations give very good qualitative results and can yield increasingly accurate quantitative results as the molecules in question become smaller. The disadvantages of ab-initio methods are that they are expensive and

take enormous amounts of computer CPU (central processing unit) time, memory, and disk space [72].

Semi-empirical models can provide results accurate enough to be useful, where there are only a few elements used extensively and the molecules are of moderate size. They are much faster than ab-initio calculations but the results can be erratic and fewer properties can be predicted reliably. If the molecule being computed is significantly different from anything in the parameterization set, the answers may be very poor. However, semi-empirical methods are not as sensitive to the parameterization set as are molecular mechanics calculations [72].

Density functional theory (DFT) has become very popular in recent years. This is justified based on the pragmatic observation that DFT is less computationally intensive than other methods with similar accuracy. DFT's recent heavy usage has been due to optimal accuracy versus CPU time. The B3LYP method with basis sets of 6-31G* or larger is the method of choice for many molecule calculations [72].

A comparison between accuracy and computational cost of theoretical models are illustrated in Figure 3.1. As can be seen from this figure selecting the method to use for a computational study usually involves finding an effective tradeoff between accuracy and computational cost. Unfortunately, high accuracy models scale unfavorably with the size of the molecule, resulting in a practical limit on how large a system can be studied. However, hybrid methods, e.g. ONIOM method, provide a means for overcoming these limitations by allowing the combination of two or more computational techniques in one calculation and make it possible to investigate the chemistry of very large systems with high precision.

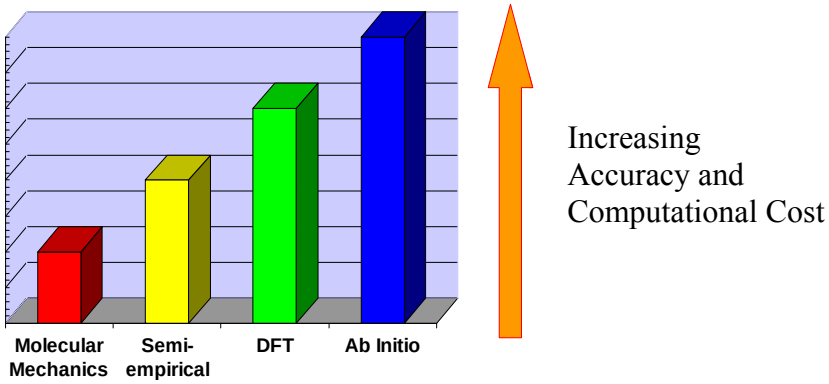

Figure 3.1 A comparison of the computational quantum chemistry models in terms of accuracy and computational cost.

3.2 ONIOM Method

In hybrid methods the region of the system where the chemical process takes place, for example bond breaking or bond formation, is treated with an appropriately accurate method, while the remainder of the system is treated at a lower level. For example, MO/MM class of hybrid methods use a molecular orbital (MO) method, which is a high level of theory ab-initio method, for the interesting or difficult portion of the system, and use a molecular mechanics (MM) method, computationally less demanding one, for the rest of the system. Alternatively, QM/MM methods are the most common class of hybrid methods, which combine a quantum mechanical (QM) method with a molecular mechanics (MM) method. The ONIOM method is a more general in the sense that it can combine any number of molecular orbital methods as well as molecular mechanics methods [74].

ONIOM stands for our own n-layered integrated molecular orbital and molecular mechanics. This computational technique that is originally developed by Morokuma et al. [75], can be used to theoretically compute energies, perform geometry optimizations, and predict vibrational frequencies and electric and magnetic properties of large systems.

The ONIOM method is applicable to large molecules in many areas of research, including enzyme reactions, reaction mechanisms for organic systems, photo-chemical processes of organic species, substituent effects and reactivity of organic and organometallic compounds, homogeneous catalysis and cluster models of surfaces and surface reactions, which are also the two research areas of this thesis study.

By explaining in depth, in an ONIOM calculation, the molecular system under investigation is divided into 2 or 3 regions, typically called layers, which are modeled using successively more accurate model chemistries [76]:

• The High Layer is the smallest region where the bond formation and breaking take place, and it is treated with the most accurate method, e.g. quantum mechanics models. This layer is also called the Small Model (SM) System. In a 2-layer ONIOM calculation, it is often simply called the Model System.

• The Low Layer consists of the entire molecule in a 2-layer ONIOM model. The calculation on this region corresponds to the environmental effects of the molecular environment on the site of interest (i.e., the high layer). The low layer is typically treated with an inexpensive model chemistry: a molecular mechanics method, a semi-empirical method, or an inexpensive ab-initio method such a Hartree-Fock with a modest basis set.

• In a 3-layer ONIOM model, a Middle Layer is defined, and it is treated with a method that is intermediate in accuracy between the high level method and the low level method. This layer consists of a larger subset of the entire molecule than the higher layer. It models the electronic effects of the molecular environment on the high layer. The combination of this layer along with the low layer is referred to as the Intermediate Model (IM) System. The entire molecule is referred by the Real (R) System.

The ONIOM method works by approximating the energy of the Real (R) System as a combination of the energies computed by less computationally expensive means. Specifically, the energy is computed as the energy of the Small Model

(SM) with corrections for the size difference between SM and R and for the method accuracy difference between the low level model chemistry and the high accuracy method used for SM (denoted low and high in the following equation) [76]:

$$E^{high}(R) \approx E^{low}(SM) + \{E^{low}(R) - E^{low}(SM)\} + \{E^{high}(SM) - E^{low}(SM)\} \qquad (3.1)$$

Size (SM → R) Level of Theory (*low* → *high*)

The preceding equation reduces to:

$$E^{ONIOM} = E^{low}(R) - E^{high}(SM) - E^{low}(SM) \qquad (3.2)$$

More specifically, in a 2-layer ONIOM (QM:MM) calculation, the equation (3.2) refers to:

$$E^{ONIOM} = E^{MM,\ real} - E^{QM,\ model} - E^{MM,\ model} \qquad (3.3)$$

The real system contains all the atoms and is calculated only at the MM level. The model system contains the part of the system that is treated at the QM level. Both QM and MM calculations need to be carried out for the model system [74].

Although the main concepts are similar, the ONIOM methods differ mainly in two aspects. One major distinction is in the treatment of covalent interaction between the two regions (boundary region). The covalent bonds have to be cut in order to generate model system. This process leaves dangling bonds at the border of the inner layer, which have to be saturated to avoid a chemically unrealistic model. The simplest approach is to use link atoms [77,78], which are usually hydrogen atoms. They are only present in the model system and their treatment differs in the different implementations. The following figure illustrates link atoms, using ethane as an example:

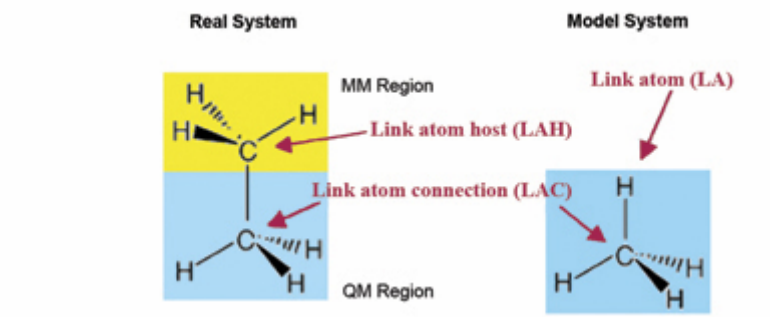

Figure 3.2 ONIOM terminology for link atoms using ethane [76].

The main alternative to link atoms is the use of frozen orbitals, which can be done through parameterization and use of *p* and *d* orbitals, describe a more accurate charge density than link atoms [79,80-82]. However, due to the required parameterization of the frozen orbitals, they lack the flexibility and generality of link atoms. Besides frozen orbitals and link atoms, pseudo potentials are also used to handle the covalent interactions between two regions [83,84].

The second main difference in all hybrid methods is the way the electrostatic interaction between the two regions is treated [85]. In its simplest form, the interaction between the QM and MM region is completely described by MM style terms. This includes the electrostatic interaction, which is then evaluated as the interaction of the MM partial charges with partial (point) charges assigned to the atoms in the QM region. This approach is usually referred to as *classical* or *mechanical embedding*. In the second approach, the charge distribution of the MM region interacts with the actual charge distribution of the QM region. This technique incorporates the partial charges of the MM region into the quantum mechanical Hamiltonian, thereby providing a better description of the electrostatic interaction between the QM and MM regions and allows the QM wave function to be polarized. This approach is referred to as *electronic embedding* [74].

In Gaussian 03, MO:MM ONIOM calculations can optionally take advantage of electronic embedding within ONIOM calculations. ONIOM geometry optimizations can also optionally use a quadratic coupled (QC) algorithm which takes into account the coupling between atoms using internal coordinates

(typically, those in the Small Model system) and those in Cartesian coordinates (typically, the atoms only in the MM layer) in order to produce more accurate steps. Note that optimizations in ONIOM proceed using the normal algorithms and procedures. ONIOM affects only the energy and gradient computations (ONIOM optimizations do *not* consist of independent, per-layer optimizations). The use of an integrated potential surface also enables vibrational analysis to be performed and related properties to be predicted [76].

3.3 Surface Models and Computational Methods

In this thesis work, water adsorption mechanisms on rutile (110), and water and ammonia adsorption mechanisms on anatase (001) surfaces of TiO_2 are investigated by using ONIOM cluster method. In addition, water and ammonia adsorption mechanisms on anatase TiO_2 (001) slab surface are investigated by means of periodic DFT method and the results are compared with the ones of ONIOM cluster method.

ONIOM cluster calculations are performed by application of Gaussian 03 [87] software, whereas periodic DFT calculations are carried out using VASP [95] (Vienna ab-initio simulation package) code.

3.3.1 ONIOM Cluster Method

3.3.1.1 Surface Models

The first step applied to obtain ONIOM surface models is forming the crystalline structures of bulk TiO_2 (rutile and anatase). To do this the experimental parameters of the bulk material; its space group, lattice parameters, atom positions and unit cell formula, should be known. In Table 3.1 the experimental parameters of bulk rutile TiO_2 which are obtained from Wyckoff, 1963 [86] are tabulated.

Table 3.1 Experimental parameters of TiO_2 (Rutile).

Space Group	$P4_2/mnm$
International Table No	136
Lattice Parameters	a = b = 4.59373 A c = 2.95812 A u = 0.3053 A
Atom Positions	Ti : (2a) 000; 1/2 1/2 1/2
	O : (4f) ± (uu0; u+1/2,1/2-u,1/2)

Data from [86].

The atomic parameters (X, Y, Z), called fractional coordinates, are determined by applying atom positions to each atom considering their Wyckoff positions (2a) or (4f). Table 3.2 illustrates the fractional coordinates of TiO_2 (rutile) that are evaluated by using atom positions given in Table 3.1.

Table 3.2 Atomic parameters (Fractional coordinates) of TiO_2 (Rutile).

Atom	Position	X	Y	Z
Ti	(2a)	0.00000000	0.00000000	0.00000000
Ti	(2a)	0.50000000	0.50000000	0.50000000
O	(4f)	0.30530000	0.30530000	0.00000000
O	(4f)	0.80530000	0.19470000	0.50000000
O	(4f)	-0.30530000	-0.30530000	0.00000000
O	(4f)	-0.80530000	-0.19470000	-0.50000000

The fractional coordinates are then multiplied by the respective lattice parameters to find the Cartesian coordinates. Table 3.3 shows the Cartesian coordinates of TiO_2 (rutile) which are obtained by multiplying fractional coordinates shown in Table 3.2 with the respective lattice parameters given in Table 3.1.

Table 3.3 Atomic parameters (Cartesian coordinates) of TiO_2 (Rutile).

Atom	Position	X	Y	Z
Ti	(2a)	0.00000000	0.00000000	0.00000000
Ti	(2a)	2.29686500	2.29686500	1.47906000
O	(4f)	1.40246577	1.40246577	0.00000000
O	(4f)	3.69933077	0.89439923	1.47906000
O	(4f)	-1.40246577	-1.40246577	0.00000000
O	(4f)	-3.69933077	-0.89439923	-1.47906000

The Cartesian coordinates constitute the smallest repeated unit that is called unit cell. TiO_2 has a bimolecular unit cell so its unit cell formula is Ti_2O_4. The structure of unit cell (Ti_2O_4) and the completed tetragonal cell (Ti_9O_6) are formed in Gaussian 03 and presented in Figure 3.3 (a) and (b) respectively.

(a) **(b)**

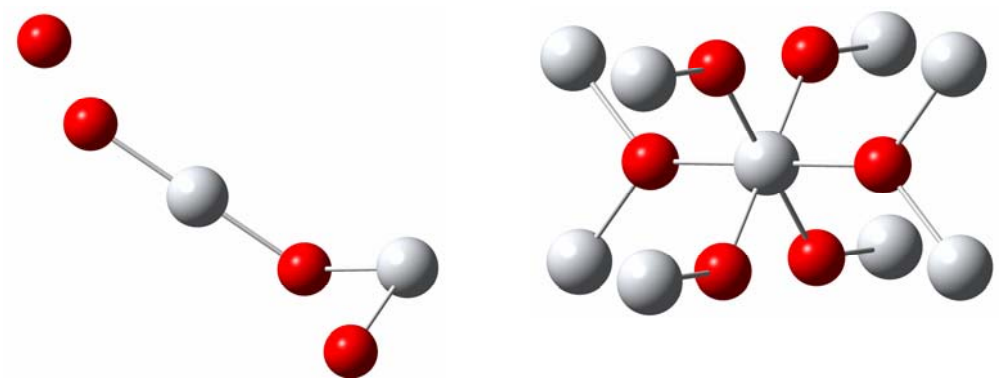

Figure 3.3 (a) TiO_2 (rutile) unit cell (Ti_2O_4). **(b)** The completed tetragonal cell (Ti_9O_6). Red balls are oxygen and gray ones are titanium atoms.

The coordinates of the rest of the crystalline structure that are the repetitions of the unit cell can be found by applying the symmetry operations to the atomic coordinates of the unit cell. Several times enlargement of the unit cell in various directions is desirable for creating a surface structure. The TiO_2 (rutile) unit cell is decided to be enlarged 3 times in each 3 directions (x, y, and z) by means of Excel and formed in Gaussian 03 (See Figure 3.4).

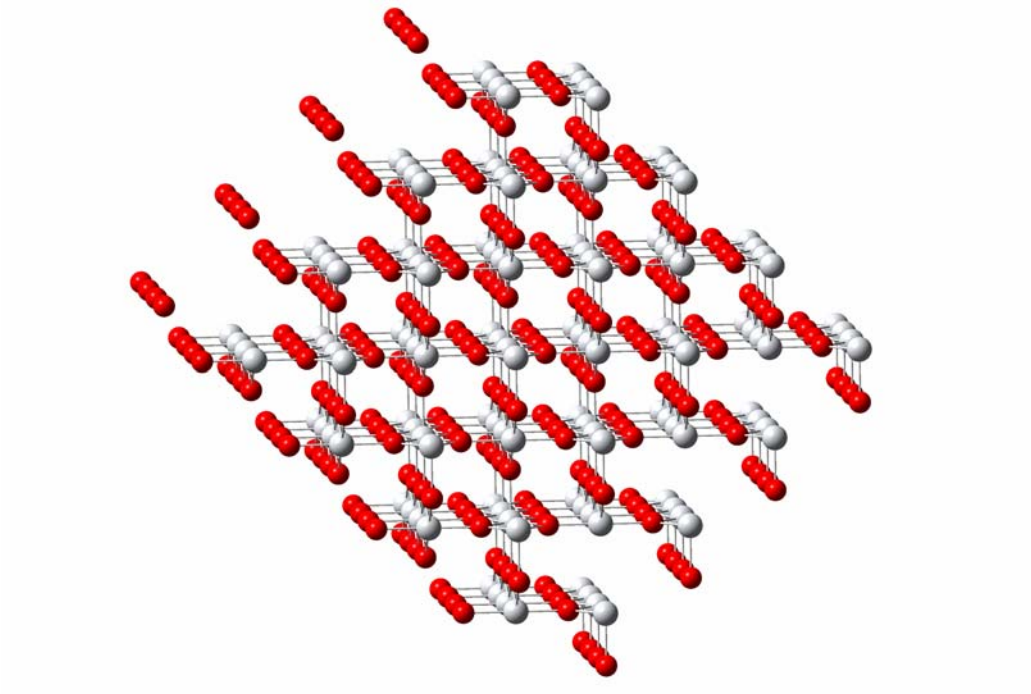

Figure 3.4 The 3-D structures of enlarged (3x-3y-3z) TiO_2 (rutile) cluster. Red balls are oxygen and gray ones are titanium atoms.

Finally, the cluster surface, which is considered to be studied, is obtained by selecting the surface and deleting undesired atoms by use of Gaussian 03. TiO_2 rutile (110) cluster surface and its ONIOM method applied version are presented in Figure 3.5 (a) and (b), respectively.

(a)

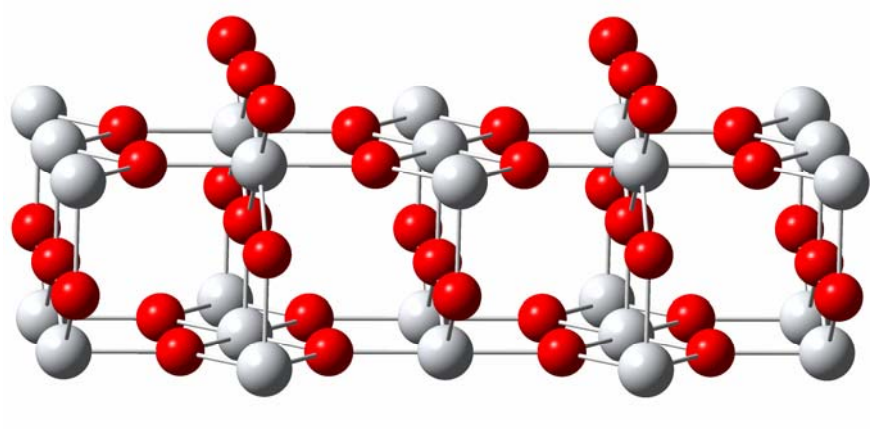

(b)

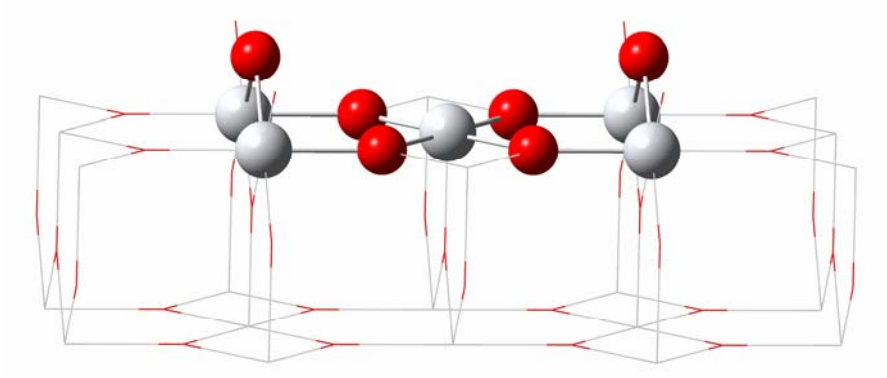

Figure 3.5 (a) TiO_2 Rutile (110) cluster surface. **(b)** ONIOM TiO_2 Rutile (110) cluster surface. [Perspective view] Red balls are oxygen and gray ones are titanium atoms. QM region is represented by ball and bond type view and MM region is represented by wireframe view.

Figure 3.5 (b) illustrates the ONIOM rutile $Ti_{25}O_{37}$ cluster that is modeled by a 2-region: (I) Quantum Mechanics (QM) region, and (II) Molecular Mechanics (MM) region. QM region is represented by ball and bond type view and MM region is represented by wireframe view in Gaussian 03. In quantum mechanics (QM) region, there are 5 Ti and 6 O atoms and in molecular mechanics (MM) region, there are 20 Ti and 31 O atoms.

The same procedure is applied to obtain ONIOM (anatase) TiO_2 (001) cluster model and explained briefly in the following statements. The experimental parameters of bulk anatase TiO_2 are obtained from Wyckoff, 1963 [86] and tabulated in Table 3.4.

Table 3.4 Experimental parameters of TiO_2 (Anatase).

Space Group	$I4_1/amd$
International Table No	141
Lattice Parameters	a = b = 3.785 A c = 9.514 A u = 0.2066 A
Atom Positions	Ti : (4a) 000; 0 ½ ¼ B.C.
	O : (8e) 00u; 00-u; 0, ½, u+¼; 0, ½, ¼-u; B.C.

Data from [86].

Table 3.5 illustrates the fractional coordinates of TiO_2 (anatase) which are determined by means of atom positions given in Table 3.4.

Table 3.5 Atomic parameters (Fractional coordinates) of TiO_2 (Anatase).

Atom	Position	X	Y	Z
Ti	(4a)	0.0000000	0.0000000	0.0000000
Ti	(4a)	0.5000000	0.5000000	0.2500000
Ti	(4a)	0.5000000	0.5000000	0.5000000
Ti	(4a)	0.5000000	1.0000000	0.7500000
O	(8e)	0.0000000	0.0000000	0.2066000
O	(8e)	0.0000000	0.0000000	-0.2066000
O	(8e)	0.0000000	0.5000000	0.4566000
O	(8e)	0.0000000	0.5000000	0.0434000
O	(8e)	0.5000000	0.5000000	0.7066000
O	(8e)	0.5000000	0.5000000	0.2934000
O	(8e)	0.5000000	1.0000000	0.9566000
O	(8e)	0.5000000	1.0000000	0.5434000

Table 3.6 illustrates the Cartesian coordinates of TiO_2 (anatase) which are evaluated by multiplying fractional coordinates of TiO_2 (anatase) shown in Table 3.5 with the respective lattice parameters given in Table 3.4.

Table 3.6 Atomic parameters (Cartesian coordinates) of TiO_2 (Anatase).

Atom	Position	X	Y	Z
Ti	(4a)	0.000000	0.000000	0.000000
Ti	(4a)	0.000000	1.892500	2.378500
Ti	(4a)	1.892500	1.892500	4.757000
Ti	(4a)	1.892500	3.785000	7.135500
O	(8e)	0.000000	0.000000	1.965592
O	(8e)	0.000000	0.000000	-1.965592
O	(8e)	0.000000	1.892500	4.344092
O	(8e)	0.000000	1.892500	0.412908
O	(8e)	1.892500	1.892500	6.722592
O	(8e)	1.892500	1.892500	2.791408
O	(8e)	1.892500	3.785000	9.101092
O	(8e)	1.892500	3.785000	5.169908

The structure of unit cell (Ti_2O_4) and the completed tetragonal cell ($Ti_{11}O_{18}$) are formed in Gaussian 03 and presented in Figure 3.6 (a) and (b) respectively.

(a) **(b)**

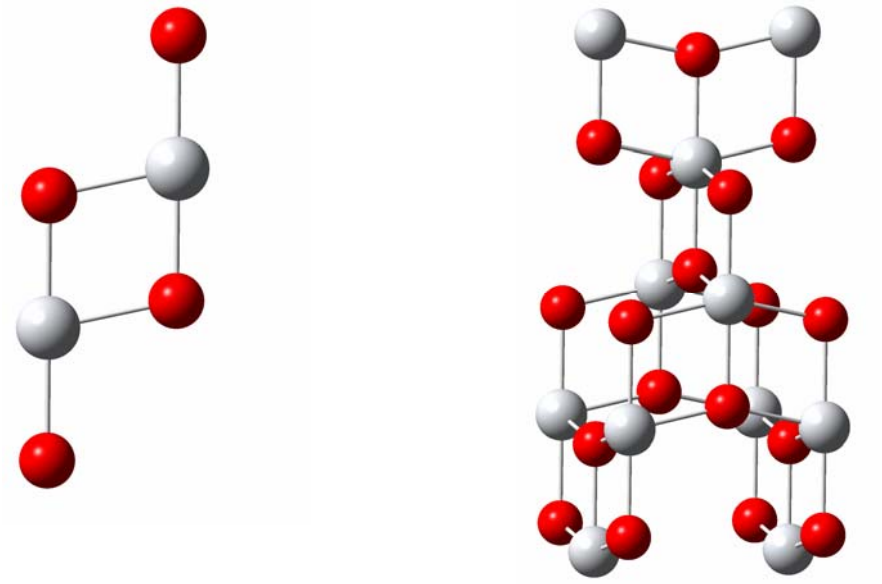

Figure 3.6 (a) TiO_2 (anatase) unit cell (Ti_2O_4). **(b)** The completed tetragonal cell ($Ti_{11}O_{18}$). Red balls are oxygen and gray ones are titanium atoms.

The TiO_2 (anatase) unit cell is decided to be enlarged three times in x and y directions and one time in z direction by using Excel. In Figure 3.7 the enlarged TiO_2 (anatase) cluster is represented by application of Gaussian 03.

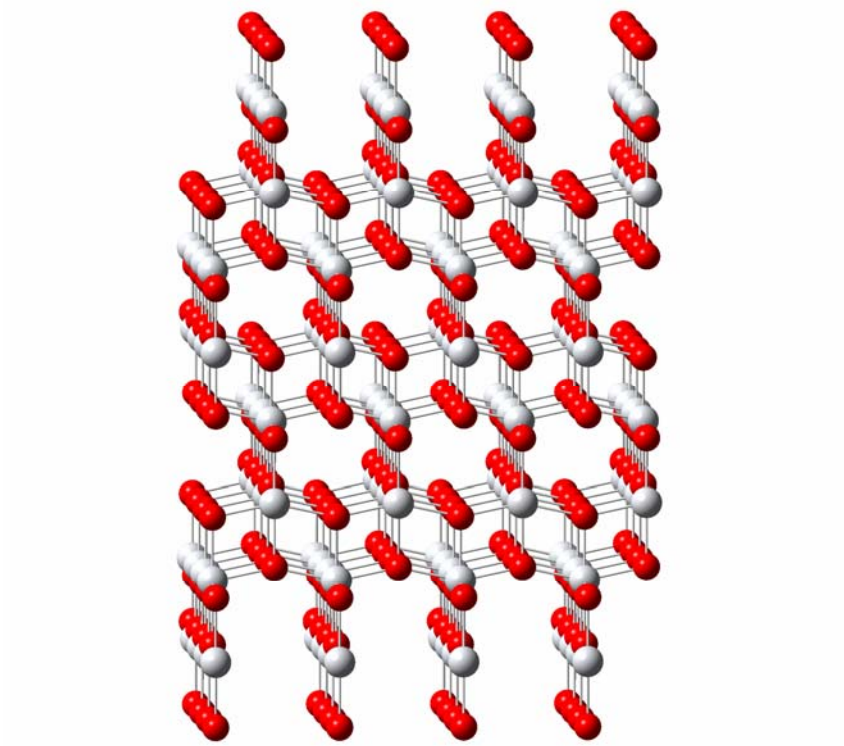

Figure 3.7 The 3-D structures of enlarged (3x-3y-1z) TiO_2 (anatase) cluster. Red balls are oxygen and gray ones are titanium atoms.

Finally, TiO_2 anatase (001) cluster surface and its ONIOM method applied version are presented in Figure 3.8 (a) and (b), respectively by means of Gaussian 03.

(a)

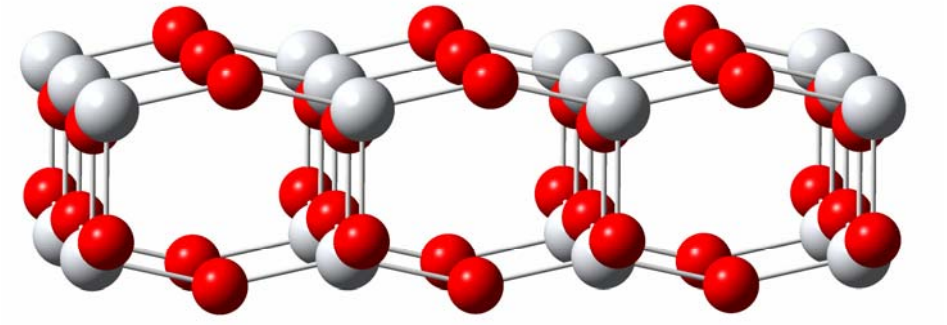

(b)

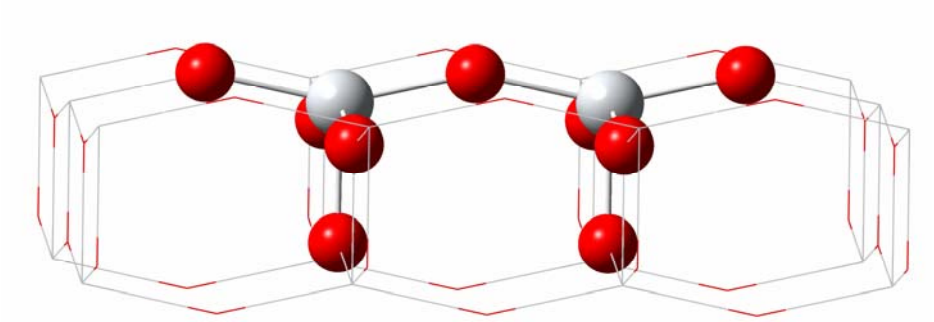

Figure 3.8 (a) TiO_2 Anatase (001) cluster surface. **(b)** ONIOM TiO_2 Anatase (001) cluster surface. [Perspective view] Red balls are oxygen and gray ones are titanium atoms. QM region is represented by ball and bond type view and MM region is represented by wireframe view in Gaussian 03.

Figure 3.8 (b) shows the ONIOM anatase $Ti_{20}O_{35}$ cluster that is modeled by a 2-region: (I) Quantum Mechanics (QM) region, and (II) Molecular Mechanics (MM) region. QM region is represented by ball and bond type view and MM region is represented by wireframe view in Gaussian 03 and there are 2 Ti and 9 O atoms in the QM region and in molecular mechanics (MM) region, there are 18 Ti and 26 O atoms.

3.3.1.2. Computational Method

Quantum chemical calculations employing ONIOM DFT/B3LYP/6-31G**-MM/UFF method provided in Gaussian 03 [87] are conducted to investigate the energetics of water adsorption on rutile TiO_2 (110), and water and ammonia adsorption on anatase (001) cluster surfaces of TiO_2.

In both ONIOM rutile and anatase cluster models, for quantum mechanical (QM) region density functional theory (DFT) [88] calculations are conducted using Becke's [89,90] three-parameter hybrid method involving the Lee et al. [91] correlation functional (B3LYP) formalism. The basis set employed in the DFT calculations is 6-31G** for all atoms. For molecular mechanics (MM) region, universal force field (UFF) [92] is used. Computations are carried out for partially relaxed cluster representation where some of the atoms on QM region are relaxed and the rest of the atoms are fixed.

The computational strategy used in this study is as follows: Initially, both the cluster and the adsorbing molecule are optimized geometrically by means of equilibrium geometry (optimized geometry or minimum-energy geometry) calculations. Then, a coordinate driving calculation is initiated by selecting a reaction coordinate distance between the adsorbing molecule and active site of the cluster. Thus, the variation of the relative energy with decreasing distance is obtained. Single point energy calculations are also performed where necessary by locating the adsorbing molecule near the catalytic cluster. Provided unrestricted calculations are performed, the $<S^2>$ value, spin contamination, is printed out and compared with the value of s(s + 1) to check whether the spin contamination error is negligible [72]. The relative energy is defined as:

$$\Delta E = E_{\text{system}} - (E_{\text{cluster}} + E_{\text{adsorbate}})$$

where E_{system} is the calculated energy of the given geometry containing the cluster and the adsorbing molecule at any interatomic distance, E_{cluster} is the energy of the cluster itself and $E_{\text{adsorbate}}$ is that of the adsorbing molecule. Once having obtained the energy profile, the geometry with the minimum energy on the energy profile

is re-optimized by means of the EG (equilibrium geometry) calculations to obtain the final geometry for the reaction. For the calculated final geometry, vibration frequencies are computed by the single point energy calculations. In this re-optimization calculation, the reaction coordinate is not fixed. Finally, the geometry with the highest energy from the energy profile is taken as the input geometry for the transition state geometry calculations, and starting from these geometries, the transition state structures with only one negative eigenvalue in Hessian matrix are obtained. The synchronous quasi-Newtonian method of optimization, (QST3) [93] is applied for transition state calculations.

Thermodynamic function values (ΔH°, ΔG°, and ΔS°), for anatase phase only*, are also calculated at specific temperatures which correspond to approximately the experimental temperatures. The relevant equations are as follows:

$$\Delta H^\circ(\mathrm{T}) = (\varepsilon_0 + H_{corr})_{\text{product}} - (\varepsilon_0 + H_{corr})_{\text{reactant}} \quad (1)$$

$$\Delta G^\circ(\mathrm{T}) = (\varepsilon_0 + G_{corr})_{\text{product}} - (\varepsilon_0 + G_{corr})_{\text{reactant}} \quad (2)$$

$$\Delta G^\circ(\mathrm{T}) = \Delta H^\circ(\mathrm{T}) - \mathrm{T}\Delta S^\circ(\mathrm{T}) \quad (3)$$

where $(\varepsilon_0 + H_{corr})$ represents "sum of electronic and thermal enthalpies" and $(\varepsilon_0 + G_{corr})$ represents "sum of electronic and thermal free energies" which are evaluated from a vibrational frequency calculation in an optimized DFT geometry calculation (See Table B.2 in Appendices). In equations (1-3) the product is assumed as cluster and adsorbate system together (molecular or dissociative) and the reactant as cluster and water or ammonia molecule separately in which adsorbate is located at a non-interacting height above the cluster system.

The equations used for computing thermodynamic data in a vibrational frequency calculation in Gaussian 03 are equivalent to those given in standard statistical texts such as Statistical Mechanics by McQuarrie [94] and the analysis used for is the rigid-rotator/harmonic-oscillator (RRHO) approximation.

---

*Since adsorption energy values at specific temperatures for rutile phase TiO_2 are not be obtained from the literature, the thermodynamic functions are not be calculated in this phase.

3.3.2. Periodic DFT Method

3.3.2.1 Surface Model and Computational Method

The periodic DFT calculations are carried out by means of VASP [95] code, which uses periodic plane wave basis sets. The electronic interactions are described with PAW (projector augmented-wave) [96,97], and GGA (generalized gradient approximation) [98] and the exchange and the correlation energy proposed by Perdew and Wang (PW91) [99]. Except for the molecules and atoms in the gas phase, dipole corrections are included for the asymmetric slab calculations, where the top sides of the slabs are used. The cut-off energies and k-points (Monkhorst Pack) used are; 500 eV and (3x3x1) for 4 layer p(2x2) anatase TiO_2 (001) slab (Figure 3.9). All the results reported in this work are carried out by optimizing the respective structures until the net force acting on the atoms are smaller than 0.01 eV/Å. The atoms and the molecules in the gas phase are represented with the same level of precision by surrounding the species with a vacuum layer of minimum 10 Å in all directions.

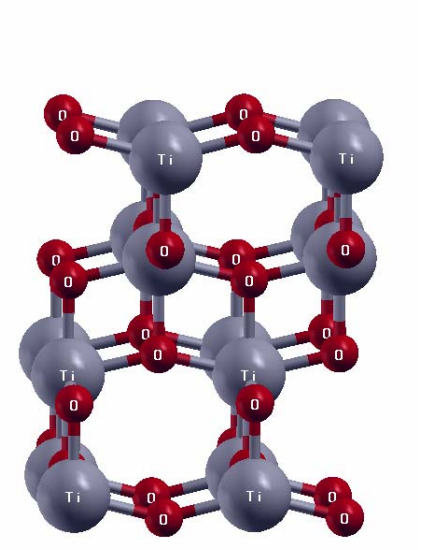

Figure 3.9 Four layer p(2x2) TiO_2 anatase (001) slab.

Anatase TiO_2 (001) surface slab (Figure 3.9) is prepared by initially optimizing the respective crystal and then cutting the crystal along (001) plane and placing a 15 Å vacuum layer above.

The adsorption energy is calculated for adsorbate on the clean surface as follows:

$$E_{\text{adsorption}} = E_{\text{adsorbate/surface}} - (E_{\text{adsorbate}} + E_{\text{surface}})$$

where $E_{\text{adsorbate}}$ is the energy of the isolated molecule (H_2O or NH_3) in the vacuum. E_{surface} is the energy of a clean anatase (001) surface, and $E_{\text{adsorbate/surface}}$ is the total energy of the molecule adsorbed together with the (001) anatase TiO_2 surface. One side of the slab is occupied by adsorbed molecules. The coverage of adsorbed molecules is taken as θ=0.25 with respect to surface Ti atoms.

The vibrational frequencies of adsorbed surface species are also calculated, after the optimizations to equilibrium geometries as described above. This is done by using the "IBRION = 5" parameter that turns on the calculation of the exact Hessian matrix. The Hessian matrix is calculated based on a finite difference approach with a step size of 0.02 for the displacements of the individual atoms of the adsorbate along each direction. The frequencies are calculated for the optimized geometries of minimas, by turning off the symmetry parameters. The frequencies of the unfrozen surface atoms (phonons) are also calculated, however they are not reported herein.

CHAPTER 4

RESULTS AND DISCUSSION

4.1 ONIOM Cluster Method

4.1.1 Water Adsorption on Rutile TiO_2 (110) Cluster Surface

4.1.1.1 Optimization of Cluster

Optimization (equilibrium geometry calculations) of ONIOM rutile TiO_2 (110) cluster is conducted by using DFT method, B3LYP formalism, 6-31G** basis set for QM region, and UFF for MM region. Computations are carried out taking the total charge as neutral, the spin multiplicity as 6, and for partially relaxed cluster representation where some of the atoms on QM region, (Ti1, O1 and O2), are relaxed and the rest of the atoms are fixed. Optimized geometry of 2-region ONIOM $Ti_{25}O_{37}$ cluster is shown in Figure 4.1.

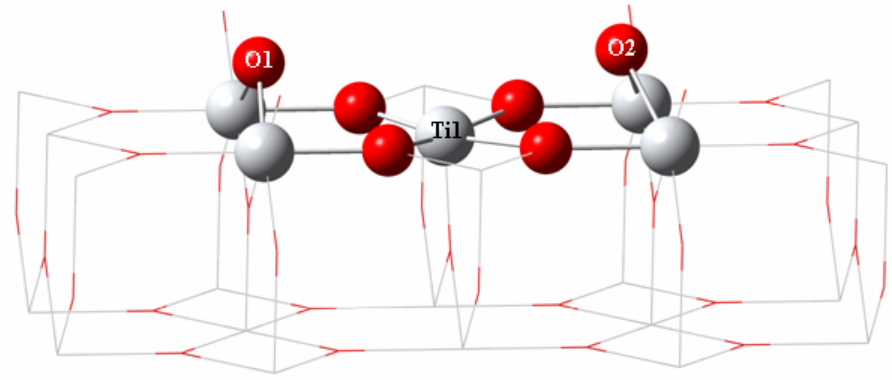

Figure 4.1 Optimized geometry of 2-region ONIOM rutile TiO_2 (110) cluster model. QM region is represented by ball and bond type view and MM region is represented by wireframe view.

The comparison of atomic displacements away from the rutile TiO_2 (110) surface relative to an ideal bulk structure with the available literature data is illustrated in Table 4.1. The variation in the distance of Ti1 from the surface in z-direction (Δz) is calculated to be -0.14 Å. The corresponding results in the experimental literatures are -0.19 ± 0.03 Å [100], -0.16 ± 0.05 Å [101] and in the theoretical literatures is - 0.17 Å [102]. The variation (Δz) in the distance of O2 from the surface is calculated to be -0.14 Å. The corresponding results in the experimental and theoretical literatures are 0.10 ± 0.05 Å [100] and -0.27 ± 0.08 Å [101] and -0.01 Å [102], respectively. Table 4.1 points out that the results obtained in this study agree very well with the literature values (See Figure 4.1 for Ti1 and O2).

Table 4.1 The comparison of the atomic displacements away from the rutile TiO_2 (110) surface relative to an ideal bulk structure with the available literature values.

Atom		**This study** [d]	Experimental		Other Theoretical	
			LEED-IV[a]	SXRD[b]	HF[c]	DFT-LDA[c]
Ti1	Δz (Å)	**-0.14**	-0.19 ± 0.03	-0.16 ± 0.05	-0.17	-0.17
O2	Δz (Å)	**0.05**	0.10 ± 0.05	-0.27 ± 0.08	-0.01	-0.01

[a] Lindsay et al. [100]
[b] Charlton et al. [101]
[c] Swamy et al. [102]
[d] Erdogan et al. [112]

4.1.1.2 Molecular Adsorption Mechanism

For molecular water adsorption on rutile TiO_2 (110) surface, a reaction coordinate is selected as the distance between the O atom (O3) of the water molecule and the fivefold coordinated Ti atom (Ti1) in QM region. As seen from the equilibrium geometry and energy profile (see Figure 4.2), molecular water adsorption occurs on partially relaxed ONIOM cluster with an exothermic relative energy difference of 22.4 kcal/mol and with (Ti1-O3) distance of 2.32 Å, and (H2-O2) distance of 1.95 Å.

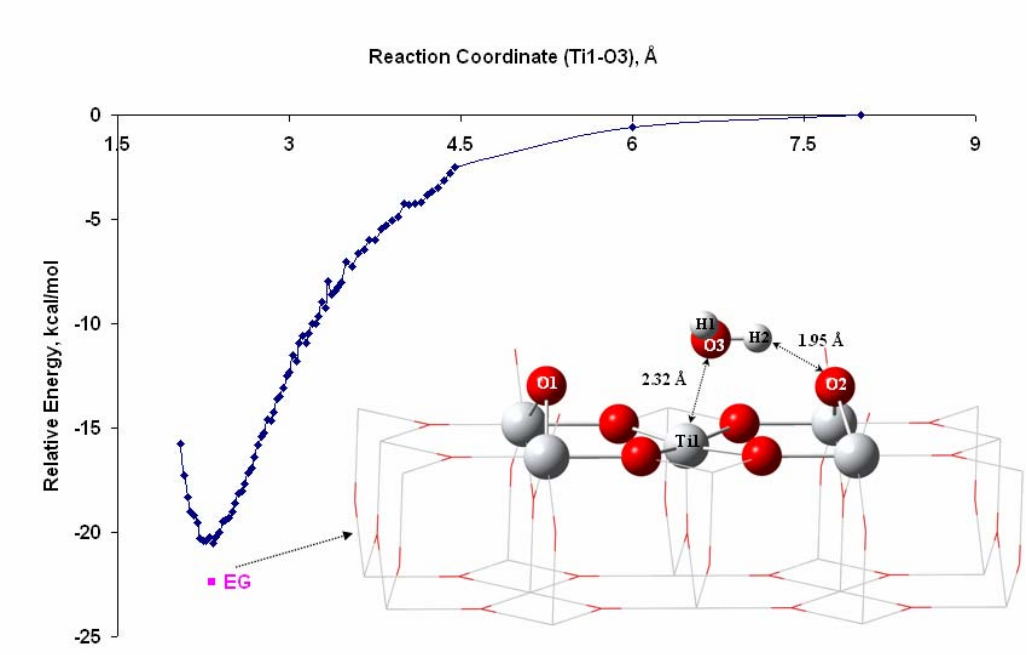

Figure 4.2 Relative energy profile and equilibrium geometry of molecular H_2O adsorption on rutile TiO_2 (110) surface. QM region is represented by ball and bond type view and MM region is represented by wireframe view.

4.1.1.3 Dissociative Adsorption Mechanism

Dissociative water adsorption is achieved on rutile TiO_2 (110) surface starting from the optimized geometry of molecular water adsorption. For this purpose, a reaction coordinate is selected as the distance between the hydrogen atom (H2) of the water molecule and the bridging oxygen atom (O2) of the cluster. (See Figure 4.4 for H2 and O2). As can be observed from the energy profile obtained for this reaction, illustrated in Figure 4.3, water dissociatively adsorbs on the surface with an activation barrier value of 23.2 kcal/mol.

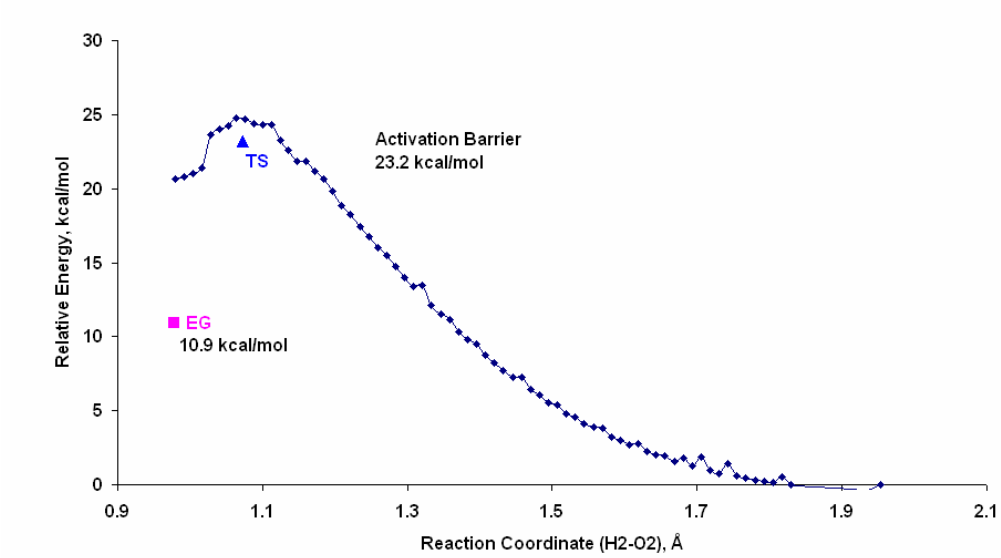

Figure 4.3 Relative energy profile for dissociative H_2O adsorption on rutile TiO_2 (110) surface.

Figure 4.4 (a) shows equilibrium geometry of dissociative water adsorption on rutile TiO_2 (110) surface. H_2O is dissociatively adsorbed on the surface with (Ti1-O3) distance of 1.84 Å, (H2-O3) distance of 2.41 Å, and (H2-O2) distance of 0.98 Å. Transition state geometry of this interaction is also illustrated in Figure 4.4 (b). One imaginary frequency is found as -776 cm^{-1} at transition state mode. The corresponding distances (Ti1-O3), (H2-O3), (H2-O2) for the transition state geometry are 2.23 Å, 1.44 Å, and 1.07 Å, respectively.

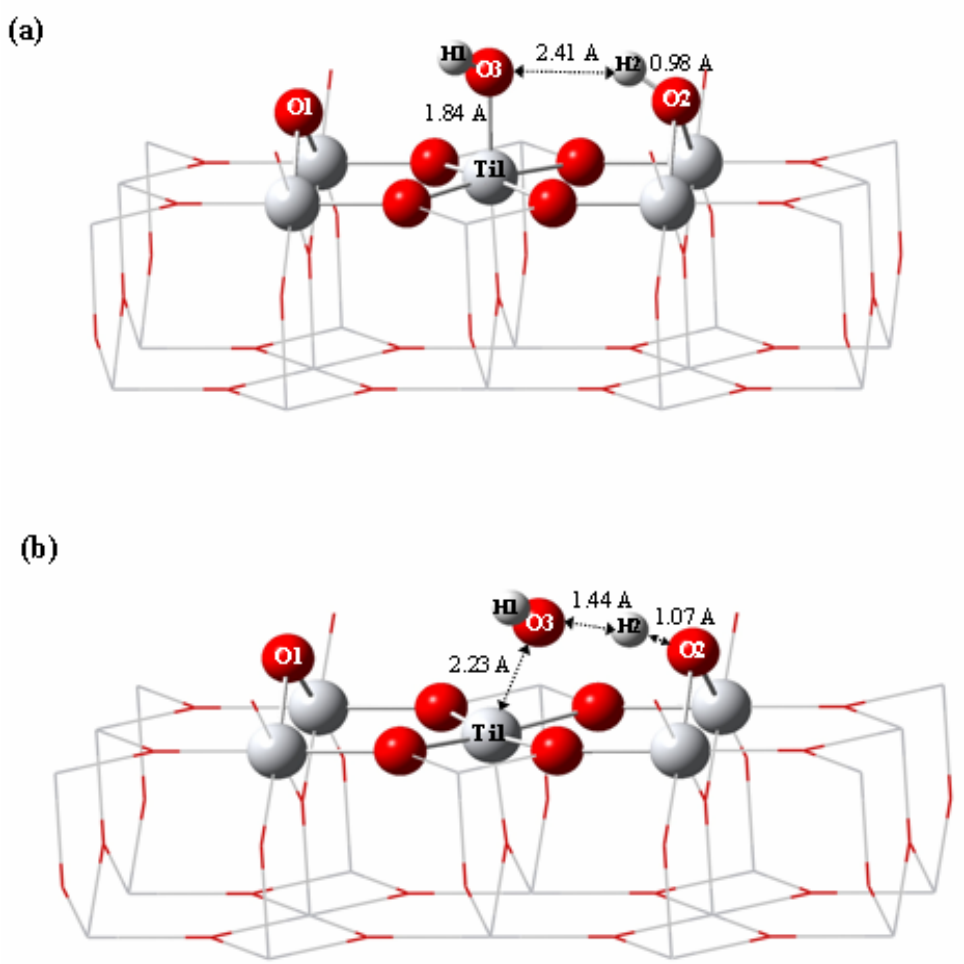

Figure 4.4 Dissociative H_2O adsorption on rutile TiO_2 (110) surface. **(a)** Equilibrium geometry, **(b)** Transition state geometry. QM region is represented by ball and bond type view and MM region is represented by wireframe view.

Relative energy diagram of reaction steps of molecular and dissociative H_2O adsorption on rutile TiO_2 (110) surface is formed and shown in Figure 4.5. As seen from that figure, overall dissociative adsorption energy is calculated to be -11.5 kcal/mol.

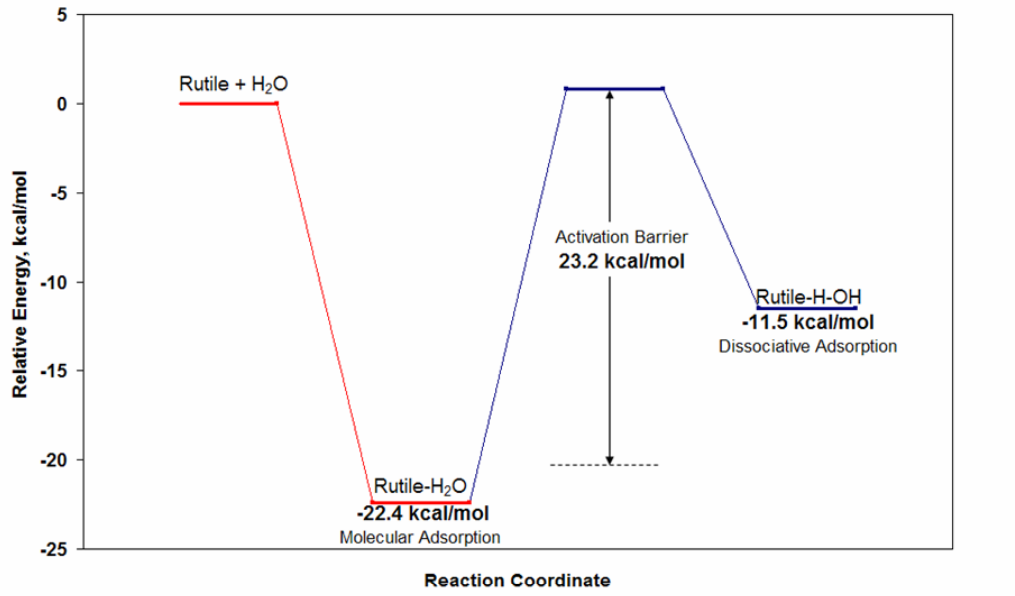

Figure 4.5 Relative energy diagram of reaction steps of molecular and dissociative H_2O adsorption on rutile TiO_2 (110) surface.

4.1.1.4 Comparison of Adsorption Energies with Literature Values

Calculated energies of water adsorption and activation barrier for the defect-free rutile TiO_2 (110) surface are compared with the available experimental and theoretical data in Table 4.2. As it is obvious from the table, our molecular H_2O adsorption energy value (-22.4 kcal/mol) is in the range of experimentally determined values -(14-24 kcal/mol) [36-38] and also agrees with some of the theoretical values [42,43,45,46]. As a comparison with other theoretical studies, our results agree well with results of Wendt et al. [48]. They found a high activation barrier (27 kcal/mol) for the diffusion of the two OH groups via periodic slab calculations that corresponds to our calculated activation barrier (23.2 kcal/mol). The activation barrier value calculated in this study also agrees well with the result of Lindan and Zhang [49]. They determined an activation barrier value of 5.8 kcal/mol at 1 ML water coverage and they pointed out that the barrier increases with decreasing coverage. To sum up, the results of our DFT calculations show that dissociative water adsorption is not favorable because of such a high activation barrier.

Table 4.2 The comparison of the calculated energies of H_2O adsorption and activation barrier on rutile TiO_2 (110) surface with the theoretical and experimental values in the literature.

References	Energy, kcal/mol			Method and *Software*
	Molec. Ads.	Disso. Ads.	Act. Barr.	
				Theoretical
Lindan et al. 1998 [42]	-22.9	-21.0	-	DFT-GGA-PW91 1 ML *CASTEP*
Casarin et al. 1998 [43]	-19.3	-	-	DFT-LDA-GGA-BP A*DF*
Stefanovich et al. 1999 [44]	-34.5	-7.9	-	LCAO:HF LANL1-CEP
	-34.9	-22.6	-	LCAO:B3LYP LANL1-CEP
	-34.4	-18.0	-	LCAO:MP2 *Gaussian 92*
Menetrey et al. 2003 [45]	-22.1	-29.3	-	DFT-GGA-PW91 9L 1/3ML *VASP*
Bandura et al. 2004 [46]	-22.5	-11.5	-	LCAO:HF LANL1-CEP *Gaussian 98*
	-21.9	-18.4	-	PW:DFT-GGA-PW91 5L *CASTEP*
Wendt et al. 2005 [47]	-15.2	-18.2	-	PW:DFT-GGA-RPBE *DACAPO*
Wendt et al. 2006 [48]	-	-	27.0	PW:DFT-GGA-RPBE
Lindan and Zhang 2005 [49]	-11.8	-6.5	5.8	DFT-GGA-PW91 5L 1ML *CASTEP*
Kamisaka et al. 2007 [51]	-18.4	-13.4	-	DFT-GGA-PW91 1/3 ML
	-16.1	-10.6	-	DFT-GGA-PBE 1/3 ML *VASP*
Erdogan et al. 2009 [112]	**-22.4**	**-11.5**	**23.2**	**ONIOM DFT/B3LYP/6-31G** -MD/UFF** *Gaussian 03*
				Experimental
Hugenshimidt et al.1994 [36]	-(17-21.5)			XPS, TPD, work function
Henderson et al. 1996 [37]	-(17-19)			TPD
Brinkley et al. 1998 [38]	-(14-24)			TPD, Modulated Beams

There are also controversial results in theoretical literature regarding water adsorption on perfect rutile TiO_2 (110) surface as can be seen in Table 4.2. The variations in the results of theoretical literature may be explained by the usage of different quantum chemical methods, cluster models, basis sets, coverages, etc. The result obtained in this study for molecular adsorption energy value (-22.4 kcal/mol) agrees well with the result (-19.3 kcal/mol) reported by Casarin et al. [43]. However, they did not study or could not find a dissociation case. Results in the study of Lindan and Zhang [49] are different from this study and it may be due to the coverage effect as they studied adsorption at high water coverage (1

monolayer), whereas we used low water coverage. The most probable reasons for the difference from the results of Stefanovich et al. [44] may be that they used different quantum chemical methods, functionals and basis sets and a very old version software program (Gaussian 92). Unlike most of other theoretical results, Menetrey et al. [45] predicted that dissociative adsorption on rutile TiO_2 (110) surface is more favorable than molecular one and the reason for the disagreement is unclear. It may not be related with coverage effect since when they decrease the coverage; the trend (dissociative adsorption's being favorable) is maintained. However, recent VASP study published by Kamisaka et al. [51] and cluster study reported by Bandura et al. [46] support our results for molecular and dissociative water adsorption energies. Results obtained in this study for molecular and dissociative water adsorption energy values (-22.4 kcal/mol and -11.5 kcal/mol, respectively) are quite similar to what Kamisaka et al. [51] determined (-18.4 kcal/mol vs. -13.4 kcal/mol, respectively) using VASP and exactly same to what Bandura et al. [46] obtained (-22.5 kcal/mol vs. -11.5 kcal/mol, respectively) using Gaussian 98.

4.1.1.5 Vibrational Frequency Studies

Table 4.3 presents the structural and vibrational properties of molecularly, and dissociatively adsorbed H_2O molecule on rutile TiO_2 (110) surface with relevant experimental data. Asymmetric OH, symmetric OH, and bending HOH vibration data of 3705, 3489, 1566 cm^{-1} for molecular water adsorption are in agreement with the experimental [37] values of 3625, 3420, 1625 cm^{-1}, respectively. The frequency of terminal hydroxyl for dissociative water adsorption is computed in this study as 3668 cm^{-1} that is in agreement with the experimental value of 3690 cm^{-1} reported by Henderson et al. [37]. They also reported that the small amount of water dissociation observed by HREELS on ideal TiO_2 (110) surface under UHV conditions; but that dissociation may be linked to structural and/or point defects. Frequency of deposited proton is computed as 3536 cm^{-1} and relevant experimental data is not available in the literature.

Table 4.3 Structural and vibrational properties of adsorbed H_2O molecule (molecularly and dissociatively) on rutile TiO_2 (110) surface via ONIOM DFT/B3LYP/6-31G**-MD/UFF calculations [c].

	Molecularly Ads. H_2O	Dissociatively Ads. H_2O
$r_{Ti1\text{-}O3}$ (Å)	**2.32** (2.21) [a]	**1.84**
$r_{H2\text{-}O2}$ (Å)	**1.95**	**0.98**
υ_{asymOH} (cm^{-1})	**3705** (3625) [b]	-
υ_{symOH} (cm^{-1})	**3489** (3420) [b]	**3668** (3690) [b]
δ_{HOH} (cm^{-1})	**1566** (1625) [b]	-
υ_{symH} (cm^{-1})	-	**3536**

[a] Allegretti et al. [103]
[b] Henderson M.A. [37]
[c] Erdogan et al. [112]
Scaling factor recommended for reproducing experimental fundamentals (frequency values) is 0.9613 for B3LYP method [104].
Experimental values are in parentheses.

4.1.2 Water and Ammonia Adsorption on Anatase TiO_2 (001) Cluster Surface

4.1.2.1 Optimization of Cluster

Optimization of ONIOM anatase TiO_2 (001) cluster is conducted by using DFT method, B3LYP formalism, 6-31G** basis set for QM region, and UFF for MM region. Computations are carried out by taking the total charge as neutral, the spin multiplicity as 2, and for partially relaxed cluster representation where some of the atoms on QM region, (Ti1, O1 and Ti2), are relaxed and the rest of the atoms are fixed. Optimized geometry of 2-region ONIOM $Ti_{20}O_{35}$ cluster model is shown in Figure 4.6.

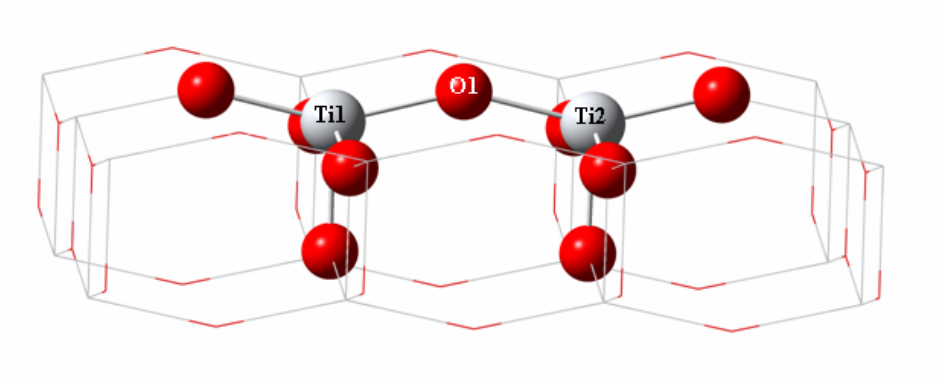

Figure 4.6 Optimized geometry of 2-region ONIOM anatase TiO_2 (001) cluster model. QM region is represented by ball and bond type view and MM region is represented by wireframe view.

Fivefold coordinated titanium atoms (Ti1 and Ti2) (act as Lewis acid sites) and the surface oxygen atoms (O1) (have Bronsted base properties) were reported as the catalytic active sites of TiO_2 anatase in [55,57] and illustrated in Figure 4.6.

4.1.2.2 Water Adsorption on Anatase TiO_2 (001) Cluster Surface

4.1.2.2.1 Molecular Adsorption Mechanism

For molecular water adsorption a coordinate driving calculation is performed by selecting the reaction coordinate as the distance between the O atom (O2) of the water molecule and one of the fivefold coordinated Ti atom (Ti1) in QM region of the cluster. Figure 4.7 depicts the energy profile for the adsorption of single water molecule on (001) anatase TiO_2 surface (See Figure 4.8 (a) for O2 and Ti1).

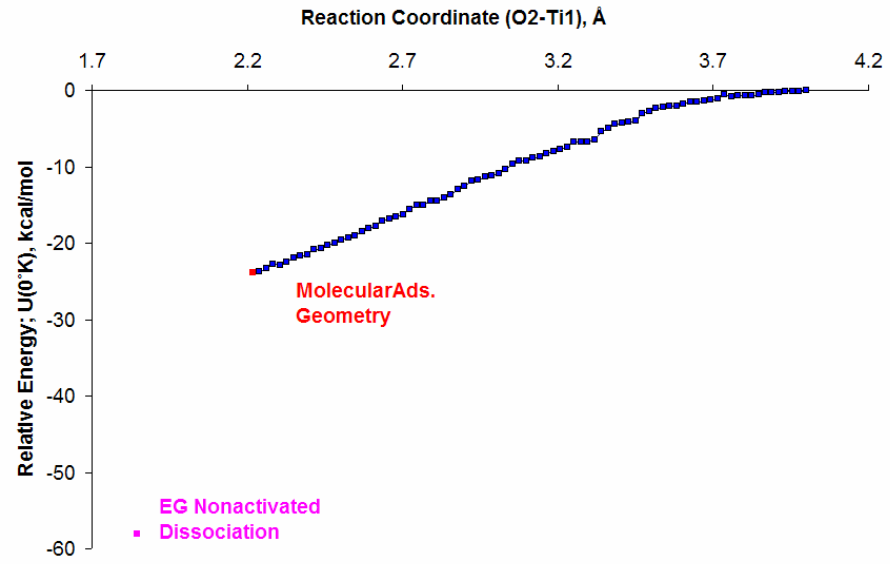

Figure 4.7 Relative energy profile for the adsorption of single water molecule on (001) anatase TiO_2 surface.

As seen from Figure 4.7, molecular adsorption energy value for water adsorption on anatase TiO_2 (001) surface is evaluated as -23.9 kcal/mol from a reaction coordinate study. It is checked whether the spin contamination error is negligible for the cluster system described in Figure 4.7 and seen that there is no spin contamination error as spin contamination $<S^2>$ value is equal to 0 for singlet spin. For molecular adsorption geometry, the distances of H1-O1, H1-O2, and Ti1-O2 are computed as 1.589 Å, 1.012 Å, and 2.218 Å, respectively (see Figure 4.8 (a)).

4.1.2.2.2 Dissociative Adsorption Mechanism

The final geometry for the reaction is found by means of an EG (equilibrium geometry) calculation as given in Figure 4.8 (b). It is observed that water molecule is dissociated on the cluster surface by a non-activated process with an exothermic relative energy difference of 58.12 kcal/mol in Figure 4.7. For the EG of the nonactivated dissociative water adsorption, the distances of H1-O1 H1-O2, and Ti1-O2 are computed as 0.982 Å, 1.679 Å, and 1.845 Å, respectively (see Figure 4.8 (b)).

(a)

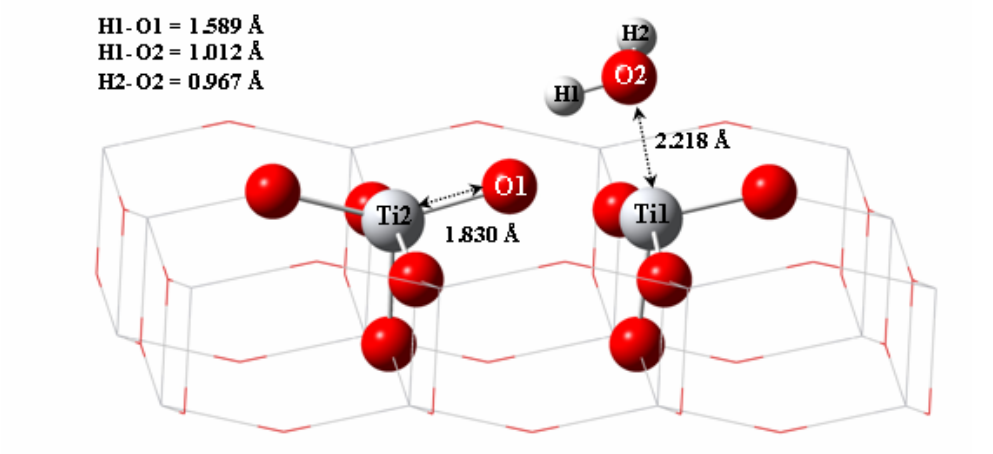

(b)

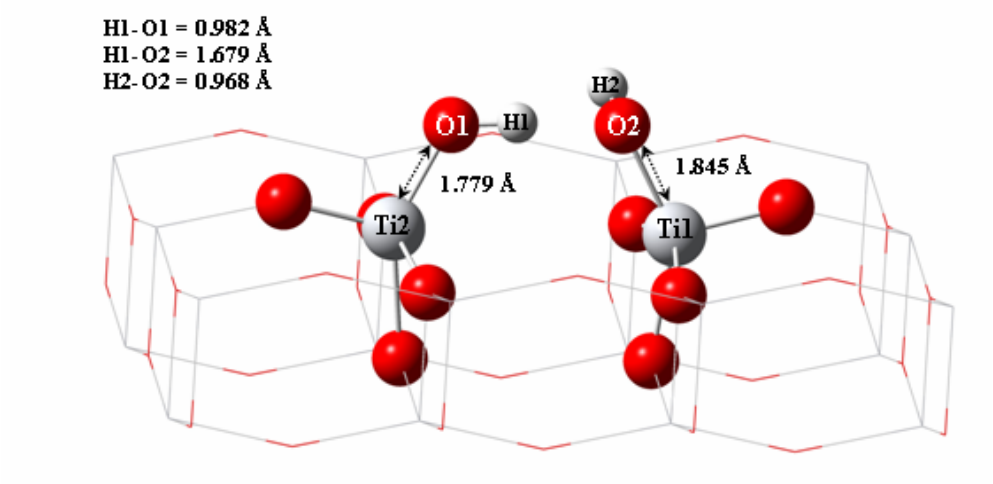

Figure 4.8 (a) Molecular H_2O adsorption geometry on anatase TiO_2 (001) surface. **(b)** Equilibrium geometry of dissociative H_2O adsorption on anatase TiO_2 (001) surface. QM region is represented by ball and bond type view and MM region is represented by wireframe view.

4.1.2.2.3 Comparison of Adsorption Energies with Literature Values

The computed molecular and dissociative adsorption energy values for water on anatase TiO_2 surface (001) are given in Table 4.4 with the available theoretical and experimental literature data for comparison. Experimental studies by Srnak et al. [52] and Munuera et al. [53] have reported molecular adsorption of water on TiO_2 (anatase) surface only. As also observed from Table 4.4, in our study and other published studies [13,60-62,64-66,68-70], water molecule is dissociated by a non-activated process or the computed adsorption energy value for dissociative adsorption is lower than the molecular one. Thus, dissociative adsorption of water molecule is energetically favored on anatase TiO_2 (001) surface.

Table 4.4 A comparison of the calculated H_2O adsorption energies (kcal/mol) on perfect anatase TiO_2 (001) surface with the theoretical and experimental values in the literature.

Authors and References	Method		Adsorption Energy	
			Molec.	Dissoc.
	Theoretical			
Fahmi and Minot 1994 [60]		Periodic	-14.34	-28.68
Bredow et al. 1995 [61]	MO/SINDO1	4x4x3 cluster	-25.33	-31.79
		3x3x3 cluster	-32.50	-38.72
		2x2x3 cluster	-35.61	-52.82
Vittadini et al. 1998 [13]	PW:DFT-GGA	Car-Parrinello	-18.68	-33.21
Nair 2004 [64]		DFT	-18.64	-32.98
Arrouvel et al. 2004 [65]	PW:DFT-GGA	KS	-	-(24-39)
Jug et al. 2005 [62]		MSINDO	-23.90	-49.71
Gong and Selloni 2005 [66]	PW:DFT-GGA	Car-Parrinello	-	-28.80
		1/6 ML		
		1/3 ML	-	-25.60
		1/2 ML	-	-26.98
Ignatchenko et al. 2006 [68]		DN-PW91 1/2 ML	-	-45.30
		DNP-PW91 1/2 ML	-	-41.00
		DNP-PBE 1/2 ML	-	-39.90
		DNP-PBE (1xn) H_2O add.	-	-38.50
Wahab et al. 2008 [69]		MSINDO	-17.69	-24.62
Onal et al. 2006 [70]	DFT-B3LYP/6-31G**	Relax.	-24.93	-54.00
Erdogan et al. 2009 [113]	**ONIOM**	**DFT/B3LYP/ 6-31G**-MD/UFF**	**-23.90**	**-33.67**
	Experimental			
Srnak et al. 1992 [52]	TPD	Anatase TiO_2	-11, -18	
Munuera et al. 1999 [53]	TPD	Anatase TiO_2	-12	

4.1.2.2.4 Vibrational Frequency Studies

The vibration frequency values of dissociatively adsorbed H_2O on (001) anatase TiO_2 surface are calculated by single point energy calculations. A comparison of the results with the available experimental literature is given in Table 4.5. As seen in the table, the O–H stretching vibration value of 3657 cm^{-1} computed for dissociative water adsorption agrees well with the experimental values of (3665, 3715 cm^{-1}) where (001) anatase surface was assumed [105] and it is also in the experimentally predicted range (3600–3800 cm^{-1}) reported by another reference [106].

Table 4.5 Vibrational frequencies (cm^{-1}) of dissociatively adsorbed H_2O molecule on anatase TiO_2 (001) surface as obtained from ONIOM DFT/B3LYP-6-31G**-MD/UFF calculations.

	This work [c] Anatase *(001)* TiO_2	Experimental Anatase TiO_2
$\upsilon_{symOH\ stret.}$	**3657**	3665[a], 3715[a], 3600-3800[b]

[a] Primet et al. [105]
[b] Morterra et al. [106]
[c] Erdogan et al. [113]
Scaling factor recommended for reproducing experimental fundamentals (frequency values) is 0.9613 for B3LYP method [104].

4.1.2.2.5 Thermochemical Data at Specific Temperatures

Table 4.6 shows calculated reaction enthalpy, free energy (kcal/mol) and entropy (cal/mol.K) values at 0 K and at specific experimental temperatures (170, 260 K) [52] for molecular or dissociative H_2O adsorption on anatase TiO_2 (001) surface. As can be seen from the table, there is no remarkable difference between the calculated reaction enthalpies in this range of temperatures. Our results also indicate that calculated reaction enthalpies for molecular water adsorption at 170 K and 260 K (-22.2 kcal/mol and -22 kcal/mol, respectively) are approximately close to one of the experimentally obtained desorption enthalpies of adsorbed states of water (-18 kcal/mol) [52]. It should be noted that these experimental

results are obtained for titania (anatase) material, which may include all types of surfaces rather than the specific (001) surface.

Table 4.6 Calculated ΔH°, ΔG° (kcal/mol), and ΔS° (cal/mol.K) values at 0 K and specific experimental temperatures (170, 260 K) [52] for H_2O adsorption on anatase TiO_2 (001) surface [b].

		Molecularly Adsorbed H_2O	Dissociatively Adsorbed H_2O
At 0 K	$\Delta H^{\circ} = \Delta G^{\circ}$	-23.9	-58.1
At 170 K	ΔH°	-22.2 (-18)[a]	-51.9
	ΔG°	-21.7	-50.9
	ΔS°	-2.8	-6.2
At 260 K	ΔH°	-22.0 (-11)[a]	-52.0
	ΔG°	-21.5	-50.3
	ΔS°	-2.2	-6.8

[a] Srnak et al. [52]
[b] Erdogan et al. [113]
Experimental values are in parentheses and belong to titania (anatase) material which may include many types of surfaces and not specifically (001) surface.

4.1.2.3 Ammonia Adsorption on Anatase TiO_2 (001) Cluster Surface

4.1.2.3.1 Molecular Adsorption Mechanism

For molecular ammonia adsorption on anatase TiO_2 (001) surface a reaction coordinate is selected as the distance between the nitrogen atom (N1) of the ammonia molecule and the fivefold coordinated titanium atom (Ti1) in QM region of the cluster surface. As seen from the resultant energy profile calculations (see Figure 4.9), molecular ammonia adsorption occurs on partially relaxed ONIOM cluster with an adsorption energy of -23.28 kcal/mol. The equilibrium geometry of this reaction is illustrated in the same figure. Ammonia is molecularly adsorbed on the surface having a N1–Ti1 distance of 2.225 Å, a H2-O1 distance of 2.685 Å and a H1-O1 distance of 2.561 Å.

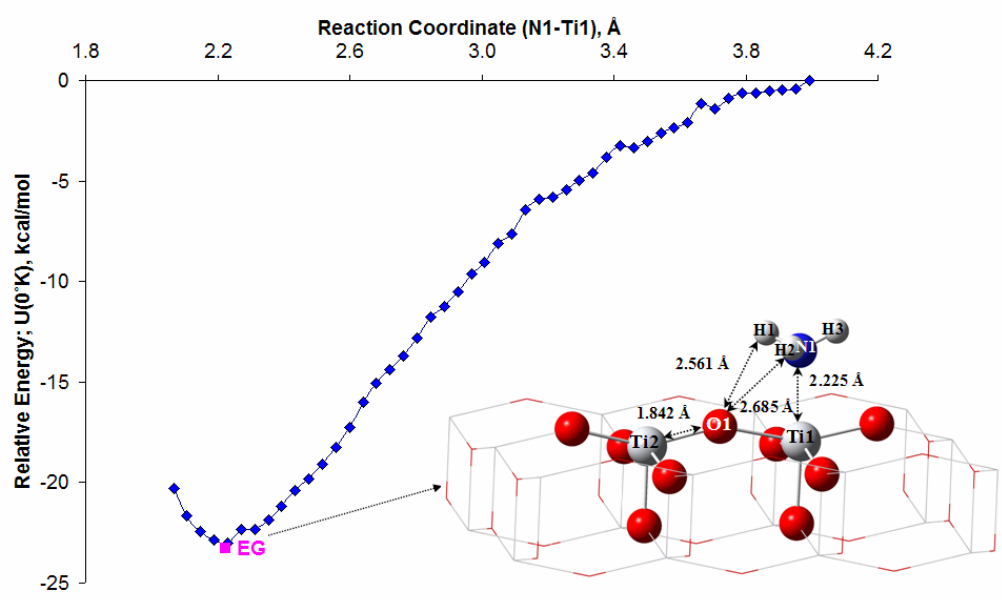

Figure 4.9 Relative energy profile and equilibrium geometry of molecular NH_3 adsorption on anatase TiO_2 (001) surface. QM region is represented by ball and bond type view and MM region is represented by wireframe view.

4.1.2.3.2 Dissociative Adsorption Mechanism

Dissociative ammonia adsorption is also studied on anatase TiO_2 (001) surface starting from the optimized geometry of molecular ammonia adsorption given in Figure 4.9. Coordinate driving calculations are performed by choosing the distance between the hydrogen atom (H1) of the ammonia molecule and the surface oxygen atom (O1) of the cluster. (See Figure 4.9 for H1 and O1). The resultant energy profile calculation, given in Figure 4.10, shows that ammonia molecule is dissociatively adsorbed on the surface with an exothermic relative energy difference of 13.89 kcal/mol and a small activation barrier value of 2.68 kcal/mol.

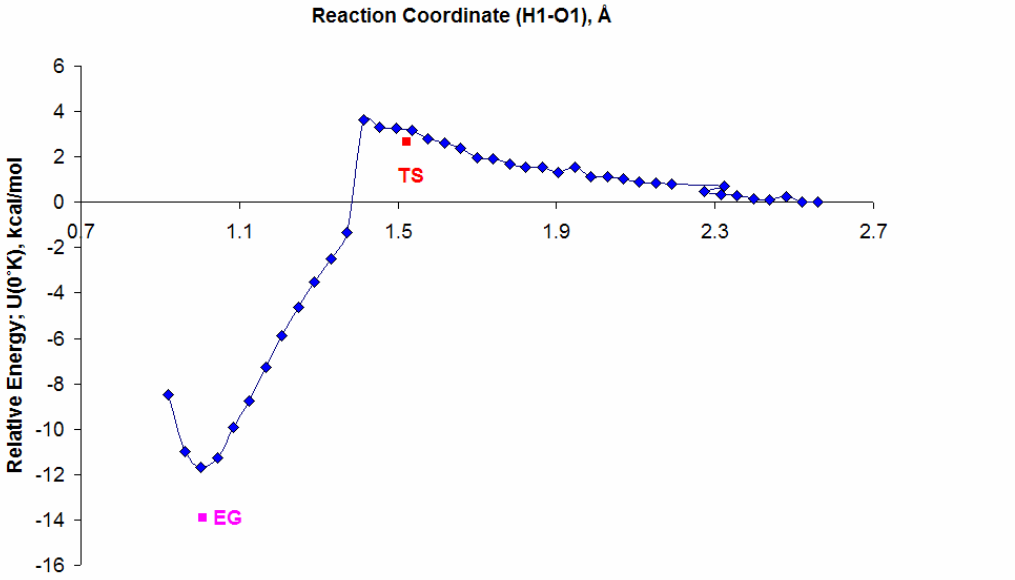

Figure 4.10 Relative energy profile for dissociative NH_3 adsorption on anatase TiO_2 (001) surface.

The equilibrium geometry (EG) of this interaction including the bond lengths is given in Figure 4.11 (a). The distances of N1–Ti1 and O1–H1 are calculated as 1.950 Å and 1.008 Å, respectively. Transition state (TS) geometry of this interaction is also illustrated in Figure 4.11 (b). One imaginary frequency is found as -137 cm^{-1} at transition state mode. The corresponding distances N1–Ti1, N1-

H1, and O1–H1 for the transition state geometry are 2.163 Å, 1.074 Å, and 1.522 Å, respectively.

(a)

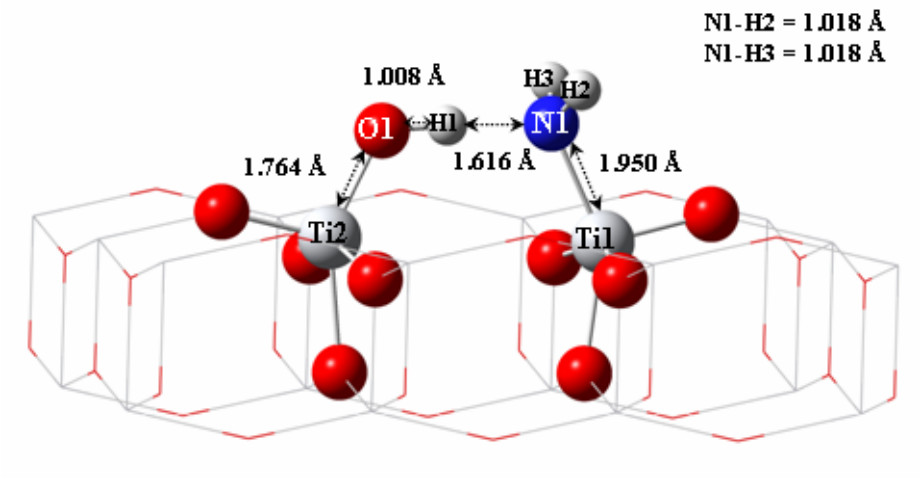

(b)

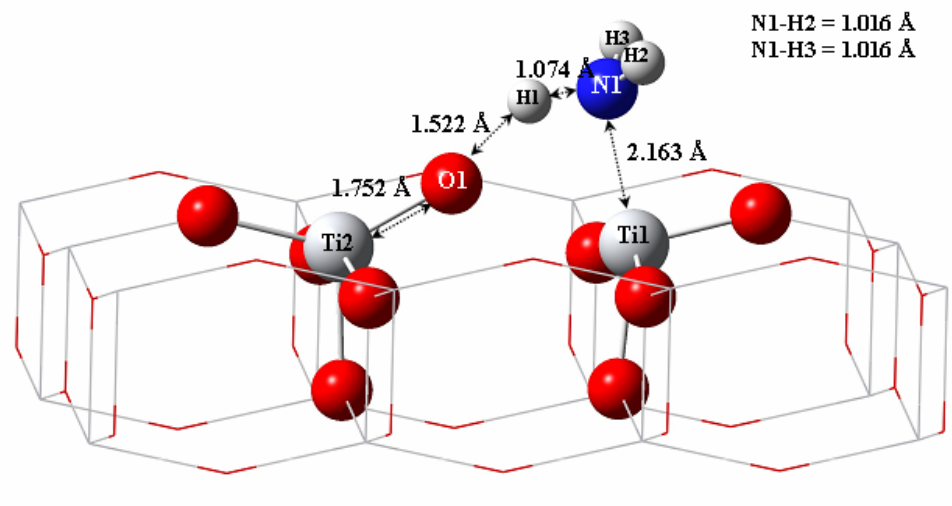

Figure 4.11 Geometries of dissociative NH_3 adsorption on anatase TiO_2 (001) surface. **(a)** Equilibrium geometry, **(b)** Transition state geometry. QM region is represented by ball and bond type view and MM region is represented by wireframe view.

A summary energy diagram of molecular and dissociative NH_3 adsorption on anatase TiO_2 (001) surface is shown in Figure 4.12. As seen from that figure, overall dissociative adsorption energy is calculated to be -37.17 kcal/mol. The result of our ONIOM-DFT calculations point out that dissociative ammonia adsorption on anatase TiO_2 (001) surface is an energetically more favorable than molecular one (-37.17 kcal/mol vs. -23.28 kcal/mol). However, there seems to be no experimental data concerning this aspect.

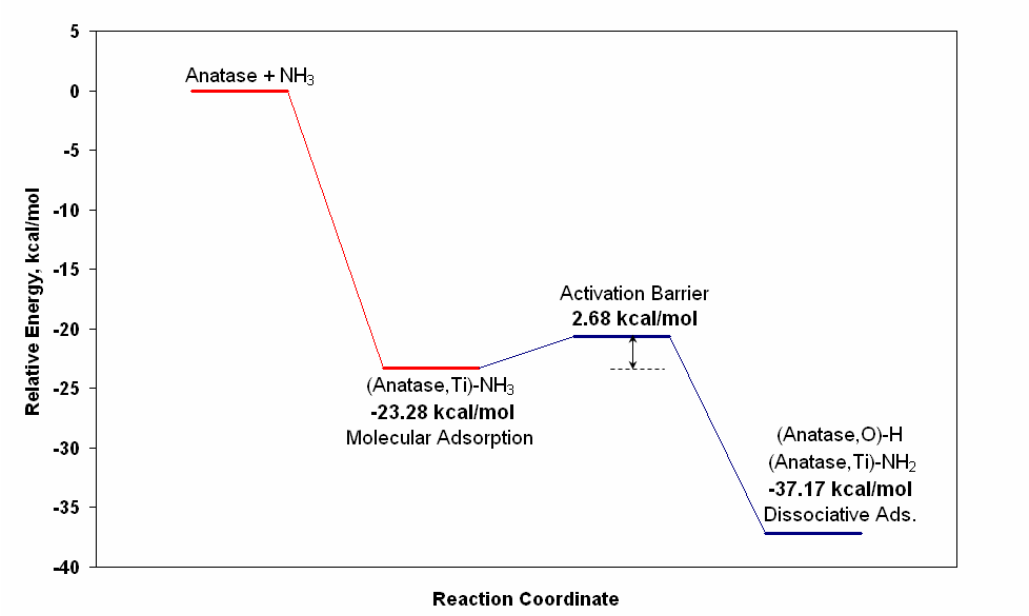

Figure 4.12 A summary energy diagram of molecular and dissociative NH_3 adsorption on anatase TiO_2 (001) surface.

4.1.2.3.3 Comparison of Adsorption Energies with Literature Values

The computed adsorption energy and activation barrier values for the ammonia adsorption on the defect-free anatase TiO_2 (001) surface are compared with the available literature and given in Table 4.7.

Table 4.7 A comparison of the calculated NH_3 adsorption energies on anatase TiO_2 (001) surface with the theoretical and experimental values in the literature.

Authors and References	Method	Adsorption Energy, kcal/mol		
		Molec.	Dissoc.	Act. Barrier
	Theoretical			
Onal et al. 2006 [70]	DFT-B3LYP-6-31G**	-26.57	-36.32	3.63
Calatayud et al 2004 [71]	DFT	-19.40		-
Erdogan et al. [113]	**ONIOM DFT/B3LYP/6-31G**-MD/UFF**	**-23.28**	**-37.17**	**2.68**
	Experimental (*Anatase TiO_2)*			
Srnak et al. 1992 [52]	TPD	-14, -27		
Sprinceana et al. 1999 [59]	XRD BET	-(31-36)		

Experimental works involving TPD [52] and XRD, BET [59] studied NH_3 adsorption on TiO_2 (anatase) only. However, the computed molecular NH_3 adsorption energy value of -23.28 kcal/mol is comparable with -27 kcal/mol of NH_3 desorption enthalpy value reported by Srnak et al. [52]. The slight deviation is reasonable in view of the fact that (001) surface is minority in anatase as previously mentioned. There seems to be only two theoretical studies concerning NH_3 adsorption on (001) anatase TiO_2 [70,71]. Molecular and dissociative NH_3 adsorption energy values (-23.28 kcal/mol and -37.17 kcal/mol, respectively) obtained in this study are quite comparable to what Onal et al. [70] obtained (-26.57 kcal/mol vs. -36.32 kcal/mol, respectively) using SPARTAN'04 software. The activation barrier value (2.68 kcal/mol) calculated in this study also agrees well with their activation barrier value of 3.63 kcal/mol. Calatayud et al. [71] reported a molecular NH_3 adsorption energy as -19.4 kcal/mol using periodic DFT calculations. However, they did not study or could not find a dissociation case.

4.1.2.3.4 Vibrational Frequency Studies

Vibration frequencies for ammonia adsorption on anatase TiO_2 (001) cluster surface are also calculated by single point energy calculations. Table 4.8 shows the vibrational properties of molecularly and dissociatively adsorbed NH_3 molecule on the (001) surface with available experimental data reported for anatase surfaces in general.

Table 4.8 The vibrational frequency (cm^{-1}) properties of molecularly and dissociatively adsorbed NH_3 molecule on anatase TiO_2 (001) surface as obtained from ONIOM DFT/B3LYP-MD/UFF calculations with the experimental literature values [e].

	Molecularly Ads. NH_3	Dissociatively Ads. NH_3	
	EG	EG	TS
$\upsilon_{asymHNH\ stret.}$	**3485, 3494** (3400[c])	**3463**	**3482**
$\upsilon_{symHNH\ stret.}$	**3347** (3350[c])	**3365**	**3395**
$\delta_{asymHNH\ bend.}$	**1576, 1586** (1599[a], 1600[c])	-	**1573**
$\delta_{symHNH\ bend.}$	**1086** (1190[a], 1225[a], 1215[b])	-	**1082**
$\upsilon_{HNH\ scis.}$	-	**1464** (1480[c], 1540[d])	**1514**

[a] Amores et al. [107]
[b] Teramura et al. [108]
[c] Schneider et al. [109]
[d] Lietti et al. [110]
[e] Erdogan et al. [113]
Scaling factor recommended for reproducing experimental fundamentals (frequency values) is 0.9613 for B3LYP method [104].
Experimental values are in parentheses and particular surface of the TiO_2 (anatase) has not been reported.

As it is seen from the Table 4.8, symmetric bending frequency value of 1086 cm^{-1} and asymmetric stretching frequency data of (3485 cm^{-1}, 3494 cm^{-1}) for molecular ammonia adsorption deviate significantly from the experimental values of 1190 cm^{-1}, 1225 cm^{-1} [107] and 1215 cm^{-1} [108] and of 3400 cm^{-1} [109], respectively. On the other hand, asymmetric bending (1576 cm^{-1}, 1586 cm^{-1}), and symmetric stretching (3347 cm^{-1}), vibration data for molecular ammonia adsorption are in agreement with the experimental values of (1599 cm^{-1} [107], 1600 cm^{-1} [109]), and 3350 cm^{-1} [109], respectively. And also, vibration frequency value (1464 cm^{-1}) for scissoring mode of NH_2 species for the

dissociative ammonia adsorption is quite comparable with the experimental value of 1480 cm^{-1} [109]. For the transition state of dissociative ammonia adsorption, vibrational frequency values are also evaluated and illustrated in Table 4.8. To sum up, it can be concluded from the findings given in Table 4.8 that the results are reasonable and the deviations from the experimental studies could be expected since the particular surface of the TiO_2 (anatase) on which NH_3 adsorbed was not determined in the real catalyst surface in these studies, and it is known that (001) surface is minority in anatase.

4.1.2.3.5 Thermochemical Data at Specific Temperatures

Table 4.9 illustrates calculated ΔH°, ΔG° (kcal/mol), and ΔS° (cal/mol.K) values at 0 K and at specific experimental temperatures (150, 360 K [52], and 423 K [59]) for molecular or dissociative NH_3 adsorption on anatase TiO_2 (001) surface. As can be seen from Table 4.9, calculated reaction enthalpy for dissociative ammonia adsorption at 423 K (-32 kcal/mol) obtained in this study is quite comparable to what Sprinceana et al. [59] obtained (-(31–36) kcal/mol) using experimental XRD and BET techniques. For this reason, the experimental value may belong to dissociative ammonia adsorption. In addition, calculated reaction enthalpies for molecular ammonia adsorption at 150 K and 360 K (-20.9 kcal/mol and -20.7 kcal/mol, respectively) are close to the experimentally obtained desorption enthalpy of strongly adsorbed state of ammonia (-27 kcal/mol) [52]. As in the case of water, it should be noticed that the experimental results are obtained for titania (anatase) material which may include many types of surfaces and not specifically (001) surface.

Table 4.9 Calculated ΔH°, ΔG° (kcal/mol), and ΔS° (cal/mol.K) values at 0 K and specific experimental temperatures (150, 360 K [52], and 423 K [59]) for NH_3 adsorption on anatase TiO_2 (001) surface [c].

		Molecularly Adsorbed NH_3	Dissociatively Adsorbed NH_3
At 0 K	$\Delta H^{\circ} = \Delta G^{\circ}$	-23.3	-37.2
At 150 K	ΔH°	-20.9 (-27)[a]	-32.0
	ΔG°	-20.2	-30.9
	ΔS°	-4.4	-7.2
At 360 K	ΔH°	-20.7 (-14)[a]	-32.1
	ΔG°	-19.4	-29.3
	ΔS°	-3.5	-7.9
At 423 K	ΔH°	-20.5	-32.0 -(31–36)[b]
	ΔG°	-19.2	-28.8
	ΔS°	-3.2	-7.7

[a] Srnak et al. [52]
[b] Sprinceana et al. [59]
[c] Erdogan et al. [113]
Experimental values are in parentheses and belong to titania (anatase) material which may include many types of surfaces and not specifically (001) surface.

4.2 Periodic DFT Method

4.2.1 Water and Ammonia Adsorption on Anatase TiO_2 (001) Slab Surface

4.2.1.1 Optimization of Slab Geometry

Optimized geometry of 4 layer p(2x2) anatase TiO_2 (001) surface slab (Figure 4.13) is prepared by initially relaxing the crystal and then cutting the crystal along (001) plane and placing a 15 Å vacuum layer above. The optimization of the bulk crystal is carried out to determine the optimal lattice parameters, which are calculated as a=b=3.822 Å, and c=9.670 Å. These values are in a good agreement with the experimentally reported values, 3.785 Å and 9.514 Å [86].

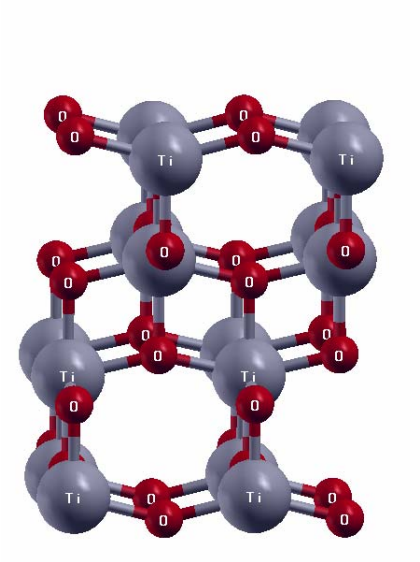

Figure 4.13 Optimized slab geometry of 4 layer p(2x2) TiO_2 anatase (001) slab.

4.2.1.2 Water Adsorption on Anatase TiO_2 (001) Slab Surface

4.2.1.2.1 Molecular Adsorption Mechanism

By using a slab geometry and a periodic DFT approach, water adsorption on anatase TiO_2 (001) surface is investigated. Molecular adsorption energy is evaluated from total energy calculations as -14.62 kcal/mol. Figure 4.14 depicts the optimized geometry of molecular H_2O adsorption on anatase TiO_2 (001) slab model. For the molecular adsorption geometry, the distances between hydrogen and oxygen of water molecule (H_w-O_w) and oxygen of water molecule and fivefold coordinated titanium (O_w-Ti) are computed as 0.972 Å, and 2.171 Å, respectively.

(a)

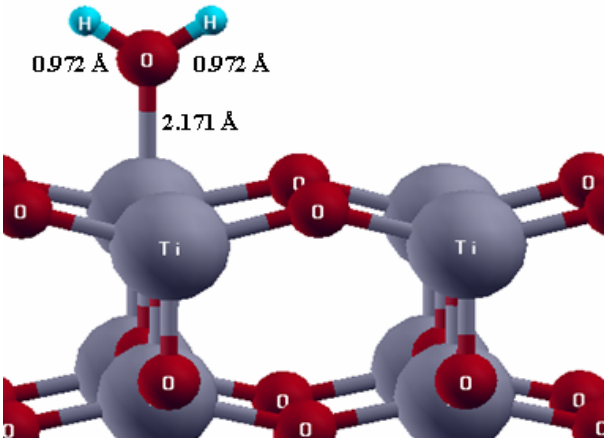

(b)

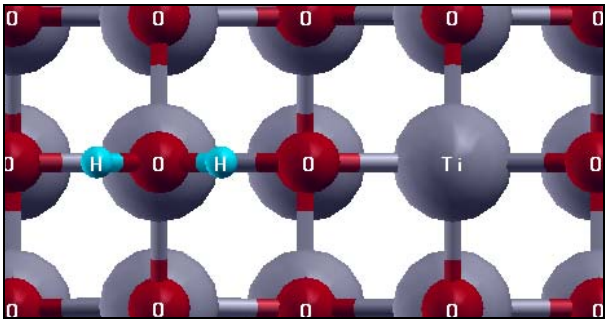

Figure 4.14 Optimized geometry of molecular H_2O adsorption on anatase TiO_2 (001) slab model. **(a)** Perspective view, **(b)** Top view.

4.2.1.2.2 Dissociative Adsorption Mechanism

For the case of dissociative adsorption mechanism, it is observed that water molecule is dissociated on (001) anatase TiO_2 slab surface with an exothermic relative energy difference of 32.28 kcal/mol. For the optimized geometry of this reaction (see Figure 4.15), the distances between hydrogen and oxygen of water molecule (H_{left}-O_w), hydrogen of water molecule and surface oxygen (H_{right}-O_s), and oxygen of water molecule and fivefold coordinated titanium (O_w-Ti) are computed as 0.971 Å, 0.982 Å, and 1.892 Å respectively.

(a)

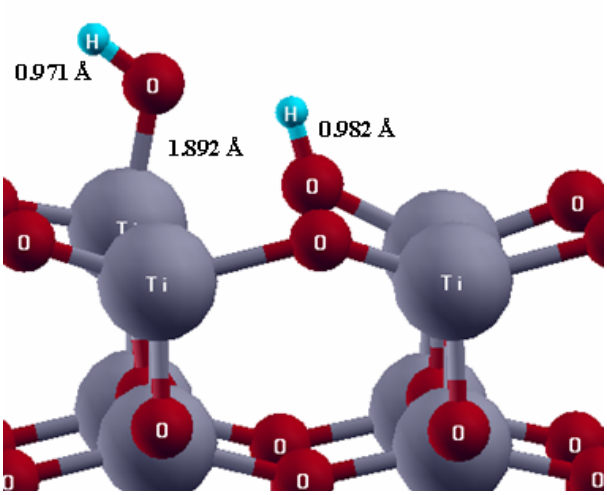

(b)

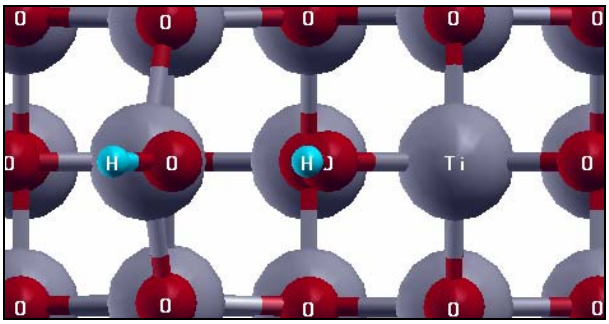

Figure 4.15 Optimized geometry of dissociative H_2O adsorption on anatase TiO_2 (001) slab model. **(a)** Perspective view, **(b)** Top view.

4.2.1.2.3 Comparison of Adsorption Energies with Literature Values

The calculated molecular and dissociative water adsorption energy values on (001) anatase TiO_2 surface are -14.62 kcal/mol and -32.28 kcal/mol, respectively. These values are comparable with the available theoretical and experimental literature data given in Table 4.10.

Table 4.10 A comparison of the calculated H_2O adsorption energies (kcal/mol) on perfect anatase TiO_2 (001) surface with the theoretical and experimental values in the literature.

Authors and References	Method	Adsorption Energy	
		Molecular	Dissociative
	Theoretical		
Fahmi and Minot 1994 [60]	Periodic	-14.34	-28.68
Vittadini et al. 1998 [13]	PW:DFT-GGA Car-Parrinello 1/2 ML	-18.68	-33.21
Nair 2004 [64]	DFT	-18.64	-32.98
Jug et al. 2005 [62]	MSINDO	-23.90	-49.71
Arrouvel et al. 2004 [65]	PW:DFT-GGA KS	-	-(24.1-39.4)
Gong and Selloni 2005 [66]	PW:DFT-GGA Car-Parrinello 1/6 ML	-	-28.80
	1/3 ML	-	-25.60
	1/2 ML	-	-26.98
Onal et al. 2006 [70]	DFT-B3LYP/6-31G** Relax	-24.93	-54.00
Wahab et al. 2008 [69]	MSINDO	-17.69	-24.62
Erdogan et al. 2009 [113]	ONIOM DFT/B3LYP/6-31G**-MD/UFF	-23.90	-33.67
Erdogan et al. 2009 [114]	**PW:DFT-GGA-PW91**	**-14.62**	**-32.28**
	Experimental		
Srnak et al. 1992 [52]	TPD Anatase TiO_2	-11, -18	
Munuera et al. 1999 [53]	TPD Anatase TiO_2	-12	

4.2.1.2.4 Vibrational Frequency Studies

A comparison of the computed vibration frequency values of dissociatively adsorbed H_2O on (001) anatase TiO_2 surface with the available experimental literature is given in Table 4.11. As can be seen in the table, the symmetric O–H stretching vibration value of 3767 cm^{-1} is in the experimentally predicted range (3600–3800 cm^{-1}) reported by [106] and agrees well with the experimental value of (3715 cm^{-1}) where (001) anatase surface was assumed [105].

Table 4.11 Vibrational frequencies (cm^{-1}) of dissociatively adsorbed H_2O molecule on anatase TiO_2 (001) surface as obtained from periodic DFT (PW:DFT-GGA) calculations.

	This work [c] **Anatase *(001)* TiO_2**	Experimental Anatase TiO_2
$\upsilon_{symOH\ stret.}$	**3560, 3767**	3665[a], 3715[a], 3600-3800[b]

[a] Primet et al. [105]
[b] Morterra et al. [106]
[c] Erdogan et al. [114]
Scaling factor recommended for reproducing experimental fundamentals (frequency values) is 0.9613 for B3LYP method [104].

4.2.1.3 Ammonia Adsorption on Anatase TiO_2 (001) Slab Surface

4.2.1.3.1 Molecular Adsorption Mechanism

Adsorption energy for molecular ammonia on anatase TiO_2 (001) slab model is computed from the total energy calculations as -25.44 kcal/mol. Optimized geometry of this reaction is illustrated in Figure 4.16 and it is found that ammonia is molecularly adsorbed on the surface having a N–Ti distance of 2.26 Å.

(a)

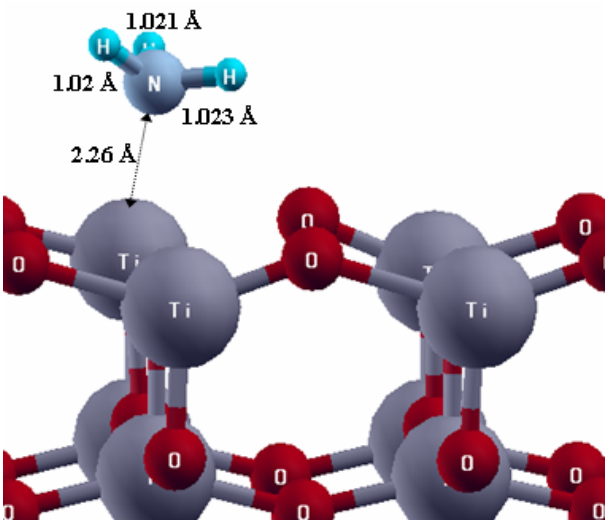

(b)

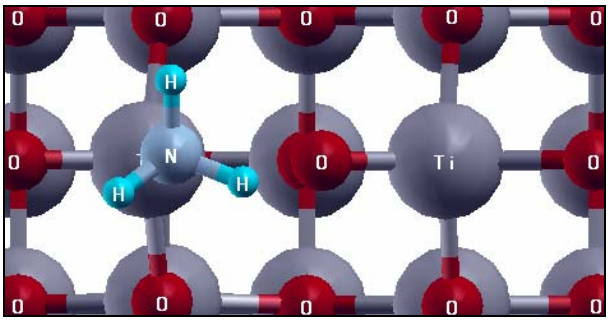

Figure 4.16 Optimized geometry of molecular NH_3 adsorption on anatase TiO_2 (001) slab model. **(a)** Perspective view, **(b)** Top view.

4.2.1.3.2 Comparison of Adsorption Energies with Literature Values

A comparison of the computed adsorption energy values obtained from periodic DFT method for NH_3 adsorption on anatase TiO_2 (001) surface with the available literature is given in Table 4.12. Experimental TPD [52] and XRD, BET [59] studies investigated NH_3 adsorption on real TiO_2 (anatase) catalyst surface and therefore the slight deviation is reasonable in view of the fact that (001) surface is minority in anatase as previously mentioned. However, molecular NH_3 adsorption energy value (-25.44 kcal/mol) obtained from periodic DFT calculations in this study is quite comparable to the results of our preceding relaxed [70] and ONIOM [113] cluster studies (-26.57 kcal/mol and -23.28 kcal/mol, respectively).

Table 4.12 A comparison of the calculated NH_3 adsorption energies on perfect anatase TiO_2 (001) surface with the theoretical and experimental values in the literature.

Authors and References	Method	Adsorption Energy, kcal/mol		
		Molec.	Dissoc.	Act.Barr
	Theoretical			
Calatayud et al. 2004 [71]	PW:DFT-GGA KS	-19.40	-	
Onal et al. 2006 [70]	Relaxed cluster DFT-B3LYP-6-31G**	-26.57	-36.32	3.63
Erdogan et al. 2009 [113]	ONIOM cluster DFT/B3LYP6-31G**-MD /UFF	-23.28	-37.17	2.68
Erdogan et al. 2009 [114]	**Periodic slab PW:DFT-GGA-PW91**	**-25.44**	**-**	**-**
	Experimental			
Srnak et al. 1992 [52]	TPD AnataseTiO$_2$	-14, -27		
Sprinceana et al. 1999 [59]	XRD BET AnataseTiO$_2$	-(31-36)		

4.2.1.3.3 Vibrational Frequency Studies

A vibration frequency study for ammonia adsorption is also performed and a comparison of the vibrational properties of molecularly adsorbed NH_3 molecule on the (001) surface with the available experimental data reported for anatase surfaces in general is given in Table 4.13. As this table shows, a symmetric bending frequency value of 1094 cm^{-1} and asymmetric stretching frequency data of (3510, 3535 cm^{-1}) for molecular ammonia adsorption deviate significantly from the experimental values of 1190, 1225 and 1215 cm^{-1} [107,108] and of 3400

cm^{-1} [109], respectively. The deviations from the experimental studies could be expected since the particular surface of the TiO_2 (anatase) on which NH_3 adsorbed has not been reported in these studies and it is known that (001) surface is minority in anatase. For the molecular ammonia adsorption asymmetric bending (1573 cm^{-1}, 1609 cm^{-1}), and symmetric stretching (3385 cm^{-1}), vibration data are in agreement with the experimental values of (1599 cm^{-1} [107], 1600 cm^{-1} [109]), and 3350 cm^{-1} [109], respectively.

Table 4.13 A comparison of the vibrational frequencies (cm^{-1}) of molecularly adsorbed NH_3 molecule on anatase TiO_2 (001) surface as obtained from periodic DFT (PW:DFT-GGA) calculations with the experimental literature values [e].

	Molecularly Ads. NH_3
$\upsilon_{asym\ HNH\ stret.}$	**3510, 3535** (3400[c])
$\upsilon_{sym\ HNH\ stret.}$	**3385** (3350[c])
$\delta_{asym\ HNH\ bend.}$	**1573, 1609** (1599[a], 1600[c])
$\delta_{sym\ HNH\ bend.}$	**1094** (1190[a], 1225[a], 1215[b])

[a] Amores et al. [107]
[b] Teramura et al. [108]
[c] Schneider et al. [109]
[e] Erdogan et al. [113]
Scaling factor recommended for reproducing experimental fundamentals (frequency values) is 0.9613 for B3LYP method [104].
Experimental values are in parentheses and particular surface of the TiO_2 (anatase) has not been reported.

CHAPTER 5

CONCLUSIONS

In this thesis, water adsorption on rutile TiO_2 (110) surface represented by partially relaxed $Ti_{25}O_{37}$ ONIOM cluster and water and ammonia adsorption on anatase TiO_2 (001) surface represented by partially relaxed $Ti_{20}O_{35}$ ONIOM cluster models are investigated by means of quantum chemical calculations employing ONIOM DFT/B3LYP/6-31G**-MM/UFF method provided in Gaussian 03. Water and ammonia adsorption on anatase TiO_2 (001) surface is studied and compared by also performing periodic DFT calculations (PW:DFT-GGA-PW91) using VASP code.

Firstly, ONIOM cluster calculations concerning water adsorption on rutile TiO_2 (110) surface point out that the results obtained for molecular and dissociative water adsorption energy values (-22.4 kcal/mol and -11.5 kcal/mol, respectively) are quite similar to the most recent publication values (-18.4 kcal/mol vs. -13.4 kcal/mol, respectively) reported on this subject by Kamisaka et al. [51] using VASP and exactly same to what Bandura et al. [46] obtained (-22.5 kcal/mol vs. -11.5 kcal/mol, respectively) using Gaussian 98. Furthermore, if the diffusion of the two OH groups is taken into consideration, we have calculated a reasonable activation barrier value of 23.2 kcal/mol similar to what Wendt et al. [48] obtained (27 kcal/mol) via periodic slab calculations in DACAPO. According to such a high activation barrier, ONIOM cluster calculations indicate that dissociative water adsorption on rutile TiO_2 (110) is not favorable. There is a good agreement with experimental literature regarding that molecular H_2O adsorption energy value obtained in this study (-22.4 kcal/mol) is in the range of experimentally determined values -(14-24 kcal/mol). In fact, experimental studies

involving HREELS and TPD [52] reported that water adsorbed on rutile TiO_2 (110) surface predominately in a molecular state with exothermic adsorption energy of 17-19 kcal/mol, little or no water dissociates on ideal TiO_2 (110) surface under UHV conditions; but that dissociation may be linked to structural and/or point defects.

Secondly, ONIOM cluster calculations concerning water and ammonia adsorption on anatase TiO_2 (001) cluster surface indicate that H_2O molecule is dissociated by a non-activated process with an exothermic relative energy difference of 58.12 kcal/mol. On the same surface dissociative NH_3 adsorption is energetically more favorable process than molecular NH_3 adsorption (-37.17 kcal/mol vs. -23.28 kcal/mol). In the experimental studies, H_2O and NH_3 adsorption have been studied on TiO_2 (anatase), particular surface has not been known, so direct comparison cannot be done with these studies. However, in accordance with other theoretical and experimental studies, the dissociative adsorptions of water and ammonia molecules on anatase TiO_2 (001) surface are energetically more favorable than the molecular one. Thermodynamic functions (ΔH°, ΔG°, and ΔS°), for anatase phase only, are also calculated at specific temperatures which correspond to approximately the experimental temperatures.

Thirdly, periodic DFT calculations concerning water and ammonia adsorption on anatase TiO_2 (001) slab surface indicate that H_2O molecule is dissociated on anatase TiO_2 (001) slab surface by a non-activated process with an exothermic relative energy difference of 32.28 kcal/mol. The dissociated form of water on anatase TiO_2 (001) surface is energetically more favored than the molecular form in accordance with other theoretical and experimental studies. On the same surface, molecular NH_3 adsorption energy is computed as -25.44 kcal/mol.

Finally, vibration data for the optimized geometries of adsorbed molecules on rutile TiO_2 (110) cluster surface and on anatase TiO_2 (001) cluster and slab surfaces compares well with the experimental values reported in literature.

REFERENCES

1. Emsley, J. Molecules at an Exhibition: portraits of intriguing materials in everyday life; Oxford University Press; 1999.

2. Trengove, L.; William Gregor (1761–1817) discoverer of titanium; Annals of Science 1972, 29, 36.

3. Kirk-Othmer Encyclopedia of Chemical Technology; 5th ed. Canada, John Wiley & Sons, Inc., 2007, 25, 9.

4. Diebold, U. Surf Sci Reports 2003, 48, 53.

5. Samsonov, G.V. The Oxide Handbook; IFI/Plenum; New York; 1982.

6. Ulmann's Encyclopedia of Industrial Chemistry; 7th ed., New York, Wiley Interscience; 2005, 20, 271.

7. Murray, J.L. Phase Diagrams of Binary Titanium Alloy; 1990, p.219.

8. Ramamoorthy, M.D.; Vanderbilt and R.D. King-Smith, Phys Rev B 1994, 49, 16721.

9. Satterfield, C.N. Heterogeneous Catalysis in Industrial Practice; 2nd ed., McGraw-Hill, New York, 1991.

10. Ohno, T.; Sarukawa, K.; Matsumura M. J Phys Chem B 2001, 105, 2417.

11. Hagfelt, A.; Gratzel, M. Chem Rev 1995, 95, 49.

12. Hadjivanov, K.I.; Klissurski, D.K. Chem Soc Rev 1996, 25, 61.

13. Vittadini, A.; Selloni, A.; Rotzinger, F.P.; Gratzel, M. Phys Rev Lett 1998, 81, 2954.

14. Lazzeri, M.; Vittadini, A.; Selloni, A. Phys Rev B 2001, 63, 155409.

15. Diebold, U.; Ruzycki, N.; Herman, G. S.; Selloni, A. Catal Today 2003, 85, 93.

16. Vittadini, A.; Casarin, M.; Selloni, A. Theor Chem Acc 2007, 117, 663.

17. Lazzeri, M.; Vittadini, A.; Selloni, A. Phys Rev B 2001, 63, 155409/1

18. Ando, M.; Kobayashi, T.; Haruta, M. Catal Today 1997, 36, 135.

19. Fujishima, A.; Honda, K. Nature 1972, 238, 37.

20. Dutta, P.K.; Ginwalla, A.; Hogg, B.; Patton, B.R.; Chwieroth, B; Liang, Z; Gouma, P.; Mills, M.; Akbar, S. J Phys Chem 1999, 103, 4412.

21. Kronos International, 1996.

22. Phillips, L.G.; Barbano, D.M. J Dairy Sci 1997, 80, 2726.

23. Hewitt J. Cosmet Toiletries 1999, 114, 59.

24. Poulios, I.; Spathis, P.; Tsoumparis, P.; J Environ Sci Health 34, 1999, 1455.

25. Selhofer, H. Vacuum Thin Film 1999, 15.

26. Sambrano, J.R.; Andres, J.; Beltran, A.; Sensato, F.R.; Leite, E.R.; Stamato F.M.L.G.; Longo E. Int J Quantum Chem 1997, 65, 625.

27. Mills, A.; Davies H.R.; Worsley, D. Chem Soc Rev 1993, 22, 417.

28. Maness, P.-C.; Smolinski, S.; Jacoby W.A. Appl Environ Microbiol 1999, 65, 4094.

29. Lausmaa, J.; Ask, M.; Rolander, U.; Kasemo, B. Mater Res Soc Symp Proc 1988, 110, 647.

30. Paz, Y.; Luo, Z.; Rabenberg, L.; Heller A. J Mater Res 1995, 10, 2842.

31. Garfunkel, E.; Gusev, E.; Vul (Eds.), A., Fundamental Aspects of Ultrathin Dielectrics on Si-based Devices, NATO Science Series, Kluwer Academic Publishers, Dordrecht, 1998.

32. Campbell, S.A.; Kim, H.-S.; Gilmer, D.C.; He, B.; Ma T.; Gladfelter, W.L. IBM J Res Devlop 1999, 43, 383.

33. Matsumoto, Y.; Shono, T.; Hasegawa, T.; Fukumura, T.; Kawasaki, M.; Ahmet, P.; Chikyow, T.; Koshihara, S.; Koinuma, H. Science 2001, 291, 854.

34. Bonhote, P.; Gogniat, E.; Grätzel, M.; Ashrit, P.V. Thin Solid Films 1999, 350, 269.

35. Kurtz, R.L.; Stockbauer, R.T.; Madey, E.; Roman, E.; de Segovia, J. L. Surf Sci 1989, 218, 178.

36. Hugenschmidt, M.B.; Gamble, L.; Campbell, C.T. Surf Sci 1994, 302, 329.

37. Henderson, M.A. Surf Sci 1996, 355, 151.

38. Brinkley, D.; Dietrich, M.; Engel, T.; Farrall, P.; Gantner, G.; Schafer, A.; Szuchmacher, A. Surf Sci 1998, 395, 292.

39. Brookes, I.M.; Muryn C.A.; Thornton, G. Phys Rev Lett 2001, 87, 266103/1.

40. Schaub, R.; Thostrup, P.; Lopez, N.; Lægsgaard, E.; Stensgaard, I.; Nørskov, J.K.; Besenbacher, F. Phys Rev Lett 2001, 87, 266104.

41. Goniakowski, J.; Gillan, M.J. Surf Sci 1996, 350, 145.

42. Lindan, P.J.D.; Harrison, N.M.; Gillan, M. J Phys Rev Lett 1998, 80, 762.

43. Casarin M.; Maccato, C. J Phys Chem B 1998, 102, 10745.

44. Stefanovich, E.V.; Truong, T.N. Chem Phys Lett 1999, 299, 623.

45. Menetrey, M.; Markovits, M.A.; Minot, C. Surf Sci 2003, 524, 49.

46. Bandura, A.V.; Sykes, D.G.; Shapovalov, V.; Troung, T.N.; Kubicki, J.D.; Evarestov, R.A. J Phys Chem B 2004, 108, 7844.

47. Wendt, S.; Shaub, R.; Matthiesen, J.; Vestergaard, E.K.; Wahlström, E.; Rasmussen, M.D.; Thostrup, P; Molina, L.M.; Laegsgaarrd, E.; Stensgaard, I; Hammer, B.; Besenbacher, F. Surf Sci 2005, 598, 226.

48. Wendt, S.; Matthiesen, J.; Shaub, R.; Vestergaard, E.K.; Laegsgaarrd, E.; Besenbacher, F.; Hammer, B. Phys Rev Lett 2006, 96, 066107.

49. Lindan, P.J.D; Zhang, C. Phys Rev B 2005, 72, 075439.

50. Perron, H.; Vandenborre, J.; Domain, C.; Drot, R.; Roques, J.; Simoni, E.; Ehrhardt, J.J.; Catalette, H. Surf Sci 2007, 601, 518.

51. Kamisaka H.; Yamashita, K.; Surf Sci 2007, 601, 4824.

52. Srnak, T.Z.; Dumesic, J.A.; Clausen, B.S.; Tornqvist, E.; Topsoe, N.Y. J Catal 1992, 135, 246.

53. Munuera, G.; Moreno, F.; Gonzales, F. A model for anatase TiO_2 surfaces: interpretation of some interface processes. Reactivity of solids; Proceedings of the 7th International Symposium Reaction Solids, Chapman & Hall, London 1972, 681.

54. Topsøe, N-Y.; Topsøe, H.; Dumesic, J.A. J Catal 1995, 151, 226.

55. Topsøe, N-Y.; Topsøe, H.; Dumesic, J.A. J Catal 1995, 151, 241.

56. Ramis, G.; Yi, L.; Busca, G.; Turco, M.; Kotur E.; Willey, R.J. J Catal 1995, 157, 523.

57. Ramis, G.; Yi, L.; Busca, G. Catal Today 1996, 28, 373.

58. Busca, G.; Lietti, L.; Ramis, G.; Berti, F. Appl Catal B 1998, 18, 1.

59. Sprinceana, D.; Caldararu, M.; Ionescu, N.I.; Auroux, A. J Therm Anal Calorim 1999, 56, 109.

60. Fahmi, A.; Minot, C. Surf Sci 1994, 304, 343.

61. Bredow, T.; Jug, K. Surf Sci 1995, 327, 398.

62. Jug, K.; Nair, N.N.; Bredow, T. Surf Sci 2005, 596, 108.

63. Kachurovskaya, N.A.; Mikheeva, E.P.; Zhidomirov, G.M. J Mol Catal 2000, 178, 191.

64. Nair, N.N. Molecular Dynamics Investigation of Clusters and Solids, Ph.D. Thesis; Theoretical Chemistry Institute, Hannover University, Germany, 2004.

65. Arrouvel C., Digne, M.; Breysse, M.; Toulhoat, H.; Raybaud, P. J Catal 2004, 222, 152.

66. Gong, X.-Q.; Selloni, A. J Phys Chem B Lett 2005, 109, 19560.

67. Barnard, A.S.; Zapol, P.; Curtiss, A. J Chem Theory Comput 2005, 1, 107.

68. Ignatchenko, A.; Nealon, D.G.; Dushane, R.; Humphries, K. J Mol Catal A Chemical 2006, 256, 57.

69. Wahab, H.S.; Bredow, T.; Aliwi, M. Chem Phys 2008, 354 50.

70. Onal, I.; Soyer, S.; Senkan, S. Surf Sci 2006, 600, 2457.

71. Calatayud, M.; Mguig, B.; Minot, C. Surf Sci Reports 2004, 55, 169.

72. Young, D.C. Computational Chemistry; John Wiley & Sons, Inc., New York, Chapter 27, 2001.

73. Hehre, J.W. A Guide to Molecular Mechanics and Quantum Calculations; Wavefunction, Inc., Irvine, Chapter 2 and 3, 2003.

74. Vreven, T.; Byun, K.S.; Komaromi, I.; Dapprich, S.; Montgomery, J.A. Jr.; Morokuma, K.; Frisch, M.J. J Chem Theory and Comput 2006, 2, 815.

75. Dapprich, S.; Komáromi, I.; Byun, K.S.; Morokuma, K.; Frisch, M.J. J Mol Struct (Theochem) 1999, 46, 21.

76. Gaussian, Inc., www.gaussian.com/g_whitepap/oniom_technote.htm Introduction to ONIOM, 11 Aug 2009.

77. Maseras, F.; Morokuma, K. J Comput Chem 1995, 16, 1170.

78. Derat, E.; Bouquant, J.; Humbel, S. J Mol Struct (THEOCHEM) 2003, 632, 61.

79. Warshel, A.; Levitt, M. J Mol Biol 1976, 103, 227.

80. Thery, V.; Rinaldi, D.; Rivail, J.L.; Maigret, B.; Ferenczy, G.G. J Comput Chem 1994, 15, 269.

81. Reuter, N.; Dejaegere, A.; Maigret, B.; Karplus, M. J Phys Chem A 2000, 104, 1720.

82. Gao, J.; Amara, P.; Alhambra, C.; Field, M.J. J Phys Chem A 1998, 102, 4714.

83. Zhang, Y.K.; Lee, T.S.; Yang, W.T. J Chem Phys 1999, 110, 46.

84. DiLabio, G.A.; Hurley, M.M.; Christiansen, P.A. J Chem Phys 2002, 116, 9578.

85. Bakowies, D.; Thiel, W. J Phys Chem 1996, 100, 10580.

86. Wyckoff, R.W.G. Crystal structures; John Wiley & Sons, Inc., USA, 1963 Vol. I, pp. 250.

87. Gaussian 03, Revision D.01, Frisch, M.J.; Trucks, G.W.; Schlegel, H.B.; Scuseria, G.E.; Robb, M.A.; Cheeseman, J.R.; J.A. Montgomery, Jr.,T. Vreven, K.N. Kudin, J.C. Burant, J.M. Millam, S.S. Iyengar, J. Tomasi, V. Barone, B. Mennucci, M. Cossi, G. Scalmani, N. Rega, G. A. Petersson, H. Nakatsuji, M. Hada, M. Ehara, K. Toyota, R. Fukuda, J. Hasegawa, M. Ishida, T. Nakajima, Y. H onda, O. Kitao, H . Nakai, M. Klene, X. Li, J.E.Knox, H .P. H ratchian, J.B.Cross, C. Adamo, J. Jaramillo, R. Gomperts, R.E. Stratmann, O. Yazyev, A.J. Austin, R. Cammi, C. Pomelli, J.W. Ochterski, P.Y. Ayala, K. Morokuma, G.A. Voth, P. Salvador, J.J. Dannenberg, V.G. Zakrzewski, S. Dapprich, A.D. Daniels, M.C. Strain, O. Farkas, D.K. Malick, A.D. Rabuck, K. Raghavachari, J.B. Foresman, J.V. Ortiz, Q. Cui, A.G. Baboul, S. Clifford, J. Cioslowski, B.B. Stefanov, G. Liu, A. Liashenko, P. Piskorz, I. Komaromi, R.L. Martin, D.J. Fox, T. Keith, M.A. Al-Laham, C.Y. Peng, A. Nanayakkara, M. Challacombe, P.M.W. Gill, B. Johnson, W. Chen, M.W. Wong, C. Gonzalez and J.A. Pople, Gaussian, Inc., Pittsburgh PA, 2003.

88. Kohn W.; Sham, L.J. Phys Rev 1965, 140, A1133.

89. Becke, A.D. Phys Rev B 1988, 38, 3098.

90. Becke, A.D.; Roussel, M.R. Phys Rev A 1989, 39, 3761.

91. Lee, C.; Yang W.; Parr, R.G. Phys Rev B 1988, 37, 785.

92. Rappé, A.K.; Casewit, C.J.; Colwell, K.S.; Goddard III, W.A.; Skiff, W.M. J Am Chem Soc 1992, 114, 10024.

93. Peng, C.; Schlegel, H.; Israel B. J Chem 1993, 33, 449.

94. McQuarrie, D.A.; Statistical Thermodynamics; Harper & Row Publishers; NewYork, 1973.

95. Kresse G.; Furthmüller, J. Comp Mat Sci 1996, 6, 15.

96. Kresse G.; Joubert D. Phys Rev B 1999, 59, 1758.

97. Blöchl P.E. Phys Rev B 1994, 50, 17953.

98. Perdew J.P.; Chevary J. A.; Vosko S. H.; Jackson K.A.; Pederson M.R.; Singh D.J.; Fiolhais C. Phys Rev B 1992, 46, 6671.

99. Wang Y.; Perdew J.P. Phys Rev B 1991, 44, 13298.

100. Lindsay, R.; Wander, A.; Ernst, A.; Montanari, B.; Thornton, G.; Harrison, N.M. Phys Rev Lett 2005, 94, 246102.

101. Charlton, G.P.; Howes, B.C.; Nicklin, L.; Steadman, P.; Taylor, J.S.G.; Muryn, C.A.; Harte, S.P.; Mercer, J.; McGrath, R.; Norman, D.; Turner, T.S.; Thornton, G. Phys Rev Lett 1997, 78, 495.

102. Swamy, V.; Muscat, J.; Gale, J.D.; Harrison, N.M. Surf Sci 2002, 504, 115.

103. Allegretti, F.; O'Brien S.; Polcik, M.; Aayago, D.I.; Woodruff, D.P. Surf Sci 2006, 600, 1487.

104. Wong, M.W. Chem Phys Lett 1996, 256, 391.

105. Primet, M.; Pichat, P.; Mathieu, M-V. J Phys Chem 1971, 75, 1216.

106. Morterra, C. J Chem Soc Faraday Trans 1, 1988, 84, 1617.

107. Amores, J.M.G.; Escribano, V.S.; Ramis G.; Busca, G. Appl Catal B 1997, 13, 45.

108. Teramura, K.; Tanaka T.; Funabiki, T. Langmuir 2003, 19, 1209.

109. Schneider, H.; Tschudin, S.; Schneider, M.; Wokaun, A.; Baiker, A. J Catal 1994, 147, 5.

110. Lietti, L.; Ramis, G.; Berti, F.; Toledo, G.; Robba, D.; Busca, G.; Forzatti, P. Catal Today 1998, 42, 101.

111. Pilar, F.L. Elementary Quantum Chemistry, Courier Dover Publications, 2001.

112. Erdogan, R.; Fellah, M.F.; Onal, I. "An ONIOM and DFT Study of Water Adsorption on Rutile TiO_2 (110) Cluster", International Journal of Quantum Chemistry, Accepted, DOI 10.1002/qua.22400.

113. Erdogan, R.; Onal, I. "An ONIOM and DFT Study of Water and Ammonia Adsorption on Anatase TiO_2 (001) Cluster", International Journal of Quantum Chemistry, Accepted, DOI 10.1002/qua.22501.

114. Erdogan, R.; Ozbek, O.; Onal, I. "A Periodic DFT Study of Water and Ammonia Adsorption on Anatase TiO_2 (001) Slab", submitted to Surface Science.

APPENDIX A

INTRODUCTION BACKGROUND AND THEORY OF COMPUTATIONAL QUANTUM CHEMISTRY

First Principles of Quantum Chemistry

In quantum chemistry, molecules are expressed in terms of interactions among nuclei and electrons, and molecular geometry in terms of minimum energy arrangements of nuclei [73]. All quantum chemical methods trace back to *Schrödinger equation*, which for the special case of hydrogen atom may be solved exactly. In generalized form of Schrödinger equation, the positions of nuclei and electrons within a system are described by the wave function Ψ, which in principal can be found by solving the molecular Schrödinger equation:

$$\hat{H}\,\Psi = E\Psi \tag{A.1}$$

where $\hat{H}$ is the molecular Hamiltonian operator and E is an eigenvalue of $\hat{H}$, corresponding to total energy of the system. With the information of the positions of the nuclei and electrons, the true values for all the molecular properties of interest can be found. However, because the Schrödinger equation cannot be solved exactly for multi-electron atoms and molecules system, approximation methods are necessary. These approximations neglect or simplify a variety of intra- and inter-atomic interactions.

Relativistic effects are neglected, as they only matter for very heavy atoms where the electrons approach the speed of light. The molecular Hamiltonian operator can then be written as: [111]

$$\hat{H} = \hat{T}_n + \hat{V}_n + \hat{H}_e \tag{A.2}$$

where $\hat{T}_n$ represents the kinetic energy of the nuclei, $\hat{V}_n$ represents the potential energy of nuclear-nuclear repulsions, and $\hat{H}_e$ represents all the terms involving electrons:

$$\hat{H}_e = \hat{T}_e + \hat{V}_{n-e} + \hat{H}_{e-e} \tag{A.3}$$

Here $\hat{T}_e$ represents the kinetic energy of the electrons, $\hat{V}_{n-e}$ represents electron-nucleus attraction, and $\hat{H}_{e-e}$ represents the pair wise repulsion of electrons.

One way to simplify the Schrödinger equation for molecular systems is to assume that the nuclei do not move thereby separating $\hat{T}_n$ and $\hat{V}_n$ from the problem. The ability to study electrons in a field of stationary nuclei is based on the separation of timescales; electrons respond very fast (the speed of light) to the slow movements of nuclei. This is called Born-Oppenheimer approximation, and leads to an "electronic" Schrödinger equation. This approximation is generally good, although it does not hold when there are two electronic states with very similar energies, as then even small perturbations, such as electron-nucleus interactions, can be important.

The terms in the electronic Hamiltonian operator representing the kinetic energy of the electrons ($\hat{T}_e$) and the electron-nucleus attraction ($\hat{V}_{n-e}$) act on one electron at a time. The computational bottleneck is the pair wise repulsion of electrons, $\hat{H}_{e-e}$, which depends on the coordinates of two electrons at the same time.

The orbital approximation assumes that each electron moves in its own orbital. The electron-electron interactions are de-coupled by treating the interaction between one electron and all the others in an average way: each electron interacts

with the potential field caused by the average position of all the other electrons, i.e. the electrons are uncorrelated. This reduces the $\hat{H}_{e-e}$ term to an electric potential term $\hat{V}_e$. This approximation regarding uncorrelated electrons is a major limitation, leading to a "correlation error".

To find each electron orbital, the average electric potential due to all other electron orbitals has to be known, but initially none of these are known. Trial orbitals are used which are modified iteratively until a self-consistent field (SCF) is found. This is known as the Hartree-Fock (HF) method, the most common ab-initio method.

To find the wave function (Ψ) we express it as a linear combination of basis functions, which can be thought of as atomic orbitals, and search for the set of coefficients that gives the best combination. The HF method relies on the Variation Principle, which states that the SCF with the lowest energy is the most accurate approximation to the true wave function. The linear combination of basis functions that leads to the SCF with the lowest energy is the best approximation.

Perturbation theory

Correlation can be added as a perturbation from the Hartree-Fock wave function. This is called Møller-Plesset perturbation theory. In mapping the HF wave function onto a perturbation theory formulation, HF becomes a first-order perturbation. Thus, a minimal amount of correlation is added by using the second order MP2 method. Third order (MP3) and fourth-order (MP4) calculations are also common. Beyond MP2 the theory is not always convergent (precision does not always improve), although computational cost always increases. These "post-Hartree-Fock" calculations are very slow [72].

Coupled Cluster methods

Other post-Hartree-Fock methods for estimating electron correlation are the coupled cluster (CC) methods. These allow for correlation between clusters, or groups, of molecular orbitals. The abbreviations for these methods indicate the size of the clusters considered: Singles – S, Doubles – D, Triples – T, Quadruples – Q. For example, CCSD includes the correlation of electrons in each individual orbital, as well as the pair wise correlation of electrons in every possible pair of orbitals. This is roughly equivalent to what MP2 tries to estimate. CCSDT would also include contributions from all possible groupings of three molecular orbitals. The inclusion of all n levels of excitation for an n-electron system would give the exact solution of the Schrödinger equation, within the given basis set. However, because the number of possible groupings increases rapidly with the size of the group, these methods scale poorly as the number of excitations considered is increased, and it is very rare to exceed CCSDT. Parentheses in the acronym indicate that an effect is estimated with perturbation theory, e.g. CCSD(T). This particular level of theory is often called the "gold standard" of quantum chemistry because of its high accuracy and feasible computational cost, although, scaling as n^7 with the number of basis functions, even this can be unaffordable for large molecules.

Semi-empirical methods

Although they make approximations, ab-initio methods such as Hartree Fock use no empirical information, except for fundamental constants such as the mass of an electron. To calculate the repulsion between each electron and all the others, these ab-initio methods require the computation of many integrals. In contrast, semi-empirical methods neglect some integrals (the Zero Differential Overlap assumption) and other integrals are replaced with parameters rather than being calculated. These parameters have been determined empirically to fit the results to experimental data. Semi-empirical methods are much faster than ab-initio

methods, but are less accurate and require the atoms of interest to be parameterized in advance.

Density Functional Theory methods

Since the 1990s, Density Functional Theory (DFT) methods have often been used instead of post-Hartree-Fock methods to calculate the electron correlation. These methods work directly with electron density instead of with molecular wave functions. The Hartree-Fock (HF) methods described above try to calculate the exact energy of an approximate wave function. The energy is given exactly by the Hamiltonian operator, but the wave function cannot be found without the mean-field approximation. The wave function Ψ is a function of the positions (x_i, y_i, z_i) of each of the N electrons, and the energy E is a functional of Ψ:

$$E_{\text{exact}} (\Psi (x_1, y_1, z_1, x_2, y_2, z_2, \ldots, x_N, y_N, z_N)) \qquad \text{(A.4)}$$

Although the exact form of $E(\Psi)$ is known, it cannot be solved without approximation. In contrast, density functional methods calculate the energy, E, directly from the electron density of the ground state, ρ, without the need to approximate the wave function. However, the functional used to find the energy from the electron density is an approximation. According to the Hohenberg-Kohn theorem, the functional $E(\rho)$ does exist in principle; its exact form however is unknown. Instead, a variety of approximate functionals has been developed to give good agreement with experimental data and detailed quantum calculations at higher levels of theory. DFT calculations are therefore not strictly ab-initio.

In the Kohn-Sham formalism, the ground-state electronic energy, E, is written as a sum of the kinetic energy, E_T, the electron-nuclear interaction energy, E_V, the Coulomb energy, E_J, and the exchange/correlation energy, E_{XC}.

$$E = E_T + E_V + E_J + E_{XC} \qquad \text{(A.5)}$$

The preceding equation can be written in a more open way:

$$E_{e^-} = -\frac{1}{2}\sum_i \phi_i(\vec{r}_i)\nabla^2\phi_i(\vec{r}_i)d\vec{r}_i + \sum_A \int \frac{Z_A}{\left|\vec{R}_A - \vec{r}_1\right|}\rho(\vec{r}_i)d\vec{r}_i + \frac{1}{2}\int \frac{\rho(\vec{r}_i)\rho(\vec{r}_i)}{\left|\vec{r}_1 - \vec{r}_2\right|}d\vec{r}_1 d\vec{r}_2 + E_{xc}$$

(A.6)

Notice that there are only three variables, compared to *3N* for the HF method. For large molecules, this makes DFT methods much faster than HF methods of comparable accuracy. One disadvantage of DFT methods is the lack of systematic improvement: with the HF methods one could continually add another term to the perturbation or another excitation level to the cluster operator, until satisfied that the change it makes is small; with DFT, although some functionals are probably better than others, there is no way to guarantee convergence upon the true value by changing functionals.

APPENDIX B

SAMPLE INPUT AND OUTPUT FILES

To represent the calculations those are done in this study:

Gaussian input and output files of *vibrational frequency* calculation of optimized single H_2O molecule are given in Table B.1 and Table B.2, respectively.

Gaussian input files of *coordinate driving* calculation and *transition state* calculation of dissociative NH_3 adsorption on anatase TiO_2 (001) surface are given in Table B.3 and Table B.4, respectively.

Finally, VASP files (POSCAR, K-POINTS, INCAR, and POTCAR) for *volume relaxation* calculation of anatase TiO_2 are given in Tables B.5-B.8, respectively.

Table B.1 Gaussian input file of vibrational frequency calculation of optimized single H_2O molecule.

```
%chk=H2O-opt.chk
%mem=450MW
%nprocshared=4
# freq temperature=360 b3lyp/6-31g(d,p) nosymm geom=connectivity

Title Card Required

0 1
 O          -2.49838900   0.26054600   0.00000000
 H          -1.53428300   0.30905600   0.00000000
 H          -2.77449000   1.18554900   0.00000000

 1 2 1.0 3 1.0
 2
 3
```

Table B.2 Gaussian output file of vibrational frequency calculation of optimized single H_2O molecule.

```
Entering Gaussian System, Link 0=g03
 Initial command:
 /home_eymir/rerdogan/gauss_odtu/g03/l1.exe /data/tmp/Gau-24765.inp -
scrdir=/data/tmp/
 Entering Link 1 = /home_eymir/rerdogan/gauss_odtu/g03/l1.exe PID=
24766.

 Copyright (c) 1988,1990,1992,1993,1995,1998,2003,2004, Gaussian, Inc.
                All Rights Reserved.

 This is the Gaussian(R) 03 program.  It is based on the
 the Gaussian(R) 98 system (copyright 1998, Gaussian, Inc.),
 the Gaussian(R) 94 system (copyright 1995, Gaussian, Inc.),
 the Gaussian 92(TM) system (copyright 1992, Gaussian, Inc.),
 the Gaussian 90(TM) system (copyright 1990, Gaussian, Inc.),
 the Gaussian 88(TM) system (copyright 1988, Gaussian, Inc.),
 the Gaussian 86(TM) system (copyright 1986, Carnegie Mellon
 University), and the Gaussian 82(TM) system (copyright 1983,
 Carnegie Mellon University). Gaussian is a federally registered
 trademark of Gaussian, Inc.

 This software contains proprietary and confidential information,
 including trade secrets, belonging to Gaussian, Inc.

 This software is provided under written license and may be
 used, copied, transmitted, or stored only in accord with that
 written license.

 The following legend is applicable only to US Government
 contracts under FAR:

                RESTRICTED RIGHTS LEGEND

 Use, reproduction and disclosure by the US Government is
 subject to restrictions as set forth in subparagraphs (a)
 and (c) of the Commercial Computer Software - Restricted
 Rights clause in FAR 52.227-19.

 Gaussian, Inc.
 340 Quinnipiac St., Bldg. 40, Wallingford CT 06492


 ---------------------------------------------------------------
 Warning -- This program may not be used in any manner that
```

Table B.2 (cont'd)

```
competes with the business of Gaussian, Inc. or will provide
assistance to any competitor of Gaussian, Inc.  The licensee
of this program is prohibited from giving any competitor of
Gaussian, Inc. access to this program.  By using this program,
the user acknowledges that Gaussian, Inc. is engaged in the
business of creating and licensing software in the field of
computational chemistry and represents and warrants to the
licensee that it is not a competitor of Gaussian, Inc. and that
it will not use this program in any manner prohibited above.
-----------------------------------------------------------------


Cite this work as:
Gaussian 03, Revision D.01,
M. J. Frisch, G. W. Trucks, H. B. Schlegel, G. E. Scuseria,
M. A. Robb, J. R. Cheeseman, J. A. Montgomery, Jr., T. Vreven,
K. N. Kudin, J. C. Burant, J. M. Millam, S. S. Iyengar, J. Tomasi,
V. Barone, B. Mennucci, M. Cossi, G. Scalmani, N. Rega,
G. A. Petersson, H. Nakatsuji, M. Hada, M. Ehara, K. Toyota,
R. Fukuda, J. Hasegawa, M. Ishida, T. Nakajima, Y. Honda, O. Kitao,
H. Nakai, M. Klene, X. Li, J. E. Knox, H. P. Hratchian, J. B. Cross,
V. Bakken, C. Adamo, J. Jaramillo, R. Gomperts, R. E. Stratmann,
O. Yazyev, A. J. Austin, R. Cammi, C. Pomelli, J. W. Ochterski,
P. Y. Ayala, K. Morokuma, G. A. Voth, P. Salvador, J. J. Dannenberg,
V. G. Zakrzewski, S. Dapprich, A. D. Daniels, M. C. Strain,
O. Farkas, D. K. Malick, A. D. Rabuck, K. Raghavachari,
J. B. Foresman, J. V. Ortiz, Q. Cui, A. G. Baboul, S. Clifford,
J. Cioslowski, B. B. Stefanov, G. Liu, A. Liashenko, P. Piskorz,
I. Komaromi, R. L. Martin, D. J. Fox, T. Keith, M. A. Al-Laham,
C. Y. Peng, A. Nanayakkara, M. Challacombe, P. M. W. Gill,
B. Johnson, W. Chen, M. W. Wong, C. Gonzalez, and J. A. Pople,
Gaussian, Inc., Wallingford CT, 2004.

****************************************
Gaussian 03:  IA32L-G03RevD.01 13-Oct-2005
              4-Nov-2009
****************************************
%chk=H2O-opt.chk
%mem=450MW
%nprocshared=4
Will use up to    4 processors via shared memory.
-----------------------------------------------------------------
# freq temperature=360 b3lyp/6-31g(d,p) nosymm geom=connectivity
-----------------------------------------------------------------
1/10=4,30=1,38=1,57=2,111=360000/1,3;
2/15=1,17=6,18=5,40=1/2;
```

Table B.2 (cont'd)

```
 3/5=1,6=6,7=101,11=2,16=1,25=1,30=1,74=-5/1,2,3;
 4//1;
 5/5=2,38=5/2;
 8/6=4,10=90,11=11/1;
 11/6=1,8=1,9=11,15=111,16=1,31=1/1,2,10;
 10/6=1,31=1/2;
 6/7=2,8=2,9=2,10=2,18=1,28=1/1;
 7/8=1,10=1,25=1,30=1/1,2,3,16;
 1/10=4,30=1/3;
 99//99;
 ------------------
 Title Card Required
 ------------------
 Symbolic Z-matrix:
 Charge =  0 Multiplicity = 1
 O                -2.49839   0.26055   0.
 H                -1.53428   0.30906   0.
 H                -2.77449   1.18555   0.


GradGradGradGradGradGradGradGradGradGradGradGradGradGradGradGrad
 Berny optimization.
 Initialization pass.
 Trust Radius=3.00D-01 FncErr=1.00D-07 GrdErr=1.00D-07
 Number of steps in this run=   2 maximum allowed number of steps=   2.

GradGradGradGradGradGradGradGradGradGradGradGradGradGradGradGrad

                     Input orientation:
 ---------------------------------------------------------------------
 Center     Atomic     Atomic              Coordinates (Angstroms)
 Number     Number      Type              X           Y           Z
 ---------------------------------------------------------------------
   1          8           0       -2.498389    0.260546    0.000000
   2          1           0       -1.534283    0.309056    0.000000
   3          1           0       -2.774490    1.185549    0.000000
 ---------------------------------------------------------------------
               Distance matrix (angstroms):
                    1          2          3
    1  O    0.000000
    2  H    0.965326   0.000000
    3  H    0.965330   1.518668   0.000000
Symmetry turned off by external request.
 Stoichiometry    H2O
 Framework group  CS[SG(H2O)]
```

Table B.2 (cont'd)

```
 Deg. of freedom     3
 Full point group                 CS
 Rotational constants (GHZ):    794.6747273    434.8467193    281.0538190
 Standard basis: 6-31G(d,p) (6D, 7F)
 Integral buffers will be    262144 words long.
 Raffenetti 2 integral format.
 Two-electron integral symmetry is turned off.
    25 basis functions,    42 primitive gaussians,    25 cartesian basis functions
     5 alpha electrons        5 beta electrons
       nuclear repulsion energy         9.1193905001 Hartrees.
 NAtoms=    3 NActive=    3 NUniq=    3 SFac= 7.50D-01 NAtFMM=   80
NAOKFM=F Big=F
 One-electron integrals computed using PRISM.
 NBasis=    25 RedAO= T  NBF=    25
 NBsUse=    25 1.00D-06 NBFU=    25
 Harris functional with IExCor=  402 diagonalized for initial guess.
 ExpMin= 1.61D-01 ExpMax= 5.48D+03 ExpMxC= 8.25D+02 IAcc=1
IRadAn=         1 AccDes= 1.00D-06
 HarFok:  IExCor= 402 AccDes= 1.00D-06 IRadAn=         1 IDoV=1
 ScaDFX=  1.000000  1.000000  1.000000  1.000000
 Requested convergence on RMS density matrix=1.00D-08 within 128 cycles.
 Requested convergence on MAX density matrix=1.00D-06.
 Requested convergence on             energy=1.00D-06.
 No special actions if energy rises.
 Keep R1 integrals in memory in canonical form, NReq=     1771596.
 Integral accuracy reduced to 1.0D-05 until final iterations.
 Initial convergence to 1.0D-05 achieved.  Increase integral accuracy.
 SCF Done:  E(RB+HF-LYP) =  -76.4197371213     A.U. after    9 cycles
            Convg  =    0.4819D-08             -V/T =  2.0078
            S**2   =   0.0000
 Range of M.O.s used for correlation:     1    25
 NBasis=    25 NAE=     5 NBE=     5 NFC=     0 NFV=     0
 NROrb=     25 NOA=     5 NOB=     5 NVA=    20 NVB=    20
 Symmetrizing basis deriv contribution to polar:
 IMax=3 JMax=2 DiffMx= 0.00D+00
 G2DrvN: will do    4 centers at a time, making    1 passes doing MaxLOS=2.
 FoFDir/FoFCou used for L=0 through L=2.
 DoAtom=TTT
          Differentiating once with respect to electric field.
               with respect to dipole field.
          Differentiating once with respect to nuclear coordinates.
          Store integrals in memory, NReq=      873587.
There are  12 degrees of freedom in the 1st order CPHF.
    9 vectors were produced by pass  0.
 AX will form   9 AO Fock derivatives at one time.
    9 vectors were produced by pass  1.
```

Table B.2 (cont'd)

```
    9 vectors were produced by pass  2.
    9 vectors were produced by pass  3.
    7 vectors were produced by pass  4.
    4 vectors were produced by pass  5.
 Inv2:  IOpt= 1 Iter= 1 AM= 4.70D-16 Conv= 1.00D-12.
 Inverted reduced A of dimension   47 with in-core refinement.
 Isotropic polarizability for W=    0.000000        5.35 Bohr**3.
 End of Minotr Frequency-dependent properties file   721 does not exist.

 ******************************************************************
          Population analysis using the SCF density.

 ******************************************************************

 Alpha  occ. eigenvalues --  -19.13801  -0.99731  -0.51498  -0.37102  -0.29196
 Alpha virt. eigenvalues --    0.06534   0.15122   0.75684   0.80551   0.89135
 Alpha virt. eigenvalues --    0.89353   1.01557   1.17538   1.52951   1.53765
 Alpha virt. eigenvalues --    1.64363   2.23869   2.26821   2.45005   2.64098
 Alpha virt. eigenvalues --    2.66677   3.02783   3.30718   3.53153   3.69289
        Condensed to atoms (all electrons):
             1         2         3
    1  O    8.041971   0.283940   0.283940
    2  H    0.283940   0.439602  -0.028468
    3  H    0.283940  -0.028468   0.439603
 Mulliken atomic charges:
             1
    1  O   -0.609851
    2  H    0.304925
    3  H    0.304926
 Sum of Mulliken charges=   0.00000
 Atomic charges with hydrogens summed into heavy atoms:
             1
    1  O    0.000000
    2  H    0.000000
    3  H    0.000000
 Sum of Mulliken charges=   0.00000
 APT atomic charges:
             1
    1  O   -0.481533
    2  H    0.240765
   3  H    0.240768
 Sum of APT charges=   0.00000
 APT Atomic charges with hydrogens summed into heavy atoms:
             1
    1  O    0.000000
```

Table B.2 (cont'd)

```
    2  H    0.000000
    3  H    0.000000
 Sum of APT charges=   0.00000
 Electronic spatial extent (au):  <R**2>=   237.8347
 Charge=     0.0000 electrons
 Dipole moment (field-independent basis, Debye):
    X=     1.1791    Y=     1.6684    Z=     0.0000  Tot=     2.0429
 Quadrupole moment (field-independent basis, Debye-Ang):
   XX=   -10.5855   YY=    -4.2224   ZZ=    -7.1378
   XY=    -4.4226   XZ=     0.0000   YZ=     0.0000
 Traceless Quadrupole moment (field-independent basis, Debye-Ang):
   XX=    -3.2703   YY=     3.0929   ZZ=     0.1774
   XY=    -4.4226   XZ=     0.0000   YZ=     0.0000
 Octapole moment (field-independent basis, Debye-Ang**2):
  XXX=    57.8778  YYY=    -3.5677  ZZZ=     0.0000  XYY=     9.6006
  XXY=    10.2208  XXZ=     0.0000  XZZ=    17.5139  YZZ=    -2.3114
  YYZ=     0.0000  XYZ=     0.0000
 Hexadecapole moment (field-independent basis, Debye-Ang**3):
 XXXX=  -260.9400 YYYY=    -7.3490 ZZZZ=    -5.1254 XXXY=   -19.4142
 XXXZ=     0.0000 YYYX=     7.9614 YYYZ=     0.0000 ZZZX=     0.0000
 ZZZY=     0.0000 XXYY=   -24.3018 XXZZ=   -45.0390 YYZZ=    -2.7529
 XXYZ=     0.0000 YYXZ=     0.0000 ZZXY=     5.7578
 N-N= 9.119390500099D+00 E-N=-1.988497441065D+02  KE=
7.582636293535D+01
  Exact polarizability:   6.860  -0.920   6.209   0.000   0.000   2.994
 Approx polarizability:   8.445  -1.035   7.712   0.000   0.000   3.295
 Full mass-weighted force constant matrix:
 Low frequencies ---  -44.9705  -33.5976   -0.0012   -0.0005    0.0010   32.9914
 Low frequencies --- 1664.8733 3799.6572 3912.8604
 Diagonal vibrational polarizability:
       0.2521340       0.4691807       0.0000000
 Harmonic frequencies (cm**-1), IR intensities (KM/Mole), Raman scattering
 activities (A**4/AMU), depolarization ratios for plane and unpolarized
 incident light, reduced masses (AMU), force constants (mDyne/A),
 and normal coordinates:
                      1                 2                 3
                     A'                A'                A'
 Frequencies --  1664.8733          3799.6572          3912.8604
 Red. masses --     1.0827             1.0452             1.0811
 Frc consts  --     1.7681             8.8905             9.7522
 IR Inten    --    70.3204             1.6388            20.2112
  Atom AN      X      Y      Z        X      Y      Z        X      Y      Z
   1   8     0.04   0.06   0.00    -0.03  -0.04   0.00     0.06  -0.04   0.00
   2   1     0.03  -0.70   0.00     0.70  -0.01   0.00    -0.71  -0.04   0.00
   3   1    -0.67  -0.21   0.00    -0.25   0.66   0.00    -0.20   0.67   0.00
```

Table B.2 (cont'd)

```
------------------
 - Thermochemistry -
 ------------------
 Temperature   360.000 Kelvin.  Pressure   1.00000 Atm.
 Atom  1 has atomic number  8 and mass  15.99491
 Atom  2 has atomic number  1 and mass   1.00783
 Atom  3 has atomic number  1 and mass   1.00783
 Molecular mass:    18.01056 amu.
 Principal axes and moments of inertia in atomic units:
                      1        2        3
    EIGENVALUES --    2.27104   4.15029   6.42134
          X           0.81664   0.57715   0.00000
          Y          -0.57715   0.81664   0.00000
          Z           0.00000   0.00000   1.00000
 This molecule is an asymmetric top.
 Rotational symmetry number  1.
 Rotational temperatures (Kelvin)     38.13833    20.86933    13.48844
 Rotational constants (GHZ):         794.67473   434.84672   281.05382
 Zero-point vibrational energy      56089.3 (Joules/Mol)
                                    13.40565 (Kcal/Mol)
 Vibrational temperatures:   2395.38  5466.85  5629.73
        (Kelvin)

 Zero-point correction=                          0.021363 (Hartree/Particle)
 Thermal correction to Energy=                   0.024793
 Thermal correction to Enthalpy=                 0.025933
 Thermal correction to Gibbs Free Energy=       -0.001608
 Sum of electronic and zero-point Energies=          -76.398374
 Sum of electronic and thermal Energies=             -76.394944
 Sum of electronic and thermal Enthalpies=           -76.393804
 Sum of electronic and thermal Free Energies=        -76.421345

                    E (Thermal)             CV                S
                     KCal/Mol       Cal/Mol-Kelvin    Cal/Mol-Kelvin
 Total                15.558            6.076            48.006
 Electronic            0.000            0.000             0.000
 Translational         1.073            2.981            35.545
 Rotational            1.073            2.981            12.442
 Vibrational          13.412            0.114             0.020
                           Q         Log10(Q)           Ln(Q)
 Total Bot       0.409655D+01         0.612418          1.410145
 Total V=0       0.563104D+09         8.750589         20.148975
 Vib (Bot)       0.728433D-08        -8.137610        -18.737540
 Vib (V=0)       0.100129D+01         0.000560          0.001290
 Electronic      0.100000D+01         0.000000          0.000000
 Translational   0.481299D+07         6.682415         15.386830
 Rotational      0.116846D+03         2.067613          4.760854
```

Table B.2 (cont'd)

```
---------------------------------------------------------------------
Center     Atomic                   Forces (Hartrees/Bohr)
Number     Number           X              Y              Z
---------------------------------------------------------------------
   1         8          0.000000904   -0.000000790    0.000000000
   2         1          0.000001138    0.000001917    0.000000000
   3         1         -0.000002042   -0.000001127    0.000000000
---------------------------------------------------------------------
Cartesian Forces:  Max     0.000002042 RMS     0.000001148
---------------------------------------------------------------------

 Internal Coordinate Forces (Hartree/Bohr or radian)
Cent Atom N1     Length/X     N2     Alpha/Y      N3      Beta/Z       J
---------------------------------------------------------------------------
 1  O        0.000001(   1)    -0.000001(   4)     0.000000(   7)
 2  H        0.000001(   2)     0.000002(   5)     0.000000(   8)
 3  H       -0.000002(   3)    -0.000001(   6)     0.000000(   9)
---------------------------------------------------------------------------
Internal  Forces:  Max     0.000002042 RMS     0.000001148

GradGradGradGradGradGradGradGradGradGradGradGradGradGradGradGrad
 Berny optimization.
 Search for a local minimum.
 Step number   1 out of a maximum of   2
 All quantities printed in internal units (Hartrees-Bohrs-Radians)
 Second derivative matrix not updated -- analytic derivatives used.
 The second derivative matrix:
                       X1        Y1        Z1        X2        Y2
            X1          0.59930
            Y1         -0.10050   0.52802
            Z1          0.00000   0.00000  -0.00001
            X2         -0.51737   0.00538   0.00000   0.53501
            Y2         -0.05903  -0.04637   0.00000   0.00658   0.04968
            Z2          0.00000   0.00000  -0.00005   0.00000   0.00000
            X3         -0.08193   0.09513   0.00000  -0.01764   0.05244
            Y3          0.15953  -0.48165   0.00000  -0.01196  -0.00330
            Z3          0.00000   0.00000   0.00006   0.00000   0.00000
                       Z2        X3        Y3        Z3
            Z2          0.00004
            X3          0.00000   0.09957
            Y3          0.00000  -0.14757   0.48495
            Z3          0.00001   0.00000   0.00000  -0.00007
    Eigenvalues ---    0.15519   0.77660   0.96943
 Angle between quadratic step and forces=  78.98 degrees.
 Linear search not attempted -- first point.
 TrRot=  0.000000  0.000000  0.000000  0.000000  0.000000  0.000000
 Variable       Old X    -DE/DX   Delta X   Delta X   Delta X     New X
```

Table B.2 (cont'd)

		(Linear)	(Quad)	(Total)		
X1	-4.72127	0.00000	0.00000	0.00000	0.00000	-4.72127
Y1	0.49236	0.00000	0.00000	0.00000	0.00000	0.49236
Z1	0.00000	0.00000	0.00000	0.00000	0.00000	0.00000
X2	-2.89937	0.00000	0.00000	0.00000	0.00000	-2.89937
Y2	0.58403	0.00000	0.00000	0.00000	0.00000	0.58403
Z2	0.00000	0.00000	0.00000	0.00000	0.00000	0.00000
X3	-5.24303	0.00000	0.00000	0.00000	0.00000	-5.24303
Y3	2.24036	0.00000	0.00000	0.00000	0.00000	2.24036
Z3	0.00000	0.00000	0.00000	0.00000	0.00000	0.00000

Item Value Threshold Converged?
Maximum Force 0.000002 0.000450 YES
RMS Force 0.000001 0.000300 YES
Maximum Displacement 0.000001 0.001800 YES
RMS Displacement 0.000001 0.001200 YES
Predicted change in Energy=-3.102891D-13
Optimization completed.
-- Stationary point found.

GradGradGradGradGradGradGradGradGradGradGradGradGradGradGradGrad

1\1\GINC-OAR23\Freq\RB3LYP\6-31G(d,p)\H2O1\RERDOGAN\04-Nov-2009\0\\# f
req temperature=360 b3lyp/6-31g(d,p) nosymm geom=connectivity\\Title C
ard Required\\0,1\O,-2.498389,0.260546,0.\H,-1.534283,0.309056,0.\H,-2
.77449,1.185549,0.\\Version=IA32L-G03RevD.01\HF=
76.4197371\RMSD=4.819 e-09\RMSF=1.148e
06\ZeroPoint=0.0213633\Thermal=0.0247932\Dipole=0.463
8825,0.6563812,0.\DipoleDeriv=-0.3794449,0.039338,0.,0.0393324,-0.3515
819,0.,0.,0.,-0.7135713,0.0917415,-0.0380802,0.,-0.0706459,0.2737674,0
.,0.,0.,0.3567855,0.2877034,-0.0012577,0.,0.0313135,0.0778145,0.,0.,0.
,0.3567858\Polar=6.8604279,-0.9195736,6.2091445,0.,0.,2.993667\PG=CS [
SG(H2O1)]\NImag=0\\0.59930367,-0.10050227,0.52802406,0.,0.,-0.00001418
,-0.51737323,0.00537533,0.,0.53501296,-0.05902527,-0.04637402,0.,0.006
58223,0.04967730,0.,0.,-0.00004804,0.,0.,0.00003777,-0.08193044,0.0951
2694,0.,-0.01763973,0.05244303,0.,0.09957016,0.15952754,-0.48165003,0.
,-0.01195756,-0.00330327,0.,-0.14756998,0.48495331,0.,0.,0.00006222,0.
,0.,0.00001027,0.,0.,-0.00007249\\-0.00000090,0.00000079,0.,-0.0000011
4,-0.00000192,0.,0.00000204,0.00000113,0.\\\@
IF AT FIRST YOU DON'T SUCCEED, TRY LOOKING IN
THE WASTEBASKET FOR THE DIRECTIONS.
Job cpu time: 0 days 0 hours 2 minutes 55.9 seconds.
File lengths (MBytes): RWF= 11 Int= 0 D2E= 0 Chk= 4 Scr= 1
Normal termination of Gaussian 03 at Wed Nov 4 15:34:03 2009.

Table B.3 Gaussian input file for coordinate driving calculation of dissociative NH_3 adsorption on anatase TiO_2 (001) surface. (The output "relative energy profile" is shown in Figure 4.10).

```
%chk=anatase-3x-3y-3z-001-2ti.chk
%mem=400MW
%nprocshared=2
# opt=(modredundant,loose,maxcycle=1000) oniom(b3lyp/6-
31g(d,p):uff)
nosymm geom=connectivity scf=(maxcycle=2000,conver=4)

Title Card Required

0 1 0 1 0 1
 Ti-              -1   -3.780277   -5.678187   -0.870925 L
 Ti-Ti3+4         -1   -1.887277   -5.678187    1.507075 L
 O-O_3            -1   -3.780277   -5.678187    1.094075 L
 O-O_3            -1   -1.887277   -5.678187   -0.458925 L
 O-O_3            -1   -1.887277   -3.786187    1.920075 L
 Ti-Ti3+4         -1    0.004723   -5.678187   -0.870925 L H-H_21 0
 Ti-Ti3+4         -1    1.897723   -5.678187    1.507075 L
 O-O_3            -1    0.004723   -5.678187    1.094075 L
 O-O_3            -1    1.897723   -5.678187   -0.458925 L
 O-O_3            -1    1.897723   -3.786187    1.920075 L
 Ti-              -1    3.789723   -5.678187   -0.870925 L
 O-O_3            -1    3.789723   -5.678187    1.094075 L
 Ti-Ti3+4         -1   -3.780277   -1.893187   -0.870925 L H-H_17 0
 Ti-              -1   -1.887277   -1.893187    1.507075 L H-H_22 0
 O-O_3            -1   -3.780277   -3.786187   -1.283925 L
 O-O_3            -1   -3.780277   -1.893187    1.094075 L
 O-O_3            -1   -1.887277   -1.893187   -0.458925 H
 O-O_3            -1   -1.887277   -0.001187    1.920075 L
 Ti-               0    0.004090   -1.920835   -0.889064 H
 Ti-              -1    1.897723   -1.893187    1.507075 L H-H_22 0
 O-O_3            -1    0.004723   -3.786187   -1.283925 H
 O-O_3            -1    0.004723   -1.893187    1.094075 H
 O-O_3            -1    1.897723   -1.893187   -0.458925 H
 O-O_3            -1    1.897723   -0.001187    1.920075 L
 Ti-Ti3+4         -1    3.789723   -1.893187   -0.870925 L H-H_22 0
 O-O_3            -1    3.789723   -3.786187   -1.283925 L
 O-O_3            -1    3.789723   -1.893187    1.094075 L
 Ti-Ti3+4         -1   -3.780277    1.891813   -0.870925 L H-H_32 0
 Ti-              -1   -1.887277    1.891813    1.507075 L H-H_37 0
 O-O_3            -1   -3.780277   -0.001187   -1.283925 L
 O-O_3            -1   -3.780277    1.891813    1.094075 L
 O-O_3            -1   -1.887277    1.891813   -0.458925 H
 O-O_3            -1   -1.887277    3.783813    1.920075 L
 Ti-               0    0.004453    1.899084   -0.834613 H
 Ti-              -1    1.897723    1.891813    1.507075 L H-H_37 0
 O-O_3             0    0.002857    0.112321   -1.284824 H
 O-O_3            -1    0.004723    1.891813    1.094075 H
 O-O_3            -1    1.897723    1.891813   -0.458925 H
 O-O_3            -1    1.897723    3.783813    1.920075 L
```

Table B.3 (cont'd)

```
Ti-Ti3+4        -1    3.789723    1.891813   -0.870925 L H-H_38 0
O-O_3           -1    3.789723   -0.001187   -1.283925 L
O-O_3           -1    3.789723    1.891813    1.094075 L
Ti-             -1   -3.780277    5.676813   -0.870925 L
Ti-Ti3+4        -1   -1.887277    5.676813    1.507075 L
O-O_3           -1   -3.780277    3.783813   -1.283925 L
O-O_3           -1   -3.780277    5.676813    1.094075 L
O-O_3           -1   -1.887277    5.676813   -0.458925 L
Ti-Ti3+4        -1    0.004723    5.676813   -0.870925 L H-H_50 0
Ti-Ti3+4        -1    1.897723    5.676813    1.507075 L
O-O_3           -1    0.004723    3.783813   -1.283925 H
O-O_3           -1    0.004723    5.676813    1.094075 L
O-O_3           -1    1.897723    5.676813   -0.458925 L
Ti-             -1    3.789723    5.676813   -0.870925 L
O-O_3           -1    3.789723    3.783813   -1.283925 L
O-O_3           -1    3.789723    5.676813    1.094075 L
N-N_3            0    0.076971   -1.773815   -3.107569 H
H-H_             0    0.011323   -2.685768   -3.551398 H
H-H_             0    0.953207   -1.318295   -3.348198 H
H-H_             0   -0.679341   -1.160896   -3.399117 H

1 3 1.0 4 1.0 15 1.0
2 3 1.0 4 1.0 5 1.0 8 1.0
3
4 6 1.0
5 14 1.0
6 8 1.0 9 1.0 21 1.0
7 8 1.0 9 1.0 10 1.0 12 1.0
8
9 11 1.0
10 20 1.0
11 12 1.0 26 1.0
12
13 15 1.0 16 1.0 17 1.0 30 1.0
14 16 1.0 17 1.0 18 1.0 22 1.0
15
16
17 19 1.0
18 29 1.0
19 21 1.0 22 1.0 23 1.0 36 1.0
20 22 1.0 23 1.0 24 1.0 27 1.0
21
22
23 25 1.0
24 35 1.0
25 26 1.0 27 1.0 41 1.0
26
27
28 30 1.0 31 1.0 32 1.0 45 1.0
29 31 1.0 32 1.0 33 1.0 37 1.0
30
31
32 34 1.0
33 44 1.0
34 36 1.0 37 1.0 38 1.0 50 1.0
35 37 1.0 38 1.0 39 1.0 42 1.0
```

Table B.3 (cont'd)

```
 36
 37
 38 40 1.0
 39 49 1.0
 40 41 1.0 42 1.0 54 1.0
 41
 42
 43 45 1.0 46 1.0 47 1.0
 44 46 1.0 47 1.0 51 1.0
 45
 46
 47 48 1.0
 48 50 1.0 51 1.0 52 1.0
 49 51 1.0 52 1.0 55 1.0
 50
 51
 52 53 1.0
 53 54 1.0 55 1.0
 54
 55
 56 57 1.0 58 1.0 59 1.0
 57
 58
 59

B 59 36 S 40 -0.041000
```

Table B.4 Gaussian input file for transition state calculation of dissociative NH_3 adsorption on anatase TiO_2 (001) surface. (The output "transition state" point and its geometry can be seen in Figure 4.10 and Figure 4.11 (b), respectively).

```
%chk=anatase-3x-3y-3z-001-2tiqst3TS.chk
%mem=400MW
%nprocshared=2
# opt=(qst3,calcfc,noeigentest,newton,maxcycle=2000,loose) freq
oniom(b3lyp/6-31g(d,p):uff)
nosymm geom=connectivity scf=(maxcycle=2000,conver=9)

Initial Geometry

0 1 0 1 0 1
 Ti-              -1   -3.780277   -5.678187   -0.870925 L
 Ti-Ti3+4         -1   -1.887277   -5.678187    1.507075 L
 O-O_3            -1   -3.780277   -5.678187    1.094075 L
 O-O_3            -1   -1.887277   -5.678187   -0.458925 L
 O-O_3            -1   -1.887277   -3.786187    1.920075 L
 Ti-Ti3+4         -1    0.004723   -5.678187   -0.870925 L H-H_21 0
 Ti-Ti3+4         -1    1.897723   -5.678187    1.507075 L
 O-O_3            -1    0.004723   -5.678187    1.094075 L
 O-O_3            -1    1.897723   -5.678187   -0.458925 L
 O-O_3            -1    1.897723   -3.786187    1.920075 L
 Ti-              -1    3.789723   -5.678187   -0.870925 L
 O-O_3            -1    3.789723   -5.678187    1.094075 L
 Ti-Ti3+4         -1   -3.780277   -1.893187   -0.870925 L H-H_17 0
 Ti-              -1   -1.887277   -1.893187    1.507075 L H-H_22 0
 O-O_3            -1   -3.780277   -3.786187   -1.283925 L
 O-O_3            -1   -3.780277   -1.893187    1.094075 L
 O-O_3            -1   -1.887277   -1.893187   -0.458925 H
 O-O_3            -1   -1.887277   -0.001187    1.920075 L
 Ti-               0    0.004090   -1.920835   -0.889064 H
 Ti-              -1    1.897723   -1.893187    1.507075 L H-H_22 0
 O-O_3            -1    0.004723   -3.786187   -1.283925 H
 O-O_3            -1    0.004723   -1.893187    1.094075 H
 O-O_3            -1    1.897723   -1.893187   -0.458925 H
 O-O_3            -1    1.897723   -0.001187    1.920075 L
 Ti-Ti3+4         -1    3.789723   -1.893187   -0.870925 L H-H_23 0
 O-O_3            -1    3.789723   -3.786187   -1.283925 L
 O-O_3            -1    3.789723   -1.893187    1.094075 L
 Ti-Ti3+4         -1   -3.780277    1.891813   -0.870925 L H-H_32 0
 Ti-              -1   -1.887277    1.891813    1.507075 L H-H_37 0
 O-O_3            -1   -3.780277   -0.001187   -1.283925 L
 O-O_3            -1   -3.780277    1.891813    1.094075 L
 O-O_3            -1   -1.887277    1.891813   -0.458925 H
 O-O_3            -1   -1.887277    3.783813    1.920075 L
 Ti-               0    0.004453    1.899084   -0.834613 H
 Ti-              -1    1.897723    1.891813    1.507075 L H-H_37 0
 O-O_3             0    0.002857    0.112321   -1.284824 H
 O-O_3            -1    0.004723    1.891813    1.094075 H
 O-O_3            -1    1.897723    1.891813   -0.458925 H
 O-O_3            -1    1.897723    3.783813    1.920075 L
```

Table B.4 (cont'd)

```
Ti-Ti3+4        -1    3.789723    1.891813   -0.870925 L H-H_38 0
O-O_3           -1    3.789723   -0.001187   -1.283925 L
O-O_3           -1    3.789723    1.891813    1.094075 L
Ti-             -1   -3.780277    5.676813   -0.870925 L
Ti-Ti3+4        -1   -1.887277    5.676813    1.507075 L
O-O_3           -1   -3.780277    3.783813   -1.283925 L
O-O_3           -1   -3.780277    5.676813    1.094075 L
O-O_3           -1   -1.887277    5.676813   -0.458925 L
Ti-Ti3+4        -1    0.004723    5.676813   -0.870925 L H-H_50 0
Ti-Ti3+4        -1    1.897723    5.676813    1.507075 L
O-O_3           -1    0.004723    3.783813   -1.283925 H
O-O_3           -1    0.004723    5.676813    1.094075 L
O-O_3           -1    1.897723    5.676813   -0.458925 L
Ti-             -1    3.789723    5.676813   -0.870925 L
O-O_3           -1    3.789723    3.783813   -1.283925 L
O-O_3           -1    3.789723    5.676813    1.094075 L
N-N_3            0    0.076971   -1.773815   -3.107569 H
H-H_             0    0.011323   -2.685768   -3.551398 H
H-H_             0    0.953207   -1.318295   -3.348198 H
H-H_             0   -0.679341   -1.160896   -3.399117 H

1 3 1.0 4 1.0 15 1.0
2 3 1.0 4 1.0 5 1.0 8 1.0
3
4 6 1.0
5 14 1.0
6 8 1.0 9 1.0 21 1.0
7 8 1.0 9 1.0 10 1.0 12 1.0
8
9 11 1.0
10 20 1.0
11 12 1.0 26 1.0
12
13 15 1.0 16 1.0 17 1.0 30 1.0
14 16 1.0 17 1.0 18 1.0 22 1.0
15
16
17 19 1.0
18 29 1.0
19 21 1.0 22 1.0 23 1.0 36 1.0
20 22 1.0 23 1.0 24 1.0 27 1.0
21
22
23 25 1.0
24 35 1.0
25 26 1.0 27 1.0 41 1.0
26
27
28 30 1.0 31 1.0 32 1.0 45 1.0
29 31 1.0 32 1.0 33 1.0 37 1.0
30
31
32 34 1.0
33 44 1.0
34 36 1.0 37 1.0 38 1.0 50 1.0
35 37 1.0 38 1.0 39 1.0 42 1.0
```

Table B.4 (cont'd)

```
 36
 37
 38 40 1.0
 39 49 1.0
 40 41 1.0 42 1.0 54 1.0
 41
 42
 43 45 1.0 46 1.0 47 1.0
 44 46 1.0 47 1.0 51 1.0
 45
 46
 47 48 1.0
 48 50 1.0 51 1.0 52 1.0
 49 51 1.0 52 1.0 55 1.0
 50
 51
 52 53 1.0
 53 54 1.0 55 1.0
 54
 55
 56 57 1.0 58 1.0 59 1.0
 57
 58
 59

Equilibrium Geometry

0 1 0 1 0 1
 Ti-             -1   -3.780277   -5.678187   -0.870925 L
 Ti-Ti3+4        -1   -1.887277   -5.678187    1.507075 L
 O-O_3           -1   -3.780277   -5.678187    1.094075 L
 O-O_3           -1   -1.887277   -5.678187   -0.458925 L
 O-O_3           -1   -1.887277   -3.786187    1.920075 L
 Ti-Ti3+4        -1    0.004723   -5.678187   -0.870925 L H-H_21 0
 Ti-Ti3+4        -1    1.897723   -5.678187    1.507075 L
 O-O_3           -1    0.004723   -5.678187    1.094075 L
 O-O_3           -1    1.897723   -5.678187   -0.458925 L
 O-O_3           -1    1.897723   -3.786187    1.920075 L
 Ti-             -1    3.789723   -5.678187   -0.870925 L
 O-O_3           -1    3.789723   -5.678187    1.094075 L
 Ti-Ti3+4        -1   -3.780277   -1.893187   -0.870925 L H-H_17 0
 Ti-             -1   -1.887277   -1.893187    1.507075 L H-H_22 0
 O-O_3           -1   -3.780277   -3.786187   -1.283925 L
 O-O_3           -1   -3.780277   -1.893187    1.094075 L
 O-O_3           -1   -1.887277   -1.893187   -0.458925 H
 O-O_3           -1   -1.887277   -0.001187    1.920075 L
 Ti-              0    0.005075   -2.122250   -0.861672 H
 Ti-             -1    1.897723   -1.893187    1.507075 L H-H_22 0
 O-O_3           -1    0.004723   -3.786187   -1.283925 H
 O-O_3           -1    0.004723   -1.893187    1.094075 H
 O-O_3           -1    1.897723   -1.893187   -0.458925 H
 O-O_3           -1    1.897723   -0.001187    1.920075 L
 Ti-Ti3+4        -1    3.789723   -1.893187   -0.870925 L H-H_23 0
 O-O_3           -1    3.789723   -3.786187   -1.283925 L
 O-O_3           -1    3.789723   -1.893187    1.094075 L
 Ti-Ti3+4        -1   -3.780277    1.891813   -0.870925 L H-H_32 0
```

Table B.4 (cont'd)

```
Ti-              -1   -1.887277    1.891813    1.507075 L H-H_37 0
O-O_3            -1   -3.780277   -0.001187   -1.283925 L
O-O_3            -1   -3.780277    1.891813    1.094075 L
O-O_3            -1   -1.887277    1.891813   -0.458925 H
O-O_3            -1   -1.887277    3.783813    1.920075 L
Ti-               0    0.005327    2.103799   -0.912863 H
Ti-              -1    1.897723    1.891813    1.507075 L H-H_37 0
O-O_3             0    0.007377    1.341705   -2.503577 H
O-O_3            -1    0.004723    1.891813    1.094075 H
O-O_3            -1    1.897723    1.891813   -0.458925 H
O-O_3            -1    1.897723    3.783813    1.920075 L
Ti-Ti3+4         -1    3.789723    1.891813   -0.870925 L H-H_38 0
O-O_3            -1    3.789723   -0.001187   -1.283925 L
O-O_3            -1    3.789723    1.891813    1.094075 L
Ti-              -1   -3.780277    5.676813   -0.870925 L
Ti-Ti3+4         -1   -1.887277    5.676813    1.507075 L
O-O_3            -1   -3.780277    3.783813   -1.283925 L
O-O_3            -1   -3.780277    5.676813    1.094075 L
O-O_3            -1   -1.887277    5.676813   -0.458925 L
Ti-Ti3+4         -1    0.004723    5.676813   -0.870925 L H-H_50 0
Ti-Ti3+4         -1    1.897723    5.676813    1.507075 L
O-O_3            -1    0.004723    3.783813   -1.283925 H
O-O_3            -1    0.004723    5.676813    1.094075 L
O-O_3            -1    1.897723    5.676813   -0.458925 L
Ti-              -1    3.789723    5.676813   -0.870925 L
O-O_3            -1    3.789723    3.783813   -1.283925 L
O-O_3            -1    3.789723    5.676813    1.094075 L
N-N_3             0   -0.002786   -1.278629   -2.620168 H
H-H_              0   -0.841903   -1.469158   -3.164268 H
H-H_              0    0.811048   -1.502694   -3.189412 H
H-H_              0    0.014603    0.337241   -2.587325 H

1 3 1.0 4 1.0 15 1.0
2 3 1.0 4 1.0 5 1.0 8 1.0
3
4 6 1.0
5 14 1.0
6 8 1.0 9 1.0 21 1.0
7 8 1.0 9 1.0 10 1.0 12 1.0
8
9 11 1.0
10 20 1.0
11 12 1.0 26 1.0
12
13 15 1.0 16 1.0 17 1.0 30 1.0
14 16 1.0 17 1.0 18 1.0 22 1.0
15
16
17 19 1.0
18 29 1.0
19 21 1.0 22 1.0 23 1.0 56 1.0
20 22 1.0 23 1.0 24 1.0 27 1.0
21
22
23 25 1.0
24 35 1.0
```

Table B.4 (cont'd)

```
 25 26 1.0 27 1.0 41 1.0
 26
 27
 28 30 1.0 31 1.0 32 1.0 45 1.0
 29 31 1.0 32 1.0 33 1.0 37 1.0
 30
 31
 32 34 1.0
 33 44 1.0
 34 36 1.0 37 1.0 38 1.0 50 1.0
 35 37 1.0 38 1.0 39 1.0 42 1.0
 36 59 1.0
 37
 38 40 1.0
 39 49 1.0
 40 41 1.0 42 1.0 54 1.0
 41
 42
 43 45 1.0 46 1.0 47 1.0
 44 46 1.0 47 1.0 51 1.0
 45
 46
 47 48 1.0
 48 50 1.0 51 1.0 52 1.0
 49 51 1.0 52 1.0 55 1.0
 50
 51
 52 53 1.0
 53 54 1.0 55 1.0
 54
 55
 56 57 1.0 58 1.0
 57
 58
 59

Approx TS

0 1 0 1 0 1
 Ti-             -1   -3.780277   -5.678187   -0.870925 L
 Ti-Ti3+4        -1   -1.887277   -5.678187    1.507075 L
 O-O_3           -1   -3.780277   -5.678187    1.094075 L
 O-O_3           -1   -1.887277   -5.678187   -0.458925 L
 O-O_3           -1   -1.887277   -3.786187    1.920075 L
 Ti-Ti3+4        -1    0.004723   -5.678187   -0.870925 L H-H_21 0
 Ti-Ti3+4         -1    1.897723   -5.678187    1.507075 L
 O-O_3           -1    0.004723   -5.678187    1.094075 L
 O-O_3           -1    1.897723   -5.678187   -0.458925 L
 O-O_3           -1    1.897723   -3.786187    1.920075 L
 Ti-             -1    3.789723   -5.678187   -0.870925 L
 O-O_3           -1    3.789723   -5.678187    1.094075 L
 Ti-Ti3+4        -1   -3.780277   -1.893187   -0.870925 L H-H_17 0
 Ti-             -1   -1.887277   -1.893187    1.507075 L H-H_22 0
 O-O_3           -1   -3.780277   -3.786187   -1.283925 L
 O-O_3           -1   -3.780277   -1.893187    1.094075 L
 O-O_3           -1   -1.887277   -1.893187   -0.458925 H
```

Table B.4 (cont'd)

```
O-O_3           -1   -1.887277   -0.001187    1.920075 L
Ti-Ti3+4         0    0.007294   -2.045197   -0.876354 H
Ti-             -1    1.897723   -1.893187    1.507075 L H-H_22 0
O-O_3           -1    0.004723   -3.786187   -1.283925 H
O-O_3           -1    0.004723   -1.893187    1.094075 H
O-O_3           -1    1.897723   -1.893187   -0.458925 H
O-O_3           -1    1.897723   -0.001187    1.920075 L
Ti-Ti3+4        -1    3.789723   -1.893187   -0.870925 L H-H_23 0
O-O_3           -1    3.789723   -3.786187   -1.283925 L
O-O_3           -1    3.789723   -1.893187    1.094075 L
Ti-Ti3+4        -1   -3.780277    1.891813   -0.870925 L H-H_32 0
Ti-             -1   -1.887277    1.891813    1.507075 L H-H_37 0
O-O_3           -1   -3.780277   -0.001187   -1.283925 L
O-O_3           -1   -3.780277    1.891813    1.094075 L
O-O_3           -1   -1.887277    1.891813   -0.458925 H
O-O_3           -1   -1.887277    3.783813    1.920075 L
Ti-              0    0.000964    1.960949   -0.847360 H
Ti-             -1    1.897723    1.891813    1.507075 L H-H_37 0
O-O_3            0   -0.003030    0.343073   -1.587548 H
O-O_3           -1    0.004723    1.891813    1.094075 H
O-O_3           -1    1.897723    1.891813   -0.458925 H
O-O_3           -1    1.897723    3.783813    1.920075 L
Ti-Ti3+4        -1    3.789723    1.891813   -0.870925 L H-H_38 0
O-O_3           -1    3.789723   -0.001187   -1.283925 L
O-O_3           -1    3.789723    1.891813    1.094075 L
Ti-             -1   -3.780277    5.676813   -0.870925 L
Ti-Ti3+4        -1   -1.887277    5.676813    1.507075 L
O-O_3           -1   -3.780277    3.783813   -1.283925 L
O-O_3           -1   -3.780277    5.676813    1.094075 L
O-O_3           -1   -1.887277    5.676813   -0.458925 L
Ti-Ti3+4        -1    0.004723    5.676813   -0.870925 L H-H_50 0
Ti-Ti3+4        -1    1.897723    5.676813    1.507075 L
O-O_3           -1    0.004723    3.783813   -1.283925 H
O-O_3           -1    0.004723    5.676813    1.094075 L
O-O_3           -1    1.897723    5.676813   -0.458925 L
Ti-             -1    3.789723    5.676813   -0.870925 L
O-O_3           -1    3.789723    3.783813   -1.283925 L
O-O_3           -1    3.789723    5.676813    1.094075 L
N-N_3            0    0.109526   -1.600169   -2.986096 H
H-H_             0   -0.664397   -1.957554   -3.537849 H
H-H_             0    0.987674   -1.875248   -3.413828 H
H-H_             0    0.056940   -0.536394   -2.691360 H

1 3 1.0 4 1.0 15 1.0
2 3 1.0 4 1.0 5 1.0 8 1.0
3
4 6 1.0
5 14 1.0
6 8 1.0 9 1.0 21 1.0
7 8 1.0 9 1.0 10 1.0 12 1.0
8
9 11 1.0
10 20 1.0
11 12 1.0 26 1.0
12
13 15 1.0 16 1.0 17 1.0 30 1.0
```

Table B.4 (cont'd)

```
14 16 1.0 17 1.0 18 1.0 22 1.0
15
16
17 19 1.0
18 29 1.0
19 21 1.0 22 1.0 23 1.0
20 22 1.0 23 1.0 24 1.0 27 1.0
21
22
23 25 1.0
24 35 1.0
25 26 1.0 27 1.0 41 1.0
26
27
28 30 1.0 31 1.0 32 1.0 45 1.0
29 31 1.0 32 1.0 33 1.0 37 1.0
30
31
32 34 1.0
33 44 1.0
34 36 1.0 37 1.0 38 1.0 50 1.0
35 37 1.0 38 1.0 39 1.0 42 1.0
36
37
38 40 1.0
39 49 1.0
40 41 1.0 42 1.0 54 1.0
41
42
43 45 1.0 46 1.0 47 1.0
44 46 1.0 47 1.0 51 1.0
45
46
47 48 1.0
48 50 1.0 51 1.0 52 1.0
49 51 1.0 52 1.0 55 1.0
50
51
52 53 1.0
53 54 1.0 55 1.0
54
55
56 57 1.0 58 1.0
57
58
59
```

Table B.5 VASP files (POSCAR, INCAR, K-POINTS, and POTCAR) for volume relaxation calculation of anatase TiO_2.

POSCAR file

```
Ti O
   1.000000000
     3.823780050    0.000000000    0.000000000
     0.000000000    3.823780050    0.000000000
     0.000000000    0.000000000    9.666313296
   4   8
Selective dynamics
Direct
  0.000000000  0.000000000  0.000000000   T   T   T
  0.000000000  0.500000000  0.250000000   T   T   T
  0.500000000  0.500000000  0.500000000   T   T   T
  0.500000000  0.000000000  0.750000000   T   T   T
  0.000000000  0.000000000  0.207275490   T   T   T
  0.000000000  0.000000000  0.792724509   T   T   T
  0.000000000  0.500000000  0.457275490   T   T   T
  0.000000000  0.500000000  0.042724509   T   T   T
  0.500000000  0.500000000  0.707275490   T   T   T
  0.500000000  0.500000000  0.292724509   T   T   T
  0.500000000  0.000000000  0.957275490   T   T   T
  0.500000000  0.000000000  0.542724509   T   T   T
```

INCAR file

```
SYSTEM = Ag2O Bulk latt param
!ISTART = 0
PREC   = HIGH
ISIF   = 3
IBRION = 1
NSW    = 150
LREAL  = Auto
ISMEAR = -5; !SIGMA = 0.1;
LWAVE = .False.
!ENCUT = 500
!IALGO = 48
EDIFFG = -0.01
```

Table B.5 (cont'd)

K-POINTS file

```
K-Points
 0
Monkhorst Pack
 15 15 15
 0  0  0
```

POTCAR file

```
PAW_GGA Ti 08Aug2001
 4.00000000000000000
 parameters from PSCTR are:
   VRHFIN =Ti: d3 s1
   LEXCH  = 91
   EATOM  =    95.1745 eV,    6.9951 Ry

   TITEL  = PAW_GGA Ti 08Aug2001
   LULTRA =        F    use ultrasoft PP ?
   IUNSCR =        1    unscreen: 0-lin 1-nonlin 2-no
   RPACOR =    2.200    partial core radius
   POMASS =   47.880; ZVAL   =    4.000    mass and valenz
   RCORE  =    2.800    outmost cutoff radius
   RWIGS  =    2.500; RWIGS  =    1.323    wigner-seitz radius
(au A)
   ENMAX  =  178.367; ENMIN  =  133.775 eV
   RCLOC  =    2.215    cutoff for local pot
   LCOR   =        T    correct aug charges
   LPAW   =        T    paw PP
   EAUG   =  328.883
   DEXC   =    -.021
   RMAX   =    3.452    core radius for proj-oper
   RAUG   =    1.300    factor for augmentation sphere
   RDEP   =    2.885    radius for radial grids
   QCUT   =   -3.621; QGAM   =    7.241    optimization
parameters
```

"The following part in POTCAR file is cut in order to save place"